**Marine Geology**
October 2018, Volume 404 Pages 41-59
http://dx.doi.org/10.1016/j.margeo.2018.07.003
http://archimer.ifremer.fr/doc/00450/56136/




# Sedimentation adjacent to atolls and volcano-cored carbonate platforms in the Mozambique Channel (SW Indian Ocean)

Counts John [1, *], Jorry Stephan [1, *], Leroux Estelle [1, *], Miramontes Elda [2, *], Jouet Gwenael [1, *]

[1] Laboratoire Géodynamique et Enregistrement Sédimentaire (GM-LGS) – Institut Français de Recherche pour l'Exploitation de la Mer (IFREMER) – Pointe du Diable, 29280 Plouzané, France
[2] CNRS, UMR6538, Laboratoire Géosciences Océan, Institute Universitaire Européen de la Mer - Université de Bretagne Occidentale (IUEM-UBO), 29280 Plouzané, France

* Corresponding authors : email addresses : John.Counts@ifremer.fr ; Stephan.Jorry@ifremer.fr ; Estelle.Leroux@ifremer.fr ; Elda.Miramontesgarcia@univ-brest.fr ; Gwenael.Jouet@ifremer.fr

**Abstract :**

Recently acquired data from the Iles Eparses (southwestern Indian Ocean) reveal new information about the geomorphology, depositional processes, and sedimentary deposits on the slopes of atolls and atoll-like platforms. The deposits discussed here lie on the deepwater flanks of isolated, inactive volcanos that are capped by shallow, relatively flat carbonate platforms 45–210 km2 in area. Much of the slope geomorphology is controlled by the underlying volcanic edifice. Steep (~25–35°) upper slopes consist of outcrops of volcanic basement, smooth banks, failure scarps, and channels. Sedimentary features seen in the lower slope and proximal basin (2000–3500 m deep) consist of channels, levees, lobes, and mass transport deposits (MTDs). In places, channels terminate 13–18 km from the platform margin, ending in lobes up to 3.5 km across, a feature not often seen in modern carbonates. In the subsurface, MTDs are present near all platforms. Within MTDs, seismic character is variable, often consists of chaotic reflections indicative of sediment gravity flow processes. Subsurface units with organized (retro- or progradational) reflections are interpreted as turbidite lobes or MTDs with compressional features. Core taken within lobes and near the base of slopes reveal decimeter-scale turbidites and debrites composed primarily of graded and massive bioclastic grainstones and packstones with abundant neritic skeletal components, interbedded with hemipelagic aragonitic and clay-rich foraminiferal ooze. Slope depositional processes are therefore primarily gravity-driven and occur at different scales; i.e., bed-scale turbidites and muds may be remobilized and redeposited through slope failure and deposition of large MTDs. Dominant wind direction may also play a role in slope sedimentation: leeward slopes are generally less rugose and show increased sedimentation at the toe of the slope. This study thus provides new insight into depositional systems surrounding atoll-like carbonate platforms, and provides a new analogue for similar deposits in the geologic record.

**Highlights**

► First study to describe the slopes of volcano-cored carbonate platforms in detail. ► Slope sediments composed of muds and platform-derived carbonate sands ► Slopes contain channels, fans, and mass transport deposits. ► Sedimentation is primarily controlled by inherited topography and dominant winds. ► Excellent example of complete source-to-sink sedimentary system

**Keywords** : Ato, ll Carbonate, Indian Ocean, Slope, Deepwater sediments

## 1. Introduction

Sediments on carbonate slopes are well-represented in the ancient geologic record (Blomeier and Reijmer, 2002, and references therein), and are an important component of carbonate depositional systems. However, a detailed, actualistic understanding of these environments in modern settings ~~has been~~ was hampered for many years by the inaccessibility of deepwater deposits in modern oceans (McIlreath and James, 1978), and much work remains to be done. Although many studies have documented the shallow-water portions of modern carbonate platforms and coral atolls

(e.g., Reijjmer et al., 2009; Gischler, 2011; Harris et al., 2011), most existing research on modern deepwater allochthonous carbonates (distinguished here as those predominantly transported into the deep sea from elsewhere, as opposed to cold-water carbonate muds and buildups precipitated *in situ*) has focused on a limited number of well-known settings (e.g., the BahamasCaribbean). Although more recent studies have expanded research into new areas (e.g., the Maldives, Papua New Guinea, NE Australia, and New Caledonia; Betzler et al., 2016; Tcherepanov et al., 2008; Dunbar and Dickens, 2000; Yamano et al., 2015, respectively), relatively few studies have been conducted in the southern Indian Ocean. More studies in new areas and in different geo-environmental settings are required in order to understand the full range of carbonate slope sedimentation around the world.

This study examines the submarine slopes of four isolated, volcano-cored atolls and atoll-like carbonate platforms in the southern Indian Ocean (Fig. 1) with the goal of improving our understanding of the depositional processes and products operating on their slopes and nearby basin floors. The deposits formed when carbonate sediments are transferred, deposited, and remobilized on the platform slopes are the focus of this paper, as well as the mechanisms responsible for such deposits. By using seismic, bathymetric, and core data, this study reveals new information about the geomorphology and

sedimentology of these unique depositional settings. Because of their relatively small size (on a scale of tens of kilometers), the entire sedimentary system of each platform can be examined as a whole, forming a complete source-to-sink picture of sedimentation. ~~.~~ This information is used to create a new, unique facies model ~~contributes to the formation of more complete depositional models~~ for the type of atoll-like carbonate platforms discussed here, which are lacking in the geological literature, and provides a point of comparison to other, genetically different carbonate systems elsewhere.

## 2. Regional Setting

The islands that are the focus of this study (Grande Glorieuse, Europa, Juan de Nova, and Bassas da India) lie within and around the modern Mozambique Channel (MC), an elongate basin in the Indian Ocean between the African continent and the island of Madagascar (Fig. 1). Together, these islands and the waters surrounding them are known as the Iles Eparses, and are part of the French Southern and Antarctic Lands. Islands are the subaerial portions of carbonate platforms that sit atop ~~conical~~ volcanic pinnacles originating from the basin floor. Platform tops are relatively flat and composed entirely of carbonate; there is no central volcanic peak. All are circular/equant in map view, except for Glorieuses, which has a roughly triangular shape.

123 The detailed origins and tectonic histories of each of
124 these structures are not well-studied, but the emergence of all
125 platforms is a result of the interplay between tectonic uplift and
126 subsidence, extrusive volcanic growth, eustasy, and the rate of
127 carbonate aggradation, all of which vary between platforms
128 (Courgeon et al., 2016). Platforms are of different ages and
129 genetic origins and may be related to localized hotspot chains
130 or mantle plumes. The Glorieuses Archipelago (Fig. 2A, 2B) is
131 at minimum Paleocene in age and is a part of a linear ridge of
132 volcanoes that also encompasses the nearby Comoros
133 (Courgeon et al., 2016). It shows no indication of any
134 significant drowning events during its lifespan, and has been
135 interpreted to now be tectonically stable (with a very slow
136 uplift of ~0.012 mm/year since ~130 ka) owing to its position
137 away from the Somalia-Nubian plate boundary (Guillaume et
138 al., 2013). Juan de Nova (Fig. 2C, 2D) has been studied very
139 little; however, it likely has a granite core (Förster, 1975) and is
140 not currently undergoing any notable uplift or subsidence
141 (Testut et al., 2016). Bassas da India (Fig. 3A, 3B) and Europa
142 (Fig. 3C. 3D) have been hypothesized to be related to the
143 Quathlamba hotspot, which formed the archipelago up to 60
144 Mya and is currently under Lesotho (Johnston and Thorkelson,
145 2000). Bassas da India specifically has also been shown to have
146 originated in the late Oligocene/early Miocene, and has been
147 volcanically active as late as the early Pleistocene (Courgeon et

al., 2017). Large-scale faulting, structural deformation, and volcanism in Bassas da India and associated submarine banks have been tied to a southern extension of the East African Rift system (Courgeon et al., 2016).

Carbonate deposition in the Iles Eparses ~~atolls~~ began between the Paleocene and Early Miocene, and continues until the present day (Courgeon et al., 2016; 2017). Sediment production was periodically interrupted by episodes of volcanism and subaerial exposure, which occurred during relative sea-level lowstands and resulted in karstification of the platform top. Platform top sediments are generally poorly understood; the sedimentology of Ile Europa was first examined from a geological perspective in the 1960s (Berthois and Battistini, 1969) and on Glorieuses in the 1970s (Battistini and Cremers, 1972; Battistini et al., 1976). These preliminary studies noted the carbonate sediment composition and basic facies asymmetry of platform tops, as well as the existence of paleo-reefs. Sediment atop the Glorieuses platform has been shown by Prat et al. (2016) to be partitioned into five asymmetric facies zones defined by hydrology, storm events, and the distribution of carbonate producing organisms. Here, sediment is remobilized by large sandwaves that ultimately likely migrate off-platform, leading to a relatively continuous supply of sand-sized sediment exported to the platform slope and beyond. Similar asymmetric facies distributions and

winnowing processes can be inferred to be occurring on the tops of other platforms as well (Jorry et al., 2016). Winds are predominantly from the south on all islands except for Glorieuses, where they are primarily from the east (Fig. 1E; Météo France, 2017). Currents come from the east at Glorieuses, but are variable surrounding other islands due to the presence of anticyclonic eddies moving southward through the channel (Schott et al., 2009).

Most Iles Eparses platforms lack the defining features of atolls; i.e., a fringing reef and central lagoon. Only Bassas da India fits the definition; the other Iles Eparses are referred to here as 'atoll-like carbonate platforms' to distinguish them from both true atolls and from more traditionally defined carbonate platforms, e.g. the Bahamas. The tops of Glorieuses and Juan de Nova platforms (Fig. 2) contain small asymmetric vegetated islands, but are mostly submerged, whereas the top of Europa (Fig. 3C, 3D) is predominantly subaerial and contains a single large tidal channel surrounded by mangrove forest. Bassas da India does contain a continuous, circular, marginal reef exposed only at low tide, with a fully enclosed inner lagoon (Fig. 3A, 3B). Today, the exposed surface area of all the islands in question (totaling approximately 42 $km^2$) is significantly smaller than the predominantly subaqueous portions (around 500 $km^2$, generally ranging between of 0-40 m water depth). All platform tops are composed of carbonate

198 sediment, with no volcanic outcrops or sediments visible, and
199 subaerially exposed islands show evidence of recent
200 karstification (Jorry et al., 2016).

201 **3. Methodology and Data Set**

202 Data used in this study were collected during three
203 research cruises in the MC: PTOLEMEE (R/V *L'Atalante*;
204 August/September 2014, Jorry, 2014), PAMELA-MOZ1 (R/V
205 *L'Atalante*; September/October 2014, Olu, 2014), and
206 PAMELA-MOZ4 (R/V *Pourquoi Pas?*; November/December
207 2015, Jouet and Deville, 2015). Dataset includes:

208 • High-resolution bathymetry and substrate
209 backscatter/reflectivity measurements of the deep
210 seafloor, using a Kongsberg EM122 multibeam
211 echosounder
212 • Seismic acquisition with high-speed multichannel
213 (high-resolution, airgun-sourced ) and CHIRP sub-
214 bottom profiler (very high-resolution, swept-frequency
215 source) methods
216 • Kullenberg and Calypso piston coring systems, used to
217 acquire up to 27 continuous meters of seafloor sediment
218 in >3000 m water depth

219 Depth conversions of seismic lines used a mean acoustic
220 velocity of approximately 1700 meters/second, based on
221 assumptions discussed in Lort et al. (1979) and DSDP Reports
222 from the region (wells 240-242 show velocities from 1.5-1.9

223 km/s for the Oligocene; Simpson et al., 1974). This method
224 provides a first approximation for sediment thickness when
225 deep core control is not available.
226 A quantitative approximation of the rugosity (roughness)
227 of the Juan de Nova slope was calculated by: 1) drawing the
228 map-view representation of the -600-meter contour line, 2)
229 measuring radii from a central point to the edge of the contour
230 line, 3) subtracting a roughly circular shape to correct for
231 overall shape of the platform, 4) assessing the standard
232 deviations of corrected radii lengths. With this method, higher
233 rugosity or roughness of the slope results in higher standard
234 deviations. Measurement of several thousand radii was
235 automated using a custom Python script. Standard deviations
236 were then compared for the leeward vs windward sides of the
237 platform to quantitatively measure slope rugosity.
238 Core sediments were initially described visually, and
239 selected intervals were selected for further analysis. Grain size
240 was measured with a Malvern Mastersizer 3000 laser
241 diffraction particle size analyzer, capable of measuring all
242 grains from 10 nm to 2 mm. Carbonate sand composition was
243 determined by counting several hundred individual grains
244 under a reflected light binocular microscope: samples were
245 sieved and split into three size fractions above 63 µm, and
246 results were combined to provide a bulk composition.
247 Sediments, both ~~sands and~~ muds (<63µm) and carbonate

grainstones/packstones (dominant particle size >63 µm), were imaged and analyzed with a FEI Quanta 200 scanning electron microscope (SEM) equipped with an Oxford Instruments Energy Dispersive Spectroscopy (EDS) detector. X-Ray diffraction (XRD) for mineralogy of muds was performed in-house using a Bruker AXS diffractometer.

## 4. Results

### *4.1 Geomorphologic elements*

#### *4.1.1 Platform tops and terraces*

Overall, platforms and their volcanic edifices have a conical morphology with a small, relatively flat top (Fig. 4). The volume of carbonate sediment that has accumulated atop each volcano is unknown; neither deep cores nor deep seismic have been acquired on the tops or upper slopes of the platforms. All investigations of platform tops (by dredging or coring), however, have only yielded carbonates. On Glorieuses and Bassas da India, the main platform tops are attached to deeper submarine terraces 700-750 and 400-500 m below sea level, respectively (Figs. 4A, 4B). The terrace on the northwestern side of Glorieuses is small (3.9 $km^2$; Fig. 4A), and lies between the main platform and a submarine volcanic pinnacle without a flat top (labeled 'T' in Fig. 2A). On Bassas da India, the submerged terrace is separated from the main platform by a large fault (Figs. 3A, 4B); previous studies (Courgeon et al.,

2017) interpret the terrace as a product of Pliocene-Pleistocene fault movement. Volcanic rocks and small volcanic clasts within sediment have been found on the submarine terrace of Bassas da India.

### *4.1.2 Smooth surfaces and basement outcrops*

All platform tops show a relatively sharp transition from the shallow, flat top to a steep upper slope with a 25-35 degree gradient (Fig. 4). These upper slope surfaces have the highest overall gradient of anywhere between the platform top and the adjacent abyssal plain, and are smoother than the mid-slope below (Fig 4C). In general, the broad, smooth areas of upper slopes are more contiguous on the leeward side of islands. Seismic lines taken on the middle slope of Europa (Fig. 4D) show that these areas likely contain only a thin veneer of sedimentary cover. Smooth ~~U~~upper slopes may be interrupted, however, by steep-sided (generally 30-50 degrees) outcrops of basement (e.g., Fig. 4C). Basement outcrops are highly variable in size, and in seismic are characterized by low- to variable-amplitude reflections that differ from the overlying sedimentation patterns (Fig. 4D). These outcrops are more abundant slightly lower in the slope where the gradient decreases to 12-20 degrees. Basement is likely composed of volcanics, as previously interpreted by Lort et al., 1979, and Bassias et al., 2016.

### *4.1.3 Escarpments*

298 The smooth topography and gradient of upper slope
299 surfaces may also be broken by escarpments and slope failure
300 scars. On the Glorieuses platform, a linear escarpment at a
301 water depth ranging between 700 and 850 meters is traceable
302 for approximately 70 km around the platform's perimeter (Fig.
303 4A and inset). This escarpment is most prominent on the
304 northwest side of the platform, and reaches around 120 meters
305 in height with a slope of 50-80 degrees. It lies at the same
306 bathymetric depth as the small terrace to the northwest of the
307 main platform. Similar long, well-developed linear escarpments
308 are not seen on other platform slopes.
309 *4.1.4 Slope failure scars*
310 Elsewhere, smaller, discrete scarps (c.f. Hampton and
311 Lee, 1996) are evident on several sites in the upper slope. On
312 Juan de Nova, multiple arcuate scarps 400-2000 m across incise
313 60-150 m into the upper slope surface (Fig. 5A-5B). At least 10
314 of these are present around the islands' perimeter, all of which
315 occur where the surrounding slope gradient ranges from 22°-
316 28°. Arcuate scarps, however, are not distributed evenly; they
317 are more abundant on the windward south side of the platform,
318 with the leeward side having a quantitatively smoother, lower
319 rugosity slope (Fig. 5C). The morphology of scarps are also
320 different—scarps on the leeward slope generally have less
321 relief, on the order of 50-60 meters as opposed to 100 meters or
322 more on windward sides. As a first approximation, the volume

of sediment once filling these scarps was calculated using a series of three-dimensional wedges, based on the gradient found above and below the scar in question (Table 1). Individual scarp volumes range from approximately 1 to 10 $km^3$, with the caveat that true volumes are slightly smaller due to their irregular shape (Fig. 5A, 5B), a factor not included in the calculation. These small individual scarps are not present on the slopes of other platforms; however, on Bassas da India a scallop-shaped indentation on the platform top (4 km across; see Fig~~ure~~ 6A) may also be the product of past slope failure on a much larger scale. The slope just below this indentation is highly rugose and is the source of channels that extend to the basin floor. Large areas of erosion are also seen on the southern side of Europa (Fig. 6B), but do not have the distinctive arcuate morphology seen on Juan de Nova.

*4.1.5 Gullies and channels*

Below the smooth uppermost slopes (greater than 20°-25°), mid-slope (from 20°-25° to 10°) and lower-slope (0-10°) zones contain a series of basement outcrops, linear ~~channels~~gullies, and sedimentary deposits (Figs. 2 and 3). In the mid-slope, gullies ~~channels~~ incise into the basement substrate (Fig 4D) and are separated by volcanic outcrops, but are generally not deep or narrow enough to be considered canyons, though the distinction is not based on quantitative criteria (Hay, 2014). These gullies gradationally transition into

true channels as the slope decreases. In seismic, channel floors can be seen to be composed of high-amplitude, relatively continuous reflections up to ~85 m thick, but without a distinct base (Fig. 4D). In map view, channels are generally straight, with flat bottoms and walls generally between 40 and 100 m high (Fig. 4C), though this varies considerably. In lower slopes, channels may erode into sediments rather than basement. Further details of sedimentary deposits associated with channels and their geomorphologic elements are discussed below.

*4.2 Sediments of the slope and proximal basin*

*4.2.1 Distribution*

Most sediment in the Iles Eparses slopes accumulates in the lower slope, where the gradient is less than 10°. Seismic and bathymetric data reveal that lower slopes contain a wedge-shaped sedimentary package ~~wedge~~ that extends to up to 30 kilometers from the platform top (Figs. 2, 3 and 7; seismic data showing sedimentary nature of lower slope ~~wedge~~ sediments in Fig. 7A). Th~~i~~ese sediments ~~wedge is~~ are elevated relative to the generally flat basin floor (Figs. 2 and 3), and ha~~s~~ve a higher gradient (usually 3°-6°, vs. 0-3°). The change in slope gradient marks the slope base; sediments beyond this point are considered to be in the adjacent basin. Where bathymetric data is available around the entire slope perimeter, lower slopes can often be seen to have asymmetric distribution around the

platform, with bathymetric highs occurring more prominently on leeward sides of at least some platforms (especially in Europa, Glorieuses, and Juan de Nova; see Figs. 2 and 3). Representative slope profiles on windward and leeward sides of the platforms are shown in Figure 7B-D. Although upper slopes may similar or steeper on either side, in each instance the lower slope ~~wedge~~ extends further from the platform top on the leeward side.

*4.2.2 Lithologies*

Cores acquired on lower platform slopes (locations in Figs. 2 and 3) reveal the character of sediments in the shallow subsurface. A selection of representative core is shown in Figure 8A-D, all of which consist predominantly of foraminiferal ~~muds~~ ooze interbedded with beds of unlithified carbonate ~~sand~~grainstones, packstones, or wackestones. ~~Carbonate sand~~ These coarser-grained carbonate beds make up a minor but significant proportion of core thicknesses, usually between <1 and 20%. The dominant grain size in these beds is generally fining-upward, with most constituent particles ~~carbonate sands ranging from fine- to medium-grained~~less than 0.5 mm (Fig. 8E), although ~~,~~ many beds have a basal lag with coarser skeletal fragments. Carbonate sediments within these beds are unlithified and well-sorted, ~~carbonate grainstones or packstones,~~ without clear sedimentary structures other than occasional horizontal laminae. The sand-sized component of

~~grainy~~ coarser units (shown in blue in Fig. 8A-8D) is composed of 100% calcareous material, including many taxa normally found in the photic zone: coral and algal fragments, echinoid spines, and well-preserved gastropods (Figs. 8F, 8G). The tests of planktonic and benthic foraminifers also make up a significant portion of these sands (up to 35% of identifiable grains; Fig. 8F). Interbedded with these sediments are thicker beds of ~~sandy~~ foraminiferal carbonate ~~muds~~ooze.~~, with the sand-sized portion predominantly made up of benthic and planktonic foraminifera.~~ The clay-sized fraction of these background micritic muds~~muds~~ is not identifiable petrographically, however, SEM images (Fig. 8H) reveal the presence of needle-like crystals, as well as platy grains. EDS analysis (Fig. 8H) shows that intervals dominated by needle-like crystals are enriched in calcium and oxygen, suggesting a carbonate mineralogy, whereas those dominated by platy grains have elevated amounts of silicon, aluminum, and oxygen—all elements that are components of ~~phyllo~~silicate minerals. To better understand the composition of this component of the mud, XRD analysis was performed on a sample from the same approximate interval (MOZ4-CS09, 100-102 cm). Results show the presence of quartz, feldspar, and various clay minerals, confirming the siliciclastic nature of some of these grains (Fig. 8H).

*4.2.3 Channels, lobes, and levees*

~~In the lower slope~~Upper slope gullies (*sensu* Amblas et al., 2018) ~~,~~ evolve distally into channels that are traceable through their increased reflectivity (backscatter) values (shown in red in Figs. 2B, 2D, 3B, 3D, and 9A-9C). All lower slope channels are extremely straight, with most sinuosities above 0.9, typical gradients between 5° and 10°, and with walls that range between 40-100 m above the channel floor. Like the overall slope, the gradient of channels floors decreases steadily basinward (see inset of Figure 4C, showing gradient decrease from ~30° to ~10° over the course of 5 km). In map view, most channels originate in the upper slope and continue downslope to reach the basin floor. Areas of increased backscatter intensity often taper basinward to a point (e.g., Fig. 9A), although channel forms may be seen in bathymetric relief to continue further downslope. In several places, however, an individual upper slope incised channel splits into multiple channels in the mid-slope (e.g., the eastern side of Europa, denoted by an arrow in Fig. 2D, and the northeastern side of Bassas da India; Fig. 9B). This point of channel bifurcation most often occurs where the slope gradient decreases to around 10°. The lower slope channels that radiate outward from this point are smaller and also straight, and often reach the basin floor. On the northwestern side of Glorieuses, some slope channels contain a regularly-spaced series of escarpments, 450-750 m apart and

15-60 m high , resembling cyclic stepsthat form an undulatory topography within the channel (Fig. 9B).

On the northern side of Europa, at least one lower slope channel is bounded by a well-defined raised sedimentary deposits with a 'bird-wing' shape in cross-sectionasymmetric levee, seen in seismic data in Figures 9D and 9E and interpreted as a levee deposit. These deposits levee and the channel axis are visible in bathymetric data as well, though the channel itself shows no increased backscatter values. In seismic, levee deposits are transparent with faint, but continuous, reflections (Facies E, described below), and -reach a maximum thickness of 280 meters in the seismic profile shown in Fig 9D. Height from the channel floor to the highest part of the levee is 70 meters or less. The central channel floor is characterized by higher amplitude reflections, as are the deposits several kilometers beyond the levee boundaries. Levee deposits eventually merge into transparent, furrowed sediments on the basin floor, shown on the right side of Figure 9D and visible in on the seafloor in Figure 3C (labeled). A 27-m core (MOZ4-CS23; see portion in Fig. 8D) taken directly atop the levee shown in Figure 9D and 9E consists almost entirely of foraminiferal carbonate mud, with carbonate sand beds occurring only near its base.

Channels may terminate in a fan lobe near the bottom of the lower slope or on the basin floor, although fans lobes are

not always present. A distinct ~~fan~~ lobe (visible in backscatter imagery; Fig. 9C) on the northeastern side of Bassas da India was selected for more detailed investigation and was ~~penetrated~~ sampled by core MOZ1-KS27 (Fig. 8A). The ~~fan~~ lobe is approximately 4 kilometers across at its widest visible point, is estimated to range from 0 to tens of meters thick based on seismic data, and begins where the slope gradient is around 3°. Core MOZ1-KS27 (Fig. 8A), despite only being 4 m long, contains multiple lithofacies indicative of the ~~fan~~lobe's composition. Above background foraminiferal muds, a ~30-cm thick bed with a sharp lower surface contains a basal layer of large (10-15 mm) coral and algal fragments within a matrix of very coarse, bioclastic calcareous ~~sand~~grainstone. This coarse skeletal grainstone facies is overlain by a one-meter thick unit of ~~muddy~~ carbonate ~~sand~~ packstone-wackestone (dominant grain size around 0.3 mm) that contains irregular clasts of mud 2-20 cm in diameter, which roughly increase in size upward through the unit. This facies is in turn overlain by a 20-cm thick, well-sorted, fining-upward bed ~~of sands,~~ containing fine- to medium-grained carbonate grainstones ~~calcareous sands~~ (Fig. 8E) with a similar composition to those seen elsewhere.

*4.2.4 Subsurface seismic facies*

Seismic lines acquired on the lower slopes and proximal basins of Iles Eparses platforms show several distinct types of sedimentary deposits, which can be classified based on the

amplitude, continuity, and orientation of their internal reflections (Table 2). Seismic facies are found in different locations surrounding each platform, and not all facies are present surrounding each locality.

Sediments comprising the basin floor are typically characterized by horizontal to sub-horizontal, continuous, high-amplitude reflections that extend to the outer limits of seismic data (Facies A; Figs. 10 and 11) and that onlap onto the lower slopes of platforms. These are seen in all seismic lines that intersect the basin floor. On the eastern side of Juan de Nova, sSediments of this facies originateing from the Madagascar shelf deposit and form thick, laterally continuous sediment packages into the basin, separated by clearly identifiable onlap surfaces (Figs. 10BC, 11B10D). Here, this facies interfingers with Facies B (transparent, chaotic reflections; Fig. 10B10C), which is contained within discrete units that taper away from the Juan de Nova platform. interfingers with sediments coming from the incised continental slope of western Madagascar. Sediments originating from the Madagascar shelf deposit thick, laterally continuous sediment packages into the basin, separated by clearly identifiable onlap surfaces (Figs. 10B, 11B). These sSubsurface units originateing from the JDN platform (e.g., those identified in Fig. 11B10D), are 30-40 m thick, and extend seven or more kilometers into the basin. Internal character in these units is consistently transparent and shows little proximal-

distal evolution. On the northwestern side of the Glorieuses platform, chaotic, transparent Facies B is present in dip line 315 around 120 m below the seafloor surface (Fig. 11A~~10C~~, ~~11C~~11B). Here, the unit containing ~~Facies B~~this facies extends only ~2 km away from its origin point, forming a thicker, shorter seismic unit that is laterally adjacent to Facies D (discussed below).

In Bassas da India, a large, amalgamated unit of Facies C (chaotic facies of mixed amplitude) makes up a significant portion of the subsurface on the northeastern side of the island (Figs. 10A, ~~11A~~10B). The deposit sits directly atop basement, and decreases in thickness over the course of approximately 15 km. This unit shows little interfingering with adjacent hemipelagic basinal sediments; up to 320 meters of flat basin sediments unconformably onlap the unit. Internally, this unit contains at least one strongly reflective basement-parallel surface, and contains both high- and low-amplitude chaotic reflection~~or~~s.

Units containing both the chaotic reflections of Facies C and the more organized reflections of Facies D are present within discrete units on the northwestern side of Glorieuses in dip lines 315 and 319 (Figs. ~~10C~~11A, 11B,~~10D~~12~~, 11C~~). The most prominent unit containing these facies, up to ~80 m thick, forms a wedge-shaped sediment package ~~(Facies D described above)~~ extending approximately 12 km basinward from its

origin point on the lower slope. In this unit, seismic Facies D contains both platform-and basinward-dipping high-amplitude reflections. Reflections in this unit become thinner and increasingly horizontal, ultimately terminating into the continuous, high amplitude, 'railroad tracks' that make up Facies A in the deep basin away from platforms. Just to the northwest of this line, a different unit containing organized, inclined reflections (Facies D; ~~(~~l Line 319, Fig ~~10D~~12) comprises a significant portion of the subsurface, forming an irregular unit that tapers basinward and is not well-separated from the underlying sediments. In this ~~area~~unit, the seafloor surface contains a series of irregular, arcuate or linear ridges that are 10s to 100s of meters in relief with 25-50 m amplitudes (decreasing basinward), and wavelengths of 700-1200 m (Fig. ~~10D~~12). Seismic Line 319 crosses these ridges, and shows that they are the surface expression of concave-downward seismic structures that originate deeper in the subsurface. These structures are characterized by a series of high-amplitude reflections that dip back toward the platform and gradually become tangential to a subhorizontal surface approximately 120 m deep (labeled on Fig. ~~10D~~12).

Facies E (Fig. ~~6A~~9D) is seen on the northern side of Europa in the birdwing-shaped levee and channel deposits that make up the lower slope. Reflections in this facies are mostly continuous and low amplitude, though amplitude and continuity

572 are somewhat variable across the observed deposit. In strike
573 line 015 (Fig. 9D), reflections within the levee are parallel to
574 each other and to the seafloor surface. In dip profile (Fig. 7A)
575 this facies can be seen to grade into horizontal, parallel
576 reflections on the basin floor, which increase in amplitude
577 basinward to conformably become Facies A (Table 2).

578 **5. Discussion**

579 *5.1 Interpretation of sedimentary deposits*

580 *5.1.1 Facies diversity*

581 Cores reveal that deposits on the slopes and in the
582 proximal basins surrounding platforms are a combination of
583 pelagic and platform-derived sedimentation. Within muddy
584 deposits, clay minerals (Fig. 8H) are likely the product of
585 weathering, suspension and transport of clastic sediments in
586 seawater, and subsequent deposition through pelagic rain
587 (Facies G of Pickering et al., 1986). These lithologies are
588 present in all cores and may originate from the African
589 continent (Kolla et al., 1976; Wiles et al., 2017), ~~or~~ Madagascar
590 (the nearby Betsiboka River exports large volumes of fine-
591 grained sediment; Raharimahefa and Kusky, 2010), or
592 elsewhere. While the carbonate platforms discussed here are
593 themselves unlikely to generate significant amounts of
594 aluminosilicate clays found in seafloor muds, the submarine
595 weathering of basalt and other volcanics can produce smectite
596 and other clay minerals (Kolla et al., 1976) and thus may be the

origin of some of the sediment seen here. Coccoliths and planktonic forams also form a significant portion of the fine-grained background sediment—these too are the result of pelagic rain, and may also have been transported long distances (van Sebille et al., 2015). Aragonite needles found in some samples are produced in shallow water on or near carbonate platforms (Milliman et al., 1993). This aragonite is therefore interpreted to have been winnowed from the platform top during times of flooding, as has been hypothesized by Jorry et al (2016).

Coarser -grainstone-packstone ~~ed (sand-dominated and above)~~ units found in core also show evidence of a nearby shallow-water origin. Bioclastic grains (e.g., corals and calcareous algae) are the skeletal remains of organisms that live primarily within the photic zone; they provide unambiguous evidence that at least part of the sediments forming these beds are allochthonous, and come from the tops of nearby platforms. The exact process by which sediment is transferred off of the platform top is unknown, however, wind-related or tide-related currents are both ~~however, winds, currents, and tidal forces are all~~ active on the shallow water portion of platforms. Elsewhere, density cascading has been proposed as a mechanism for the off-platform transfer of sediment (Wilson and Roberts, 1995), a process which is not likely to be ~~may also be~~ active here as it is

dependent on winter cold fronts that are not present in the Mozambique Channel (Deutscher Wetterdienst, 2018).

The fining-upward profiles of some of these beds (e.g., those shown in Fig. 8A-E) are~~is~~ consistent with deposition as turbidites (Shanmugam, 2000). Other depositional processes may also occur: in core MOZ1-KS27, the size of mud clasts within the main bed increases upward. This type of ~~re~~inverse grading may occur in ~~is characteristic of~~ debrites (Mulder and Alexander, 2001), and strongly resembles cohesive flow deposits described by Lowe (1982). Inverse grading has been described previously on ancient carbonate slopes (e.g., Mullins and Cook, 1986). Ripped-up clasts of slope muds entrained within debris flows are also a common component of carbonate slope deposits (James and Jones, 2016). Fining-upward turbidites are also found stratigraphically adjacent to the debris flow unit (Fig. 8A). Turbidite facies are clearly separate, but may be related to the debris flow event (linked turbidites and debrites, c.f. Benn & Evans 2014; Talling et al. 2012). Sediments within these types of gravity flows must ultimately originate from the platform itself, as evidenced by the nature of constituent grains, though the entraining turbidity current or debris flow may originate lower on the slope.

Cores therefore reveal that sedimentation on a bed scale is a combination of hemipelagic sedimentation and gravity flow deposits. However, larger-scale sediment transport processes

are also operating on platform slopes, as depositional units seen in seismic profiles show evidence of mass transport on a kilometer scale.

*5.1.2 Subsurface expression*

Sedimentary units and associated facies seen in seismic lines and bathymetric data are interpreted to consist of three primary types of deposits:

- Basin floor pelagites
- Mass transport deposits (MTDs)
- Channels, levees, and ~~fans/~~turbidite lobes

High-amplitude, parallel reflections on the basin floor (Facies A) are interpreted to be the result of pelagic and hemipelagic sedimentation processes that are continually occurring in the deep sea (Pickering et al., 1986). This seismic facies corresponds to the foraminiferal muds that are seen in core. Thin carbonate turbidites may also be present within this facies, but are likely to be only in the area immediately surrounding each platform. Near Juan de Nova, the character of these background sediments is more variable than elsewhere (Fig. ~~10B~~10C); this is likely a result of their proximity to the western slope of Madagascar. Here, the variety of slope-related sedimentary processes creates internal surfaces and topography not seen in the abyssal basin floor elsewhere (Fig. ~~11B~~10D).

Seismic Facies B-C, characterized by low- or mixed-amplitude chaotic reflections, ~~-~~are usually restricted to discrete

671 units and contain many of the criteria used to recognize mass
672 transport deposits (MTDs), as outlined in Posamentier and
673 Martinsen (2011). Based on the geometry of the unit, as well as
674 the amplitude, continuity, and the orientation of internal
675 reflections, these MTDs are interpreted to be the result of one
676 of several depositional processes. MTDs consisting of chaotic,
677 transparent reflections (Facies B) and those with chaotic, but
678 higher amplitude reflections (Facies C) are interpreted to be the
679 result of submarine debris flows originating on the platform
680 slope. Deposits with similar chaotic seismic character have also
681 been referred to as debris flows by Carter (2001), Posamentier
682 and Kolla (2003), and Joanne et al. (2013), among others. In
683 carbonates specifically, Principaud et al. (2015) interpret
684 chaotic seismic units as mass transport complexes with a debris
685 flow component, and Janson et al. (2011) interpret units
686 characterized by discontinuous, low-amplitude reflectionslso
687 interpreted as debris flows. ~~among others.~~ Debris flow
688 processes remove original stratification during downslope
689 movement, and have the potential to travel long distances
690 (Mulder and Cochonat, 1996), features consistent with the units
691 seen here that extend for several kilometers. The amplitude of
692 the reflections that distinguishes between these facies is likely a
693 product of the lithologic heterogeneity of the source material.
694 On the eastern side of Juan de Nova, this facies contains large
695 stratified and convolute-bedded blocks on a scale of several

hundred meters (Fig. ~~10B~~10C), interpreted as large blocks of coherent or deformed sediment entrained within the mass movement.

The basinward or platform-dipping reflections in some units containing Facies D suggest that a different process is responsible for their deposition. A unit on the northwestern side of Glorieuses thins basinward and displays both progradational and retrogradational internal geometries (Figs. ~~10C~~11A, ~~11C~~11B). This unit is interpreted as a turbidite lobe, as deposits with these types of geometries have been interpreted elsewhere as turbidites (e.g., Gervais et al., 2006). It is likely the subsurface expression of the type of lobate ~~fans~~deposits seen on the current seafloor elsewhere (e.g., on Bassas da India; Fig. 8A). On the northwestern side of Glorieuses, the unit seen in Figure ~~10D~~ 12 contains a series of organized structures with platform-dipping reflections that are expressed on the seafloor surface. These deposits are interpreted as a large MTD with depositional thrusts and pressure ridges (Fig ~~10D~~12) gliding along a subsurface decollement. Such features are known to form due to the compressional regime encountered during some downslope mass movements (Posamentier and Martinsen, 2011; Alsop et al., 2017), however, this is one of the first times they have been clearly documented in a predominantly carbonate system. Sedimentary compression ridges similar to these have been noted in analogous settings in the clastic

realm—nearly identical features are described in recent, submarine sediments from multiple locations (e.g., Alfaro and Holz, 2014; Moscardelli et al., 2006; Frey-Martínez et al., 2005; Hampton and Lee., 1996; Joanne et al., 2013). Compressional features cannot explain all seafloor ridges near Glorieuses, however; smaller sediment waves are also present in the same area, and some of the seafloor topography seen in Figure 2A may be related to turbidity currents.

Transparent, continuous ~~Levee~~ deposits in Facies E are form a channel levee, and interpreted to be the result of the overbank depositional processes associated with channelized sediment gravity flows. The generally low-amplitude nature of these deposits suggests that they are of uniform composition and fine-grained, an interpretation confirmed by the predominance of muds in core MOZ4-CS23 (Fig. 8D).

*5.1.3 Seafloor surface*

Backscatter (reflectivity) data has been reliably shown to predict sedimentological facies (Dartnell and Gardner, 2004), grain size (Clarke et al., 1996; McGonigle and Collier, 2014), and degree of induration of the seafloor (Mulder et al., 2017), though has not been used previously to differentiate between carbonate sands and muds. Here, high reflectivity values are interpreted to denote areas of submarine volcanism, erosional outcrops, and active sediment transfer where coarser-grained (larger than silt-sized)~~,~~ facies are more abundant on the

seafloor. This assumption fits with observed geomorphology and is preliminarily confirmed by core data. Backscatter data shows that active deposition of coarse-grained material is currently taking place through feeder channels that funnel sediment to the basin floor (Figs. 2 and 3). High reflectivity values are interpreted to be the result of carbonate sands (grainstones) on the floors of incised channels, which respond differently to acoustic soundings than surrounding muds. Although lithified volcanic outcrops are also highly reflective, these are easily distinguished from linear sediment pathways. High-reflectivity sediments within channels may terminate on the basin floor in a lobcate fan, and channel forms may be bounded by elevated levees (Fig. 9D-E). Undulatory surface morphologies within some channels are interpreted as cyclic steps (c.f. Covault et al., 2017);. These types of bedforms, lobefans and levees are associated with deposition from turbidity currents (Shanmugam, 2000), and this is interpreted to be the primary process of sediment transfer from the platform top. Channel forms without increased reflectivity are interpreted as inactive, as is the case in the leveed channel noted in Fig. 9C. This channel and others like it may have been cut off from active deposition in the past, a hypothesis supported by the lack of recent sandy deposits in the adjacent core (MOZ4-CS23). Individual channels may therefore have a

finite lifespan, and active channels and lobes may switch with changes in sediment availability.

*5.2 Controls on deposition and geomorphology*

The nature of the volcanic edifice underlying each platform ultimately influences the size, height, and overall gradient of the slope profile, all of which influence the slope depositional architecture. Volcanic cone morphologies lead to an overall smaller platform top size, limiting the volume of bioclastic carbonate sediment that can be produced and thus reducing the available sediment supply to slopes. High gradients in the upper slope lead to little carbonate deposition; the majority of slope sedimentation takes place where gradients are less than 10°. This upper slope bypass inhibits progradation and lateral expansion of the platform top. Slope steepness is also likely responsible for straight channel morphologies (Clark et al., 1992) and the development of basin-floor fan systems, a type of deposit rarely seen in modern carbonate settings (Payros and Pujalte, 2008). The abundance of MTDs on the lower slope and proximal seafloor may also be influenced by slope steepness, although past studies (e.g., Hühnerbach and Masson, 2004) note that the number of slope failures are is relatively independent of inclination, even in volcanic islands. Active regional tectonics may also directly influence platform morphology (and thus deposition), as in the fault-generated subaqueous terrace on Bassas da India. Processes occurring on

795 the terrace may likely affect the sedimentary character of
796 platform sediments; large sand dunes (Fig. 4B, inset; lithology
797 confirmed by sediment samples) suggest that sediments may be
798 winnowed and transported by bottom currents atop the terrace
799 before subsequently moving further downslope.
800 The direction and intensity of dominant trade winds have
801 long been known to have an effect on the facies distribution on
802 carbonate platforms (Dravis and Wanless, 2017) including on
803 Glorieuses (Jorry et al., 2016; Prat et al., 2016). In the Iles
804 Eparses, most platform tops show some degree of wind-related
805 asymmetry, especially on Glorieuses and Juan de Nova.
806 Platform tops also differ in terms of their geomorphology,
807 which likely has some influence over the nature and
808 distribution of slope sediments. Open platform tops without a
809 fringing reef (Glorieuses and Juan de Nova) have a submarine
810 bank with no barriers between the top and slope break, a
811 morphology that promotes continuous deposition and sediment
812 transfer (Fig. 2). Enclosed platform tops (Bassas da India) have
813 an interior lagoon with a mostly continuous fringing reef,
814 preventing continual transferal of large amounts of sediment
815 from the inner platform to the slope, and possibly affecting the
816 sedimentological character of platform top exports by confining
817 platform-top muds (Fig. 3). On the top of Europa, sediment
818 transfer is localized, showing a strong directionality to
819 sediment export in the form of a wide tidal channel. This

channel is clearly the origin point for the largest single channel on the slope (labeled 'TC' on Fig. 4C). However, backscatter data (Fig. 3D) do not suggest that active sedimentation is appreciably increased within this specific channel axis when compared to the many other channels visible surrounding the island. Future studies of platform top sedimentology are needed to fully understand the way that sediment export is affected by platform top elements.

Wind-related asymmetry extends to the slope as well—the leeward sides of carbonate platforms elsewhere have been established to have their morphology affected by off-platform sediment transport (e.g., Hine et al., 1981). Here, leeward sides are generally smoother, with fewer high-relief outcrops. This is interpreted to be a product of increased sedimentation, which would promote faster erosion of any volcanic highs or remnant sedimentary outcrops, and would infill depressions and low areas with sediment. Windward sides of platforms are sometimes more rugose than leeward sides. This can also be attributed to increased abundance of outcrops of underlying basement, as well as from steep-sided arcuate slope failures. Decreased windward sedimentation may lead to oversteepened, sediment-starved windward slopes, which are more prone to failure.

*5.3 Summary and facies model*

Although facies models allow for real-world deviation from an idealized scenario, the character and distribution of sedimentary facies seen here is significantly different from previously established models of carbonate slopes elsewhere. Past models have generally not focused on steep, volcanic-cored platforms, however, these settings are clearly responsible for the generation of substantial amounts of carbonate sediment, and have a unique set of depositional features when compared to those elsewhere. The geomorphology, depositional elements, and sedimentary processes seen in the Iles Eparses are synthesized in a facies model shown in Figure ~~12~~13.

In summary, sediment transfer to the deep sea in the Iles Eparses is a combination of processes at a variety of scales. Carbonate sediments on the platform top are transported onto the broad, steep upper slope through the action of wind- or tide-generated water movement, shallow currents, or density cascading (Fig. ~~12A~~13A). The slope becomes increasingly channelized basinward, with sediments moving down straight channel axes in gravity flows. ~~Sands~~ Carbonate grainstones-packstones are ultimately deposited in the lower slope or proximal basin in the form of gravity flow deposits (turbidites and debrites), including levee and overbank deposits, where they are interbedded with hemipelagic foraminiferal muds. These interbedded gravity flow deposits and background muds (and possibly basement volcanics) may move further

downslope together in the form of large-scale mass transport deposits that originate on the slope itself (Fig. ~~12B~~13B). MTDs may in turn be subsequently reworked as new channels incise into lower slope sedimentary deposits (Fig. ~~12C~~13C). Any given slope deposit may therefore be the result of multiple sedimentation processes, and a range of depositional elements resulting from several different processes may be present on the seafloor at any given time. Figure ~~12~~ 13 shows a composite sketch combining many of the observed geomorphologic and depositional features seen across platforms, and general characteristics are summarized in the chart in Table 3.

*5.4 Implications*

The synthesis of observed features and processes shown in Figure ~~12~~ 13 is one of the first detailed facies models for sedimentary deposition on the slopes of carbonate atolls and atoll-like carbonate platforms. It can be compared with similar block diagrams on other carbonate slopes (e.g. Betzler et al., 2014, Grammer and Ginsberg, 1992, Mulder et al., 2017, Mullins and Cook, 1986, Mullins et al., 1984, and Payros and Pujalte, 2008, among others). Although these are very different types of carbonate platforms from those discussed here, such a comparison is essential in determining which aspects of carbonate deposition are more universal, and highlights the differences between the settings discussed here and more 'traditional' carbonate platforms. In addition, facies on the

slopes of these platforms differ from those on other volcanic islands. The island of La Réunion (Indian Ocean), for example, is characterized by a steep-sided central volcanic cone rather than a flat, carbonate-dominated platform top. Facies models developed on the submarine slopes of La Réunion therefore lack the extensive carbonate deposits seen here, and are instead dominated by large-scale flank collapses, lava flow platforms and deltas, and volcaniclastic fan systems (Babonneau et al., 2011; Saint-Ange et al., 2013; Sisavath et al., 2011). Elsewhere, the flanks of Madeira Archipelago (a series of volcanic islands in the Atlantic Ocean) are also dominated by numerous large, arcuate slope failures, as well as numerous radial gully-channel systems more similar to those seen here (Quartau et al., 2018). These channels, however, often show a well-developed dendritic pattern in map view, and coalesce into longer, larger channels that extend much further from the islands than those in the Iles Eparses.

Of note in the Iles Eparses are the presence of clear, unambiguous channel systems with lobate basin-floor fans. This type of lobate fan system has rarely been described in other modern carbonate settings: Payros and Pujalte (2008) state that "Calciclastic submarine fans are rare in the stratigraphic record and no bona fide present-day analogue has been described to date." Mullins and Cook (1986) also note the paucity of unambiguous examples in the geologic record, and

James and Jones (2016) note that submarine fans do not typically form on carbonate slopes because of the linear, rather than point-sourced, nature of slope profiles. Terminal fans seen in the Iles Eparses are likely present because sediments are concentrated into relatively few active channels that reach the basin floor. Platform-derived sediment is distributed over a relatively small area, resulting in more focused distributary systems and promoting point-sourcing of deposition.

Although the deposits seen here are relatively recent in origin, the distribution and character of these sediments may be used as an analog for deposits elsewhere. Core taken on lower slopes almost always include some component of ~~coarse-grained~~ carbonate ~~sands~~grainstones-packstones, a facies with more potential as a conventional hydrocarbon reservoir than the periplatform muds that make up the majority of core in inter-channel areas, MTDs, and levees. Goldstein et al. (2012) note the difference in reservoir potential between dispersed- and focused-flow carbonate slope systems in the Miocene of Spain; the Iles Eparses deposits are more similar to the latter. These types of small isolated platforms therefore have a different reservoir potential and sediment distribution than other, larger platforms with more dispersed depositional systems. The higher reservoir potential of more concentrated focused-flow grainstones should be tempered by the overall smaller volume, smaller distribution radius, and lower preservation potential of

these types of settings; the geologic record of atolls and carbonate platforms atop deep sea volcanoes is relatively sparse.

## 6. Conclusions

The Iles Eparses atolls, islands, and platforms are situated on isolated deepwater volcanic pedestals in and around the Mozambique Channel, making them genetically different from other, more well-known carbonate settings. This study provides a first look into the nature of carbonate slope sedimentation in this unique, little-known depositional environment, and presents the first detailed facies model for the types of atoll and atoll-like platforms discussed here. Slope sediments are a product of a range of gravity-dominated depositional processes, including hemipelagic rain, slope failure and downslope mass transport, and gravity flows (turbidites and debrites). Inherited topography of the underlying volcanic pinnacles results in steep upper slope gradients where little sedimentation takes place and arcuate slope failure scars are locally common. Platform-derived carbonates may be channelized in the lower slope, forming, in places, relatively straight channel systems that extend for tens of kilometers and may terminate in basin-floor ~~fans~~lobes, a relatively rare occurrence in modern-day carbonate settings. Elsewhere on the lower slope, turbidites and mass transport deposits are present, with the subsurface seismic facies often taking the form of chaotic units interpreted as

debris flows. Depositional thrusting and associated pressure ridges are also present in some lower slope deposits. Slopes are usually asymmetric with respect to predominant wind direction, with leeward slopes usually having a lower rugosity than windward slopes and more spatially extensive toe-of-slope deposition. The lack of data in settings analogous to the Iles Eparses underscores the need for further research, and shows the importance of the observations reported here in expanding the known spectrum of depositional carbonate depositional environments.

## 7. Acknowledgements

The oceanographic expeditions PTOLEMEE, PAMELA-MOZ1 and PAMELA-MOZ4 and Elda Miramontes' fellowship were co-funded by TOTAL and IFREMER as part of the PAMELA (Passive Margin Exploration Laboratory) scientific project. This work was supported by the "Laboratoire d'Excellence" LabexMER (ANR-10-LABX-19) and co-funded by a grant from the French government under the program "Investissements d'Avenir". Thanks to Joseph Ronzier for writing and executing the Python script used in calculating slope rugosity. Thanks to Simon Courgeon ~~and Joseph Ronzier~~ for additional data contributions and helpful discussions related to this project, Sandrine Cheron and Audrey Boissier for XRD analysis, and Nicolas Gayet for SEM assistance. We also thank

993 the captains and crews of the RVs *Atalante* and *Pourquoi Pas?*
994 during the cruises where this data was collected.
995
996

997 **Figure Captions**

998 *Table 1*: General dimensions and associated volumes of
999 selected slope failure scars on Juan de Nova. Wedge diagram
1000 shows conceptual method of volumetric calculation.

1001 *Table 2*: Interpreted seismic facies found in lower slopes and
1002 proximal basins. Interpretations are based on the amplitude,
1003 orientation, and bounding relationships of seismic reflectors
1004 within seismic units.

1005 *Table 3*: Chart summarizing scale and character of selected
1006 depositional elements observed in this study.

1007 *Figure 1*: A) Location map of platforms and other geographic
1008 and geologic features mentioned in this paper. Oceanic
1009 circulation from Brietzke et al. (2017). COM-Comoros Islands;
1010 MAY-Mayotte Island; GLO- Glorieuses Islands; JDN-Juan de
1011 Nova; DR-Davie Ridge; ZV-Zambezi Valley ; BDI-Bassas da
1012 India; EUR-Europa. B) Present-day dominant wind directions
1013 from Metéo France, sourced from over 5000 individual
1014 measurements from weather stations on the islands. Bassas da
1015 India has no weather station, but is situated close enough to Ile
1016 Europa that wind directions are not appreciably different (see
1017 location in Figure 1A).

1018 *Figure 2*: Detailed bathymetric and backscatter maps of slopes
1019 of Iles Eparses platforms Glorieuses (A, B) and Juan de Nova
1020 (C, D). Bathymetric maps are an overlaid combination of
1021 absolute seafloor depth (color) and slope gradient (greyscale),

allowing both the slope relief and seafloor topography to be seen. Reflectivity maps use an arbitrary, sliding-scale color bar to best differentiate sedimentological and geomorphologic features. GG-Grande Glorieuse Island.

*Figure 3*: Detailed bathymetric and backscatter/reflectivity maps of slopes of Iles Eparses platforms Bassas da India and Europa. Same parameters as Figure 2. A, B) Bassas da India; C, D) Europa, TC-tidal channel.

*Figure 4*: Three-dimensional views of submarine platform slopes, focusing on slope morphology. Color gradient adjusted for each platform. A) Southeast-looking view of Glorieuses, showing the platform top, Glorieuses terrace and the linear escarpment most prominent on the northwestern side (magnified view in inset). B) Northward-looking view of Bassas da India, showing large submarine terrace and its profile and associated features, notably sand dunes and gullies found on the terrace surface in 350-600 meters water depth (insets). C) Southeastern-looking view of Europa, showing strike and dip profiles and location of seismic line in Figure 4D. Channel floor visible in both bathymetric and seismic data marked with an asterisk. Also of note is the steep, smooth upper slope surface, visible here on the leeward side of the platform. D) Europa seismic line 076 (PTO-mig076_v1500_g0). This line shows the relatively thin nature of sedimentary deposits in the

mid-slope, the seismic character of the volcanic basement, and the higher-amplitude reflections in channel floors.

*Figure 5*: A-B): Evidence of slope failure on Juan de Nova; A) Leeward slope, showing generally smooth upper slope surface and two large arcuate scarps, denoted 1 and 2 in Figure 5D. B) Windward slope, with several discrete scarps highlighted (numbers 3-6). Approximate volumetric calculations for each numbered scarp shown in Table 1. C) Quantitative rugosity analysis of Juan de Nova upper slope. 1st part shows conceptual method of quantification, second part applies the same method to the 600-m contour on Juan de Nova platform. On Juan de Nova, the windward side of the platform is significantly more rugose than the windward side.

*Figure 6*: Examples of slope failure and/or erosion on Bassas da India and Europa, with along-strike profiles and dimensions.

*Figure ~~6~~7*: A) Seismic line 079 (PTO-mig079_v1500_g0), taken along the leeward side of Europa, showing sedimentary nature of the lower slope ~~wedge~~. The line is an oblique dip line, crossing channels and levees seen in Figures 8D and 8E, and clearly showing their contact with the underlying basement. B-D) Bathymetric profiles for the windward and leeward slopes of platforms. Bassas da India not included due to lack of data coverage on the windward side. Note extended lower slope on each leeward side; windward slopes often have a steeper descent to the basin floor.

*Figure ~~7~~8*: Core data from the lower slopes and proximal basins of Iles Eparses. Exact locations of core shown in Figure 2. A-D) Lithologies and core photos from four seafloor piston cores. Core MOZ4-CS23 (D) contains an additional 23 meters above the selected section that is almost entirely composed of background foraminiferal ~~muds~~ooze. (A) taken at 3089 m; (B) 3167 m; (C) 1909 m; (D) 2852 m. E) Grain-size profiles of the carbonate ~~sand~~ grainstone-packstone beds marked in red in above logs. F) Compositional data for selected intervals within carbonate ~~sand~~ grainstone-packstone beds. Locations denoted in A-D. Data shown only includes identifiable grains; unidentified grains constitute 30-40% of total grains observed. G) SEM images of carbonate ~~sands~~ grainstones in core MOZ1-KS04, interval 649-650 m, at the base of a relatively thick carbonate sand unit. Abbreviations: BF-benthic foraminifer; CA-calcareous algae; Ec-echinoid; Fo-Foraminifer; Ga-gastropod; PF-planktonic foraminifer. H) Analysis of muds/foraminiferal oozes; left side: SEM images; AN-aragonite needles; CM-clay minerals; Co-Coccolith. Right side: EDS spectra and XRD mineralogy of selected intervals.

*Figure ~~8~~9*: Examples of channels and channel-related features on Iles Eparses slopes. A) Reflectivity map of northeastern side of Glorieuses, showing numerous sub-parallel active channels that do not terminate in lob~~at~~e ~~fan~~ structures. B) and C) are overlays of reflectivity and slope data; B) Northwestern side of

Bassas da India, showing bifurcating channels, some of which terminate in a lobe~~cate fan~~. Image is an overlay of reflectivity and slope data. C) Northern side of Europa. Inactive channel crossed by seismic lines in D and E is outlined with dashed line. Other, active channels have higher backscatter values and fan outward at the slope base. D) Seismic strike line on the north side of Europa showing channel-levee complex. Note levee transparency, higher-amplitude asymmetric overbank deposits, and central channel. E) Interpretation of (D)

*Figure ~~9~~10*: Lower slope seismic lines and interpretations. Description of seismic facies in text and in Table 2. Exact locations of lines shown in Figures 2 and 3. A) Bassas da India line 017 (PTO-mig017_v1500). B) Interpretation of seismic line above in (A). ~~B~~C) Juan de Nova line 234 (PTO-mig234_v1500_g0). D) Interpretation of seismic line above in (C). Colors delineate individual stratigraphic units, similar colors denote related units.

*Figure 11*: Lower slope seismic lines and interpretations, continued. ~~C~~A) Glorieuses Line 315 (mig315_v1500_g0). B) Interpretation of seismic line above in (A).

*Figure 12*: ~~D)~~ Glorieuses Line 319 (mig319_v1500_g0) and notes on interpretation.

~~*Figure 10*: A), B), C), Interpretations of the corresponding seismic lines in Figure 9A-9C. Colors delineate individual stratigraphic units, similar colors denote related units.~~

*Figure ~~11~~13*: A-C) Simplified diagram of sedimentation processes observed in core, seafloor bathymetry, and seismic data. A) Turbidite deposition resulting in interbedded carbonate ~~sands~~ grainstone-packstones and seafloor muds B) Upper-middle slope failure, remobilizing previously deposited sediments (potentially including parts of the lithified platform) and redistributing them to the lower parts of the slope in the form of MTDs. C) Further deposition of carbonate ~~sands~~ grainstones-packstones in turbidites. Channelized deposits may erode into past MTDs and rework previously deposited material. D) Facies model that summarizes depositional elements and sedimentation processes in the Iles Eparses. Figure represents a synthesis of data from bathymetric, reflectivity, and seismic surveys of multiple platforms. Schematic only; not to scale.

## References


Alfaro, E., Holz, M., 2014. Seismic geomorphological analysis of deepwater gravity-driven deposits on a slope system of the southern Colombian Caribbean margin. Marine and Petroleum Geology 57, 294-311.

Alsop, G.I., Marco, S., Levi, T., Weinberger, R., 2017. Fold and thrust systems in Mass Transport Deposits. Journal of Structural Geology, 94, 98-115.

Amblas, D., Ceramicola, S., Gerber, T.P., Canals, M., Chiocci, F.L., Dowdeswell, J.A., Harris, P.T., Huvenne, V.A., Lai, S.Y., Lastras, G. and Iacono, C.L., Micalle, A., Mountjoy, J.J., Paull, C.K., Puig, P., and Sanchez-Vidal, A. 2018. Submarine canyons and gullies. In: Micallef, A., Krastel S., and Savini A. (eds) Submarine Geomorphology. 251-272, Springer Geology. Springer, Cham.

Babonneau, N., Delacourt, C., Cancouët, R., Sisavath, E., Bachèlery, P., Mazuel, A., Jorry, S.J., Deschamps, A., Ammann, J. and Villeneuve, N., 2013. Direct sediment transfer from land to deep-sea: Insights into shallow multibeam bathymetry at La Réunion Island. Marine Geology, 346, 47-57.

Bassias, Y., Roberts, G., Christoffersen, T., 2016. The nature of the crust offshore East Coast Africa When geology and seismic

meet potential fields in the search for hydrocarbons. East Africa: From Research to Reserves, Extended Abstract, The Geological Society of London 13-15 April 2016, 1-12.

Battistini, R., Cremers, G., 1972. Geomorphology and vegetation of Iles Glorieuses. Smithsonian Institution. Atoll Research Bulletin 159, 27 p.

Battistini, R., Gayet, J., Jouannic, C., Labracherie, M., Peypouquet, J.P., Pujol, C., Pujos-Lamy, A., Turon, J.L., 1976. Etude des sédiments et la microfaune des îles Glorieuses (Canal de Mozambique). Cahiers ORSTOM, Série Géologie 8, 147-171.

Benn, D., Evans, D.J., 2014. Glaciers and glaciation. Routledge, 816 p.

Berthois L., Battistini, R., 1969, Etude Sedimentologique de L'Ile Europa, Madagascar Revue de Geographie 15, 1-52.

Betzler, C., Lindhorst, S., Eberli, G. P., Lüdmann, T., Möbius, J., Ludwig, J., Schutter, I., Wunsch, M., Reijmer, J., Hübscher, C., 2014. Periplatform drift: the combined result of contour current and off-bank transport along carbonate platforms. Geology 42, 871-874.

Betzler, C., Hübscher, C., Lindhorst, S., Lüdmann, T., Reijmer, J.J. and Braga, J.C., 2016. Lowstand wedges in carbonate platform slopes (Quaternary, Maldives, Indian Ocean). The Depositional Record, 2, pp.196-207.

Blomeier, D.P.G., Reijmer, J. J., 2002. Facies architecture of an Early Jurassic carbonate platform slope (Jbel Bou Dahar, High Atlas, Morocco). Journal of Sedimentary Research 72, 462-475.

Breitzke, M., Wiles, E., Krocker, R., Watkeys, M.K., Jokat, W., 2017. Seafloor morphology in the Mozambique Channel: evidence for long-term persistent bottom-current flow and deep-reaching eddy activity. Marine Geophysical Research 38, 241-269.

Carter, L., 2001. A large submarine debris flow in the path of the Pacific deep western boundary current off New Zealand. Geo-Marine Letters, 21, 42-50

Clark, J.D., Kenyon, N.H., Pickering, K.T., 1992. Quantitative analysis of the geometry of submarine channels: implications for the classification of submarine fans. Geology, 20, 633-636.

Clarke, J.E.H., Mayer, L.A. and Wells, D.E., 1996. Shallow-water imaging multibeam sonars: a new tool for investigating

seafloor processes in the coastal zone and on the continental shelf. Marine Geophysical Researches, 18, 607-629.

Courgeon, S., Jorry, S.J., Camoin, G.F., BouDagher-Fadel, M.K., Jouet, G., Révillon, S., Bachèlery, P., Pelleter, E., Borgomano, J., Poli, E., Droxler, A.W., 2016. Growth and demise of Cenozoic isolated carbonate platforms: New insights from the Mozambique Channel seamounts (SW Indian Ocean). Marine Geology 380, 90-105.

Courgeon, S., Jorry, S.J., Jouet, G., Camoin, G., BouDagher-Fadel, M.K., Bachèlery, P., Caline, B., Boichard, R., Révillon, S., Thomas, Y. Thereau, E., 2017. Impact of tectonic and volcanism on the Neogene evolution of isolated carbonate platforms (SW Indian Ocean). Sedimentary Geology 355, 114-131.

Covault, J.A., Kostic, S., Paull, C.K., Sylvester, Z., Fildani, A., 2017. Cyclic steps and related supercritical bedforms: building blocks of deep-water depositional systems, western North America. Marine Geology, 393, 4-20.

Dartnell, P., Gardner, J.V., 2004. Predicting seafloor facies from multibeam bathymetry and backscatter data. Photogrammetric Engineering & Remote Sensing 70, 1081-1091.

Deutscher Wetterdienst, 2018, Klimatafel von Juan de Nova (Insel), Iles Desirades / Indischer Ozean / Frankreich https://www.dwd.de/DWD/klima/beratung/ak/ak_619700_kt.pdf. Retrieved June 20, 2018.

Dravis, J.J., Wanless, H.R., 2017. Impact of strong easterly trade winds on carbonate petroleum exploration-Relationships developed from Caicos Platform, southeastern Bahamas. Marine and Petroleum Geology 85, 272-300.

Dunbar, G.B. and Dickens, G.R., 2003. Late Quaternary shedding of shallow-marine carbonate along a tropical mixed siliciclastic–carbonate shelf: Great Barrier Reef, Australia. Sedimentology, 50, 1061-1077.

Förster, R., 1975. The geological history of the sedimentary basin of southern Mozambique, and some aspects of the origin of the Mozambique Channel. Palaeogeography, Palaeoclimatology, Palaeoecology 17, 267-287.

Frey Martinez, J., Cartwright, J., Hall, B., 2005. 3D seismic interpretation of slump complexes: examples from the continental margin of Israel. Basin Research, 17, 83-108.

Gervais, A., Savoye, B., Mulder, T., Gonthier, E., 2006. Sandy modern turbidite lobes: a new insight from high resolution seismic data. Marine and Petroleum Geology, 23, 485-502.

1247 Gischler, E., 2011. Sedimentary facies of Bora Bora, Darwin's
1248 type barrier reef (Society Islands, South Pacific): the
1249 unexpected occurrence of non-skeletal grains. Journal of
1250 Sedimentary Research, 81,.1-17.

1251 Goldstein, R.H., Franseen, E.K., Dvoretsky, R.A., Sweeney,
1252 R.J., 2012. Controls on focused-flow and dispersed-flow
1253 deepwater carbonates: Miocene Agua Amarga Basin, Spain.
1254 Journal of Sedimentary Research 82, 499-520.

1255 Grammer, G.M., Ginsburg, R.N., 1992. Highstand versus
1256 lowstand deposition on carbonate platform margins: insight
1257 from Quaternary foreslopes in the Bahamas. Marine Geology
1258 103, 125-136.

1259 Guillaume, M.M., Reyss, J.L., Pirazzoli, P.A., Bruggemann,
1260 J.H., 2013. Tectonic stability since the last interglacial offsets
1261 the Glorieuses Islands from the nearby Comoros archipelago.
1262 Coral Reefs 32, 719-726.

1263 Hampton, M., and Lee, H., 1996. Submarine Landslides,
1264 Reviews of Geophysics 34, 33-59.

1265 Harris, D.L., Webster, J.M., De Carli, E.V., Vila-Concejo, A.,
1266 2011. Geomorphology and morphodynamics of a sand apron,
1267 One Tree reef, southern Great Barrier Reef. Journal of Coastal
1268 Research, 64, 760.

1269 Hay W.W., 2014. Submarine Canyons. In: Harff J., Meschede
1270 M., Petersen S., Thiede J. (eds) Encyclopedia of Marine
1271 Geosciences. Springer, Dordrecht.

1272 Hine, A.C., Locker, S.D., Tedesco, L.P., Mullins, H.T.,
1273 Hallock, P., Belknap, D.F., Gonzales, J.L., Neumann, A.C.,
1274 Snyder, S.W., 1992. Megabreccia shedding from modern, low-
1275 relief carbonate platforms, Nicaraguan Rise. GSA Bulletin,
1276 104, 928-943.

1277 Hühnerbach, V. and Masson, D.G., 2004. Landslides in the
1278 North Atlantic and its adjacent seas: an analysis of their
1279 morphology, setting and behaviour. Marine Geology, 213, 343-
1280 362.

1281 James, N. P., Jones, B., 2016. Origin of Carbonate Sedimentary
1282 Rocks. John Wiley & Sons. 320 p.

1283 Janson, X., Kerans, C., Loucks, R., Marhx, M.A., Reyes, C.
1284 and Murguia, F., 2011. Seismic architecture of a Lower
1285 Cretaceous platform-to-slope system, Santa Agueda and Poza
1286 Rica fields, Mexico. AAPG bulletin, 95, 105-146.

1287 Joanne, C., Lamarche, G., Collot, J.Y., 2013. Dynamics of
1288 giant mass transport in deep submarine environments: the
1289 Matakaoa Debris Flow, New Zealand. Basin Research, 25, 471-
1290 488.

1291 Johnston, S.T., Thorkelson, D.J., 2000. Continental flood
1292 basalts: episodic magmatism above long-lived hotspots. Earth
1293 and Planetary Science Letters, 175, 247-256.

1294 Jorry, S., 2014. PTOLEMEE cruise, RV L'Atalante.
1295 http://dx.doi.org/10.17600/14000900

1296 Jorry, S.J., Camoin, G.F., Jouet, G., Le Roy, P., Vella, C.,
1297 Courgeon, S., Prat S., Fontanier C., Paumard V., Boulle J.,
1298 Caline B., Borgomano, J., 2016. Modern sediments and
1299 Pleistocene reefs from isolated carbonate platforms (Iles
1300 Eparses, SW Indian Ocean): A preliminary study. Acta
1301 Oecologica, 72, 129-143.

1302 Jouet, G., Deville, E., 2015. PAMELA-MOZ04 cruise, RV
1303 Pourquoi Pas ?. http://dx.doi.org/10.17600/15000700

1304 Kolla, V., Henderson, L. and Biscaye, P.E., 1976. Clay
1305 mineralogy and sedimentation in the western Indian Ocean.
1306 Deep Sea Research and Oceanographic Abstracts 23, 949-961.

1307 Lort, J.M., Limond, W.Q., Segoufin, J., Patriat, P., Delteil, J.R.,
1308 Damotte, B., 1979. New seismic data in the Mozambique
1309 Channel. Marine Geophysical Research, 4, 71-89.

1310 Lowe, D.R., 1982. Sediment gravity flows: II Depositional
1311 models with special reference to the deposits of high-density

turbidity currents. Journal of Sedimentary Research, 52, 279-297.

McGonigle, C. and Collier, J.S., 2014. Interlinking backscatter, grain size and benthic community structure. Estuarine, Coastal and Shelf Science, 147, 123-136.

McIlreath, I.A., James, N.P., 1978. Facies models 13. Carbonate slopes. Geoscience Canada, 5, 189-199.

Météo France, 2017. https://publitheque.meteo.fr/Donnees/DESC170531171564028 9.KEYu07f7D3UO9xudD2U2fU9.html 1/2

Milliman, J.D., Freile, D., Steinen, R.P. and Wilber, R.J., 1993. Great Bahama Bank aragonitic muds: mostly inorganically precipitated, mostly exported. Journal of Sedimentary Research, 63, 589-595.

Moscardelli, L., Wood, L., Mann, P., 2006. Mass-transport complexes and associated processes in the offshore area of Trinidad and Venezuela. AAPG Bulletin, 90, 1059-1088.

Mulder, T., Alexander, J., 2001. The physical character of subaqueous sedimentary density flows and their deposits. Sedimentology, 48, 269-299.

1332 Mulder, T. and Cochonat, P., 1996. Classification of offshore
1333 mass movements. Journal of Sedimentary Research, 66, 43-57.

1334 Mulder, T., Joumes, M., Hanquiez, V., Gillet, H., Reijmer,
1335 J.J.G., Tournadour, E., Chabaud, L., Principaud, M., Schnyder,
1336 J.S.D., Borgomano, J. Fauquembergue, K., 2017. Carbonate
1337 slope morphology revealing sediment transfer from bank-to-
1338 slope (Little Bahama Bank, Bahamas). Marine and Petroleum
1339 Geology, 83, 26-34.

1340 Mullins, H.T., Cook, H.E., 1986. Carbonate apron models:
1341 alternatives to the submarine fan model for paleoenvironmental
1342 analysis and hydrocarbon exploration. Sedimentary Geology,
1343 48, 37-79.

1344 Mullins, H.T., Heath, K.C., Buren, H., Newton, C.R., 1984.
1345 Anatomy of a modern open-ocean carbonate slope: northern
1346 Little Bahama Bank. Sedimentology, 31, 141-168.

1347 Olu, K., 2014. Rapport de fin de mission campagne Pamela-
1348 MOZ01. http://dx.doi.org/10.17600/14001000

1349 Payros, A., Pujalte, V., 2008. Calciclastic submarine fans: An
1350 integrated overview. Earth-Science Reviews, 86, 203-246.

1351 Pickering, K., Stow, D., Watson, M. and Hiscott, R., 1986.
1352 Deep-water facies, processes and models: a review and

1353 classification scheme for modern and ancient sediments. Earth-
1354 Science Reviews, 23, 75-174.

1355 Posamentier, H.W. and Kolla, V., 2003. Seismic
1356 geomorphology and stratigraphy of depositional elements in
1357 deep-water settings. Journal of Sedimentary Research, 73, 367-
1358 388.

1359 Posamentier, H.W., Martinsen, O.J. and Shipp, R.C., 2011. The
1360 character and genesis of submarine mass-transport deposits:
1361 insights from outcrop and 3D seismic data. In: Shipp, R.C.,
1362 Weimer, P., and Posamentier, H.W. (eds.), Mass-transport
1363 deposits in deepwater settings: Society for Sedimentary
1364 Geology (SEPM) Special Publication 96, 7-38.

1365 Prat, S., Jorry, S.J., Jouet, G., Camoin, G., Vella, C., Le Roy,
1366 P., Caline, B., Boichard, R., Pastol, Y., 2016. Geomorphology
1367 and sedimentology of a modern isolated carbonate platform:
1368 The Glorieuses archipelago, SW Indian Ocean. Marine
1369 Geology, 380, 272-283.

1370 Principaud, M., Mulder, T., Gillet, H. and Borgomano, J., 2015.
1371 Large-scale carbonate submarine mass-wasting along the
1372 northwestern slope of the Great Bahama Bank (Bahamas):
1373 Morphology, architecture, and mechanisms. Sedimentary
1374 Geology, 317, 27-42.

Quartau, R., Ramalho, R.S., Madeira, J., Santos, R., Rodrigues, A., Roque, C., Carrara, G. and da Silveira, A.B., 2018. Gravitational, erosional and depositional processes on volcanic ocean islands: Insights from the submarine morphology of Madeira Archipelago. Earth and Planetary Science Letters, 482, 288-299.

Raharimahefa, T. and Kusky, T.M., 2010. Environmental monitoring of Bombetoka Bay and the Betsiboka Estuary, Madagascar, using multi-temporal satellite data. Journal of Earth Science, 21, 210-226.

Reijmer, J.J., Swart, P.K., Bauch, T., Otto, R., Reuning, L., Roth, S. and Zechel, S., 2009. A Re-Evaluation of Facies on Great Bahama Bank I: New Facies Maps of Western Great Bahama Bank (pp. 29-46). International Association of Sedimentologists Special Publication 41, 29-46.

Saint-Ange, F., Bachèlery, P., Babonneau, N., Michon, L. and Jorry, S.J., 2013. Volcaniclastic sedimentation on the submarine slopes of a basaltic hotspot volcano: Piton de la Fournaise volcano (La Réunion Island, Indian Ocean). Marine Geology, 337, 35-52.

1395 Schott, F.A., Xie, S.P., McCreary, J.P., 2009. Indian Ocean
1396 circulation and climate variability. Reviews of Geophysics, 47,
1397 1-46.

1398 Shanmugam, G., 2000. 50 years of the turbidite paradigm
1399 (1950s—1990s): deep-water processes and facies models—a
1400 critical perspective. Marine and Petroleum Geology, 17, 285-
1401 342.

1402 Simpson, E.S.W., Schlich, R., Gieskes, J.M., Arch Girdley, W.,
1403 Leclaire, L., Marshall, B.V., Moore, C., Müller, C., Sigal, J.,
1404 Vallier, T.L., White, S.M., Zobel, B., 1974. Initial Reports of
1405 the Deep Sea Drilling Project, Sites 240-242, Volume 25,
1406 Washington (U.S. Government Printing Office) p. 65-176.

1407 Sisavath, E., Babonneau, N., Saint-Ange, F., Bachèlery, P.,
1408 Jorry, S.J., Deplus, C., De Voogd, B. and Savoye, B., 2011.
1409 Morphology and sedimentary architecture of a modern
1410 volcaniclastic turbidite system: The Cilaos fan, offshore La
1411 Réunion Island. Marine Geology, 288, 1-17.

1412 Talling, P.J., Masson, D.G., Sumner, E.J., Malgesini, G., 2012.
1413 Subaqueous sediment density flows: depositional processes and
1414 deposit types. Sedimentology, 59, 1937-2003.

1415 Tcherepanov, E.N., Droxler, A.W., Lapointe, P. and Mohn, K.,
1416 2008. Carbonate seismic stratigraphy of the Gulf of Papua

mixed depositional system: Neogene stratigraphic signature and eustatic control. Basin Research, 20, 185-209.

Testut, L., Duvat, V., Ballu, V., Fernandes, R.M., Pouget, F., Salmon, C., Dyment, J., 2016. Shoreline changes in a rising sea level context: The example of Grande Glorieuse, Scattered Islands, Western Indian Ocean. Acta Oecologica, 72, 110-119.

Van Sebille, E., Scussolini, P., Durgadoo, J.V., Peeters, F.J., Biastoch, A., Weijer, W., Turney, C., Paris, C.B. and Zahn, R., 2015. Ocean currents generate large footprints in marine palaeoclimate proxies. Nature Communications, 6, 6521.

Wiles, E., Green, A.N., Watkeys, M.K. and Jokat, W., 2017. Zambezi continental margin: compartmentalized sediment transfer routes to the abyssal Mozambique Channel. Marine Geophysical Research, 38, 227-240.

Wilson, P.A. and Roberts, H.H., 1995. Density cascading: off-shelf sediment transport, evidence and implications, Bahama Banks. Journal of Sedimentary Research, 65, 45-56.

Yamano, H., Cabioch, G., Pelletier, B., Chevillon, C., Tachikawa, H., Lefèvre, J. and Marchesiello, P., 2015. Modern carbonate sedimentary facies on the outer shelf and slope around New Caledonia. Island Arc, 24, 4-15.

1438

Highlights:

- First study to describe the slopes of volcano-cored carbonate platforms in detail
- Slope sediments composed of muds and platform-derived carbonate sands
- Slopes contain channels, fans, and mass transport deposits
- Sedimentation is primarily controlled by inherited topography and dominant winds
- Excellent example of complete source-to-sink sedimentary system

# Sedimentation adjacent to atolls and volcano-cored carbonate platforms in the Mozambique Channel (SW Indian Ocean)

John W. COUNTS* (*John.Counts@ifremer.fr* [a]

Stephan J. JORRY (*Stephan.Jorry@ifremer.fr)*[a]

Estelle LEROUX (*Estelle.Leroux@ifremer.fr)*[a]

Elda MIRAMONTES (*Elda.Miramontesgarcia@univ-brest.fr)*[b]

Gwenael JOUET (*Gwenael.Jouet@ifremer.fr)*[a]

**Corresponding author*

[a]*Laboratoire Géodynamique et Enregistrement Sédimentaire (GM-LGS) – Institut Français de Recherche pour l'Exploitation de la Mer (IFREMER) – Pointe du Diable, 29280 Plouzané, France*

[b]*CNRS, UMR6538, Laboratoire Géosciences Océan, Institute Universitaire Européen de la Mer - Université de Bretagne Occidentale (IUEM-UBO), 29280 Plouzané, France.*

**Abstract**

*Recently acquired data from the Iles Eparses (southwestern Indian Ocean) reveal new information about the geomorphology, depositional processes, and sedimentary deposits on the slopes of atolls and atoll-like platforms. The deposits discussed here lie on the deepwater flanks of isolated, inactive volcanos that are capped by shallow, relatively flat carbonate platforms 45-210 km$^2$ in area. Much of the slope geomorphology is controlled by the underlying volcanic edifice. Steep (~25-35°) upper slopes consist of outcrops of volcanic basement, smooth banks, failure scarps, and channels. Sedimentary features seen in the lower slope and proximal basin (2000-3500 m deep) consist of channels, levees, lobes, and mass transport deposits (MTDs). In places, channels terminate 13-18 km from the platform margin, ending in lobes up to 3.5 km across, a feature not often seen in modern carbonates. In the subsurface, MTDs are present near all platforms. Within MTDs, seismic character is variable, often consists of chaotic reflections indicative of sediment gravity flow processes. Subsurface units with organized (retro- or progradational) reflections are interpreted as turbidite lobes or MTDs with compressional features. Core taken within lobes and near the base of slopes reveal decimeter-scale turbidites and debrites composed primarily of graded and massive bioclastic grainstones and packstones with abundant neritic*

*skeletal components, interbedded with hemipelagic aragonitic and clay-rich foraminiferal ooze. Slope depositional processes are therefore primarily gravity-driven and occur at different scales; i.e., bed-scale turbidites and muds may be remobilized and redeposited through slope failure and deposition of large MTDs. Dominant wind direction may also play a role in slope sedimentation: leeward slopes are generally less rugose and show increased sedimentation at the toe of the slope. This study thus provides new insight into depositional systems surrounding atoll-like carbonate platforms, and provides a new analogue for similar deposits in the geologic record.*

**Keywords**: atoll; carbonate; Indian Ocean; slope; deepwater sediments

## 1. Introduction

Sediments on carbonate slopes are well-represented in the ancient geologic record (Blomeier and Reijmer, 2002, and references therein), and are an important component of carbonate depositional systems. However, a detailed, actualistic understanding of these environments in modern settings was hampered for many years by the inaccessibility of deepwater deposits in modern oceans (McIlreath and James, 1978), and much work remains to be done. Although many studies have documented the shallow-water portions of modern carbonate platforms and coral atolls (e.g., Reijmer et al., 2009; Gischler, 2011; Harris et al., 2011), most existing research on

74 modern deepwater allochthonous carbonates (distinguished
75 here as those predominantly transported into the deep sea from
76 elsewhere, as opposed to cold-water carbonate muds and
77 buildups precipitated *in situ*) has focused on a limited number
78 of well-known settings (e.g., the Caribbean). Although more
79 recent studies have expanded research into new areas (e.g., the
80 Maldives, Papua New Guinea, NE Australia, and New
81 Caledonia; Betzler et al., 2016; Tcherepanov et al., 2008;
82 Dunbar and Dickens, 2000; Yamano et al., 2015, respectively),
83 relatively few studies have been conducted in the southern
84 Indian Ocean. More studies in new areas and in different geo-
85 environmental settings are required in order to understand the
86 full range of carbonate slope sedimentation around the world.
87 This study examines the submarine slopes of four
88 isolated, volcano-cored atolls and atoll-like carbonate platforms
89 in the southern Indian Ocean (Fig. 1) with the goal of
90 improving our understanding of the depositional processes and
91 products operating on their slopes and nearby basin floors. The
92 deposits formed when carbonate sediments are transferred,
93 deposited, and remobilized on the platform slopes are the focus
94 of this paper, as well as the mechanisms responsible for such
95 deposits. By using seismic, bathymetric, and core data, this
96 study reveals new information about the geomorphology and
97 sedimentology of these unique depositional settings. Because of
98 their relatively small size (on a scale of tens of kilometers), the

entire sedimentary system of each platform can be examined as a whole, forming a complete source-to-sink picture of sedimentation. This information is used to create a new, unique facies model for the type of atoll-like carbonate platforms discussed here, which are lacking in the geological literature, and provides a point of comparison to other, genetically different carbonate systems elsewhere.

## 2. Regional Setting

The islands that are the focus of this study (Grande Glorieuse, Europa, Juan de Nova, and Bassas da India) lie within and around the modern Mozambique Channel (MC), an elongate basin in the Indian Ocean between the African continent and the island of Madagascar (Fig. 1). Together, these islands and the waters surrounding them are known as the Iles Eparses, and are part of the French Southern and Antarctic Lands. Islands are the subaerial portions of carbonate platforms that sit atop volcanic pinnacles originating from the basin floor. Platform tops are relatively flat and composed entirely of carbonate; there is no central volcanic peak. All are circular/equant in map view, except for Glorieuses, which has a roughly triangular shape.

The detailed origins and tectonic histories of each of these structures are not well-studied, but the emergence of all platforms is a result of the interplay between tectonic uplift and subsidence, extrusive volcanic growth, eustasy, and the rate of

carbonate aggradation, all of which vary between platforms (Courgeon et al., 2016). Platforms are of different ages and genetic origins and may be related to localized hotspot chains or mantle plumes. The Glorieuses Archipelago (Fig. 2A, 2B) is at minimum Paleocene in age and is a part of a linear ridge of volcanoes that also encompasses the nearby Comoros (Courgeon et al., 2016). It shows no indication of any significant drowning events during its lifespan, and has been interpreted to now be tectonically stable (with a very slow uplift of ~0.012 mm/year since ~130 ka) owing to its position away from the Somalia-Nubian plate boundary (Guillaume et al., 2013). Juan de Nova (Fig. 2C, 2D) has been studied very little; however, it likely has a granite core (Förster, 1975) and is not currently undergoing any notable uplift or subsidence (Testut et al., 2016). Bassas da India (Fig. 3A, 3B) and Europa (Fig. 3C. 3D) have been hypothesized to be related to the Quathlamba hotspot, which formed the archipelago up to 60 Mya and is currently under Lesotho (Johnston and Thorkelson, 2000). Bassas da India specifically has also been shown to have originated in the late Oligocene/early Miocene, and has been volcanically active as late as the early Pleistocene (Courgeon et al., 2017). Large-scale faulting, structural deformation, and volcanism in Bassas da India and associated submarine banks have been tied to a southern extension of the East African Rift system (Courgeon et al., 2016).

149 Carbonate deposition in the Iles Eparses began between
150 the Paleocene and Early Miocene, and continues until the
151 present day (Courgeon et al., 2016; 2017). Sediment production
152 was periodically interrupted by episodes of volcanism and
153 subaerial exposure, which occurred during relative sea-level
154 lowstands and resulted in karstification of the platform top.
155 Platform top sediments are generally poorly understood; the
156 sedimentology of Ile Europa was first examined from a
157 geological perspective in the 1960s (Berthois and Battistini,
158 1969) and on Glorieuses in the 1970s (Battistini and Cremers,
159 1972; Battistini et al., 1976). These preliminary studies noted
160 the carbonate sediment composition and basic facies
161 asymmetry of platform tops, as well as the existence of paleo-
162 reefs. Sediment atop the Glorieuses platform has been shown
163 by Prat et al. (2016) to be partitioned into five asymmetric
164 facies zones defined by hydrology, storm events, and the
165 distribution of carbonate producing organisms. Here, sediment
166 is remobilized by large sandwaves that ultimately likely
167 migrate off-platform, leading to a relatively continuous supply
168 of sand-sized sediment exported to the platform slope and
169 beyond. Similar asymmetric facies distributions and winnowing
170 processes can be inferred to be occurring on the tops of other
171 platforms as well (Jorry et al., 2016). Winds are predominantly
172 from the south on all islands except for Glorieuses, where they
173 are primarily from the east (Fig. 1E; Météo France, 2017).

Currents come from the east at Glorieuses, but are variable surrounding other islands due to the presence of anticyclonic eddies moving southward through the channel (Schott et al., 2009).

Most Iles Eparses platforms lack the defining features of atolls; i.e., a fringing reef and central lagoon. Only Bassas da India fits the definition; the other Iles Eparses are referred to here as 'atoll-like carbonate platforms' to distinguish them from both true atolls and from more traditionally defined carbonate platforms, e.g. the Bahamas. The tops of Glorieuses and Juan de Nova platforms (Fig. 2) contain small asymmetric vegetated islands, but are mostly submerged, whereas the top of Europa (Fig. 3C, 3D) is predominantly subaerial and contains a single large tidal channel surrounded by mangrove forest. Bassas da India does contain a continuous, circular, marginal reef exposed only at low tide, with a fully enclosed inner lagoon (Fig. 3A, 3B). Today, the exposed surface area of all the islands in question (totaling approximately 42 $km^2$) is significantly smaller than the predominantly subaqueous portions (around 500 $km^2$, generally ranging between of 0-40 m water depth). All platform tops are composed of carbonate sediment, with no volcanic outcrops or sediments visible, and subaerially exposed islands show evidence of recent karstification (Jorry et al., 2016).

## 3. Methodology and Data Set

Data used in this study were collected during three research cruises in the MC: PTOLEMEE (R/V *L'Atalante*; August/September 2014, Jorry, 2014), PAMELA-MOZ1 (R/V *L'Atalante*; September/October 2014, Olu, 2014), and PAMELA-MOZ4 (R/V *Pourquoi Pas?*; November/December 2015, Jouet and Deville, 2015). Dataset includes:

- High-resolution bathymetry and substrate backscatter/reflectivity measurements of the deep seafloor, using a Kongsberg EM122 multibeam echosounder
- Seismic acquisition with high-speed multichannel (high-resolution, airgun-sourced ) and CHIRP sub-bottom profiler (very high-resolution, swept-frequency source) methods
- Kullenberg and Calypso piston coring systems, used to acquire up to 27 continuous meters of seafloor sediment in >3000 m water depth

Depth conversions of seismic lines used a mean acoustic velocity of approximately 1700 meters/second, based on assumptions discussed in Lort et al. (1979) and DSDP Reports from the region (wells 240-242 show velocities from 1.5-1.9 km/s for the Oligocene; Simpson et al., 1974). This method provides a first approximation for sediment thickness when deep core control is not available.

A quantitative approximation of the rugosity (roughness) of the Juan de Nova slope was calculated by: 1) drawing the map-view representation of the -600-meter contour line, 2) measuring radii from a central point to the edge of the contour line, 3) subtracting a roughly circular shape to correct for overall shape of the platform, 4) assessing the standard deviations of corrected radii lengths. With this method, higher rugosity or roughness of the slope results in higher standard deviations. Measurement of several thousand radii was automated using a custom Python script. Standard deviations were then compared for the leeward vs windward sides of the platform to quantitatively measure slope rugosity.

Core sediments were initially described visually, and selected intervals were selected for further analysis. Grain size was measured with a Malvern Mastersizer 3000 laser diffraction particle size analyzer, capable of measuring all grains from 10 nm to 2 mm. Carbonate sand composition was determined by counting several hundred individual grains under a reflected light binocular microscope: samples were sieved and split into three size fractions above 63 μm, and results were combined to provide a bulk composition. Sediments, both muds (<63μm) and carbonate grainstones/packstones (dominant particle size >63 μm), were imaged and analyzed with a FEI Quanta 200 scanning electron microscope (SEM) equipped with an Oxford Instruments

Energy Dispersive Spectroscopy (EDS) detector. X-Ray diffraction (XRD) for mineralogy of muds was performed in-house using a Bruker AXS diffractometer.

## 4. Results

### *4.1 Geomorphologic elements*

#### *4.1.1 Platform tops and terraces*

Overall, platforms and their volcanic edifices have a conical morphology with a small, relatively flat top (Fig. 4). The volume of carbonate sediment that has accumulated atop each volcano is unknown; neither deep cores nor deep seismic have been acquired on the tops or upper slopes of the platforms. All investigations of platform tops (by dredging or coring), however, have only yielded carbonates. On Glorieuses and Bassas da India, the main platform tops are attached to deeper submarine terraces 700-750 and 400-500 m below sea level, respectively (Figs. 4A, 4B). The terrace on the northwestern side of Glorieuses is small (3.9 $km^2$; Fig. 4A), and lies between the main platform and a submarine volcanic pinnacle without a flat top (labeled 'T' in Fig. 2A). On Bassas da India, the submerged terrace is separated from the main platform by a large fault (Figs. 3A, 4B); previous studies (Courgeon et al., 2017) interpret the terrace as a product of Pliocene-Pleistocene fault movement. Volcanic rocks and small volcanic clasts within sediment have been found on the submarine terrace of Bassas da India.

273 *4.1.2 Smooth surfaces and basement outcrops*

274 All platform tops show a relatively sharp transition from
275 the shallow, flat top to a steep upper slope with a 25-35 degree
276 gradient (Fig. 4). These upper slope surfaces have the highest
277 overall gradient of anywhere between the platform top and the
278 adjacent abyssal plain, and are smoother than the mid-slope
279 below (Fig 4C). In general, the broad, smooth areas of upper
280 slopes are more contiguous on the leeward side of islands.
281 Seismic lines taken on the middle slope of Europa (Fig. 4D)
282 show that these areas likely contain only a thin veneer of
283 sedimentary cover. Smooth upper slopes may be interrupted,
284 however, by steep-sided (generally 30-50 degrees) outcrops of
285 basement (e.g., Fig. 4C). Basement outcrops are highly variable
286 in size, and in seismic are characterized by low- to variable-
287 amplitude reflections that differ from the overlying
288 sedimentation patterns (Fig. 4D). These outcrops are more
289 abundant slightly lower in the slope where the gradient
290 decreases to 12-20 degrees. Basement is likely composed of
291 volcanics, as previously interpreted by Lort et al., 1979, and
292 Bassias et al., 2016.

293 *4.1.3 Escarpments*

294 The smooth topography and gradient of upper slope
295 surfaces may also be broken by escarpments and slope failure
296 scars. On the Glorieuses platform, a linear escarpment at a
297 water depth ranging between 700 and 850 meters is traceable

298 for approximately 70 km around the platform's perimeter (Fig.
299 4A and inset). This escarpment is most prominent on the
300 northwest side of the platform, and reaches around 120 meters
301 in height with a slope of 50-80 degrees. It lies at the same
302 bathymetric depth as the small terrace to the northwest of the
303 main platform. Similar long, well-developed linear escarpments
304 are not seen on other platform slopes.

305 *4.1.4 Slope failure scars*

306 Elsewhere, smaller, discrete scarps (c.f. Hampton and
307 Lee, 1996) are evident on several sites in the upper slope. On
308 Juan de Nova, multiple arcuate scarps 400-2000 m across incise
309 60-150 m into the upper slope surface (Fig. 5A-5B). At least 10
310 of these are present around the islands' perimeter, all of which
311 occur where the surrounding slope gradient ranges from 22°-
312 28°. Arcuate scarps, however, are not distributed evenly; they
313 are more abundant on the windward south side of the platform,
314 with the leeward side having a quantitatively smoother, lower
315 rugosity slope (Fig. 5C). The morphology of scarps are also
316 different—scarps on the leeward slope generally have less
317 relief, on the order of 50-60 meters as opposed to 100 meters or
318 more on windward sides. As a first approximation, the volume
319 of sediment once filling these scarps was calculated using a
320 series of three-dimensional wedges, based on the gradient
321 found above and below the scar in question (Table 1).
322 Individual scarp volumes range from approximately 1 to 10

323 $km^3$, with the caveat that true volumes are slightly smaller due
324 to their irregular shape (Fig. 5A, 5B), a factor not included in
325 the calculation. These small individual scarps are not present on
326 the slopes of other platforms; however, on Bassas da India a
327 scallop-shaped indentation on the platform top (4 km across;
328 see Fig. 6A) may also be the product of past slope failure on a
329 much larger scale. The slope just below this indentation is
330 highly rugose and is the source of channels that extend to the
331 basin floor. Large areas of erosion are also seen on the southern
332 side of Europa (Fig. 6B), but do not have the distinctive arcuate
333 morphology seen on Juan de Nova.
334 *4.1.5 Gullies and channels*
335 Below the smooth uppermost slopes (greater than 20°-
336 25°), mid-slope (from 20°-25° to 10°) and lower-slope (0-10°)
337 zones contain a series of basement outcrops, linear gullies, and
338 sedimentary deposits (Figs. 2 and 3). In the mid-slope, gullies
339 incise into the basement substrate (Fig 4D) and are separated by
340 volcanic outcrops, but are generally not deep or narrow enough
341 to be considered canyons, though the distinction is not based on
342 quantitative criteria (Hay, 2014). These gullies gradationally
343 transition into true channels as the slope decreases. In seismic,
344 channel floors can be seen to be composed of high-amplitude,
345 relatively continuous reflections up to ~85 m thick, but without
346 a distinct base (Fig. 4D). In map view, channels are generally
347 straight, with flat bottoms and walls generally between 40 and

100 m high (Fig. 4C), though this varies considerably. In lower slopes, channels may erode into sediments rather than basement. Further details of sedimentary deposits associated with channels and their geomorphologic elements are discussed below.

*4.2 Sediments of the slope and proximal basin*

*4.2.1 Distribution*

Most sediment in the Iles Eparses slopes accumulates in the lower slope, where the gradient is less than 10°. Seismic and bathymetric data reveal that lower slopes contain a wedge-shaped sedimentary package that extends to up to 30 kilometers from the platform top (Figs. 2, 3 and 7; seismic data showing sedimentary nature of lower slope sediments in Fig. 7A). These sediments are elevated relative to the generally flat basin floor (Figs. 2 and 3), and have a higher gradient (usually 3°-6°, vs. 0-3°). The change in slope gradient marks the slope base; sediments beyond this point are considered to be in the adjacent basin. Where bathymetric data is available around the entire slope perimeter, lower slopes can often be seen to have asymmetric distribution around the platform, with bathymetric highs occurring more prominently on leeward sides of at least some platforms (especially in Europa, Glorieuses, and Juan de Nova; see Figs. 2 and 3). Representative slope profiles on windward and leeward sides of the platforms are shown in Figure 7B-D. Although upper slopes may similar or steeper on

either side, in each instance the lower slope extends further from the platform top on the leeward side.

*4.2.2 Lithologies*

Cores acquired on lower platform slopes (locations in Figs. 2 and 3) reveal the character of sediments in the shallow subsurface. A selection of representative core is shown in Figure 8A-D, all of which consist predominantly of foraminiferal ooze interbedded with beds of unlithified carbonate grainstones, packstones, or wackestones. These coarser-grained carbonate beds make up a minor but significant proportion of core thicknesses, usually between <1 and 20%. The dominant grain size in these beds is generally fining-upward, with most constituent particles less than 0.5 mm (Fig. 8E), although many beds have a basal lag with coarser skeletal fragments. Carbonate sediments within these beds are unlithified and well-sorted, without clear sedimentary structures other than occasional horizontal laminae. The sand-sized component of coarser units (shown in blue in Fig. 8A-8D) is composed of 100% calcareous material, including many taxa normally found in the photic zone: coral and algal fragments, echinoid spines, and well-preserved gastropods (Figs. 8F, 8G). The tests of planktonic and benthic foraminifers also make up a significant portion of these sands (up to 35% of identifiable grains; Fig. 8F). Interbedded with these sediments are thicker beds of foraminiferal carbonate ooze. The clay-sized fraction of

these background micritic muds is not identifiable petrographically, however, SEM images (Fig. 8H) reveal the presence of needle-like crystals, as well as platy grains. EDS analysis (Fig. 8H) shows that intervals dominated by needle-like crystals are enriched in calcium and oxygen, suggesting a carbonate mineralogy, whereas those dominated by platy grains have elevated amounts of silicon, aluminum, and oxygen—all elements that are components of silicate minerals. To better understand the composition of this component of the mud, XRD analysis was performed on a sample from the same approximate interval (MOZ4-CS09, 100-102 cm). Results show the presence of quartz, feldspar, and various clay minerals, confirming the siliciclastic nature of some of these grains (Fig. 8H).

*4.2.3 Channels, lobes, and levees*

Upper slope gullies (*sensu* Amblas et al., 2018) evolve distally into channels that are traceable through their increased reflectivity (backscatter) values (shown in red in Figs. 2B, 2D, 3B, 3D, and 9A-9C). All lower slope channels are extremely straight, with most sinuosities above 0.9, typical gradients between 5° and 10°, and with walls that range between 40-100 m above the channel floor. Like the overall slope, the gradient of channels floors decreases steadily basinward (see inset of Figure 4C, showing gradient decrease from ~30° to ~10° over the course of 5 km). In map view, most channels originate in

423 the upper slope and continue downslope to reach the basin
424 floor. Areas of increased backscatter intensity often taper
425 basinward to a point (e.g., Fig. 9A), although channel forms
426 may be seen in bathymetric relief to continue further
427 downslope. In several places, however, an individual upper
428 slope incised channel splits into multiple channels in the mid-
429 slope (e.g., the eastern side of Europa, denoted by an arrow in
430 Fig. 2D, and the northeastern side of Bassas da India; Fig. 9B).
431 This point of channel bifurcation most often occurs where the
432 slope gradient decreases to around 10°. The lower slope
433 channels that radiate outward from this point are smaller and
434 also straight, and often reach the basin floor. On the
435 northwestern side of Glorieuses, some slope channels contain a
436 regularly-spaced series of escarpments, 450-750 m apart and
437 15-60 m high that form an undulatory topography within the
438 channel (Fig. 9B).
439 On the northern side of Europa, at least one lower slope
440 channel is bounded by well-defined raised sedimentary deposits
441 with a ‘bird-wing’ shape in cross-section, seen in seismic data
442 in Figures 9D and 9E and interpreted as a levee deposit. These
443 deposits and the channel axis are visible in bathymetric data as
444 well, though the channel itself shows no increased backscatter
445 values. In seismic, levee deposits are transparent with faint, but
446 continuous, reflections (Facies E, described below), and reach a
447 maximum thickness of 280 meters in the seismic profile shown

448 in Fig 9D. Height from the channel floor to the highest part of
449 the levee is 70 meters or less. The central channel floor is
450 characterized by higher amplitude reflections, as are the
451 deposits several kilometers beyond the levee boundaries. Levee
452 deposits eventually merge into transparent, furrowed sediments
453 on the basin floor, shown on the right side of Figure 9D and
454 visible in on the seafloor in Figure 3C (labeled). A 27-m core
455 (MOZ4-CS23; see portion in Fig. 8D) taken directly atop the
456 levee shown in Figure 9D and 9E consists almost entirely of
457 foraminiferal carbonate mud, with carbonate sand beds
458 occurring only near its base.
459 Channels may terminate in a lobe near the bottom of the
460 lower slope or on the basin floor, although lobes are not always
461 present. A distinct lobe (visible in backscatter imagery; Fig.
462 9C) on the northeastern side of Bassas da India was selected for
463 more detailed investigation and was sampled by core MOZ1-
464 KS27 (Fig. 8A). The lobe is approximately 4 kilometers across
465 at its widest visible point, is estimated to range from 0 to tens
466 of meters thick based on seismic data, and begins where the
467 slope gradient is around 3°. Core MOZ1-KS27 (Fig. 8A),
468 despite only being 4 m long, contains multiple lithofacies
469 indicative of the lobe's composition. Above background
470 foraminiferal muds, a ~30-cm thick bed with a sharp lower
471 surface contains a basal layer of large (10-15 mm) coral and
472 algal fragments within a matrix of very coarse, bioclastic

calcareous grainstone. This coarse skeletal grainstone facies is overlain by a one-meter thick unit of carbonate packstone-wackestone (dominant grain size around 0.3 mm) that contains irregular clasts of mud 2-20 cm in diameter, which roughly increase in size upward through the unit. This facies is in turn overlain by a 20-cm thick, well-sorted, fining-upward bed containing fine-to medium-grained carbonate grainstones (Fig. 8E) with a similar composition to those seen elsewhere.

*4.2.4 Subsurface seismic facies*

Seismic lines acquired on the lower slopes and proximal basins of Iles Eparses platforms show several distinct types of sedimentary deposits, which can be classified based on the amplitude, continuity, and orientation of their internal reflections (Table 2). Seismic facies are found in different locations surrounding each platform, and not all facies are present surrounding each locality.

Sediments comprising the basin floor are typically characterized by horizontal to sub-horizontal, continuous, high-amplitude reflections that extend to the outer limits of seismic data (Facies A; Figs. 10 and 11) and that onlap onto the lower slopes of platforms. These are seen in all seismic lines that intersect the basin floor. On the eastern side of Juan de Nova, sediments of this facies originate from the Madagascar shelf and form thick, laterally continuous sediment packages separated by clearly identifiable onlap surfaces (Figs. 10C,

10D). Here, this facies interfingers with Facies B (transparent, chaotic reflections; Fig. 10C), which is contained within discrete units that taper away from the Juan de Nova platform. These subsurface units originate from the JDN platform (Fig. 10D), are 30-40 m thick, and extend seven or more kilometers into the basin. Internal character in these units is consistently transparent and shows little proximal-distal evolution. On the northwestern side of the Glorieuses platform, chaotic, transparent Facies B is present in dip line 315 around 120 m below the seafloor surface (Fig. 11A, 11B). Here, the unit containing this facies extends only ~2 km away from its origin point, forming a thicker, shorter seismic unit that is laterally adjacent to Facies D (discussed below).

In Bassas da India, a large, amalgamated unit of Facies C (chaotic facies of mixed amplitude) makes up a significant portion of the subsurface on the northeastern side of the island (Figs. 10A, 10B). The deposit sits directly atop basement, and decreases in thickness over the course of approximately 15 km. This unit shows little interfingering with adjacent hemipelagic basinal sediments; up to 320 meters of flat basin sediments unconformably onlap the unit. Internally, this unit contains at least one strongly reflective basement-parallel surface, and contains both high- and low-amplitude chaotic reflections.

Units containing both the chaotic reflections of Facies C and the more organized reflections of Facies D are present

523 within discrete units on the northwestern side of Glorieuses in
524 dip lines 315 and 319 (Figs. 11A, 11B,12). The most prominent
525 unit containing these facies, up to ~80 m thick, forms a wedge-
526 shaped sediment package extending approximately 12 km
527 basinward from its origin point on the lower slope. In this unit,
528 seismic Facies D contains both platform-and basinward-dipping
529 high-amplitude reflections. Reflections in this unit become
530 thinner and increasingly horizontal, ultimately terminating into
531 the continuous, high amplitude, 'railroad tracks' that make up
532 Facies A in the deep basin away from platforms. Just to the
533 northwest of this line, a different unit containing organized,
534 inclined reflections (Facies D; Line 319, Fig 12) comprises a
535 significant portion of the subsurface, forming an irregular unit
536 that tapers basinward and is not well-separated from the
537 underlying sediments. In this unit, the seafloor surface contains
538 a series of irregular, arcuate or linear ridges that are 10s to 100s
539 of meters in relief with 25-50 m amplitudes (decreasing
540 basinward), and wavelengths of 700-1200 m (Fig. 12). Seismic
541 Line 319 crosses these ridges, and shows that they are the
542 surface expression of concave-downward seismic structures
543 that originate deeper in the subsurface. These structures are
544 characterized by a series of high-amplitude reflections that dip
545 back toward the platform and gradually become tangential to a
546 subhorizontal surface approximately 120 m deep (labeled on
547 Fig. 12).

548 Facies E (Fig. 9D) is seen on the northern side of Europa
549 in the birdwing-shaped levee and channel deposits that make up
550 the lower slope. Reflections in this facies are mostly continuous
551 and low amplitude, though amplitude and continuity are
552 somewhat variable across the observed deposit. In strike line
553 015 (Fig. 9D), reflections within the levee are parallel to each
554 other and to the seafloor surface. In dip profile (Fig. 7A) this
555 facies can be seen to grade into horizontal, parallel reflections
556 on the basin floor, which increase in amplitude basinward to
557 conformably become Facies A (Table 2).

558 **5. Discussion**

559 *5.1 Interpretation of sedimentary deposits*

560 *5.1.1 Facies diversity*

561 Cores reveal that deposits on the slopes and in the
562 proximal basins surrounding platforms are a combination of
563 pelagic and platform-derived sedimentation. Within muddy
564 deposits, clay minerals (Fig. 8H) are likely the product of
565 weathering, suspension and transport of clastic sediments in
566 seawater, and subsequent deposition through pelagic rain
567 (Facies G of Pickering et al., 1986). These lithologies are
568 present in all cores and may originate from the African
569 continent (Kolla et al., 1976; Wiles et al., 2017), Madagascar
570 (the nearby Betsiboka River exports large volumes of fine-
571 grained sediment; Raharimahefa and Kusky, 2010), or
572 elsewhere. While the carbonate platforms discussed here are

573 themselves unlikely to generate significant amounts of
574 aluminosilicate clays found in seafloor muds, the submarine
575 weathering of basalt and other volcanics can produce smectite
576 and other clay minerals (Kolla et al., 1976) and thus may be the
577 origin of some of the sediment seen here. Coccoliths and
578 planktonic forams also form a significant portion of the fine-
579 grained background sediment—these too are the result of
580 pelagic rain, and may also have been transported long distances
581 (van Sebille et al., 2015). Aragonite needles found in some
582 samples are produced in shallow water on or near carbonate
583 platforms (Milliman et al., 1993). This aragonite is therefore
584 interpreted to have been winnowed from the platform top
585 during times of flooding, as has been hypothesized by Jorry et
586 al (2016).
587 Coarser grainstone-packstone units found in core also
588 show evidence of a nearby shallow-water origin. Bioclastic
589 grains (e.g., corals and calcareous algae) are the skeletal
590 remains of organisms that live primarily within the photic zone;
591 they provide unambiguous evidence that at least part of the
592 sediments forming these beds are allochthonous, and come
593 from the tops of nearby platforms. The exact process by which
594 sediment is transferred off of the platform top is unknown,
595 however, wind-related or tide-related currents are both active
596 on the shallow water portion of platforms. Elsewhere, density
597 cascading has been proposed as a mechanism for the off-

598 platform transfer of sediment (Wilson and Roberts, 1995), a
599 process which is not likely to be active here as it is dependent
600 on winter cold fronts that are not present in the Mozambique
601 Channel (Deutscher Wetterdienst, 2018).
602 The fining-upward profiles of some of these beds (e.g.,
603 those shown in Fig. 8A-E) are consistent with deposition as
604 turbidites (Shanmugam, 2000). Other depositional processes
605 may also occur: in core MOZ1-KS27, the size of mud clasts
606 within the main bed increases upward. This type of inverse
607 grading may occur in debrites (Mulder and Alexander, 2001),
608 and strongly resembles cohesive flow deposits described by
609 Lowe (1982). Inverse grading has been described previously on
610 ancient carbonate slopes (e.g., Mullins and Cook, 1986).
611 Ripped-up clasts of slope muds entrained within debris flows
612 are also a common component of carbonate slope deposits
613 (James and Jones, 2016). Fining-upward turbidites are also
614 found stratigraphically adjacent to the debris flow unit (Fig.
615 8A). Turbidite facies are clearly separate, but may be related to
616 the debris flow event (linked turbidites and debrites, c.f. Benn
617 & Evans 2014; Talling et al. 2012). Sediments within these
618 types of gravity flows must ultimately originate from the
619 platform itself, as evidenced by the nature of constituent grains,
620 though the entraining turbidity current or debris flow may
621 originate lower on the slope.

Cores therefore reveal that sedimentation on a bed scale is a combination of hemipelagic sedimentation and gravity flow deposits. However, larger-scale sediment transport processes are also operating on platform slopes, as depositional units seen in seismic profiles show evidence of mass transport on a kilometer scale.

*5.1.2 Subsurface expression*

Sedimentary units and associated facies seen in seismic lines and bathymetric data are interpreted to consist of three primary types of deposits:

- Basin floor pelagites
- Mass transport deposits (MTDs)
- Channels, levees, and turbidite lobes

High-amplitude, parallel reflections on the basin floor (Facies A) are interpreted to be the result of pelagic and hemipelagic sedimentation processes that are continually occurring in the deep sea (Pickering et al., 1986). This seismic facies corresponds to the foraminiferal muds that are seen in core. Thin carbonate turbidites may also be present within this facies, but are likely to be only in the area immediately surrounding each platform. Near Juan de Nova, the character of these background sediments is more variable than elsewhere (Fig. 10C); this is likely a result of their proximity to the western slope of Madagascar. Here, the variety of slope-related

sedimentary processes creates internal surfaces and topography not seen in the abyssal basin floor elsewhere (Fig. 10D).

Seismic Facies B-C, characterized by low- or mixed-amplitude chaotic reflections, are usually restricted to discrete units and contain many of the criteria used to recognize mass transport deposits (MTDs), as outlined in Posamentier and Martinsen (2011). Based on the geometry of the unit, as well as the amplitude, continuity, and the orientation of internal reflections, these MTDs are interpreted to be the result of one of several depositional processes. MTDs consisting of chaotic, transparent reflections (Facies B) and those with chaotic, but higher amplitude reflections (Facies C) are interpreted to be the result of submarine debris flows originating on the platform slope. Deposits with similar chaotic seismic character have also been referred to as debris flows by Carter (2001), Posamentier and Kolla (2003), and Joanne et al. (2013), among others. In carbonates specifically, Principaud et al. (2015) interpret chaotic seismic units as mass transport complexes with a debris flow component, and Janson et al. (2011) interpret units characterized by discontinuous, low-amplitude reflectionslso interpreted as debris flows. Debris flow processes remove original stratification during downslope movement, and have the potential to travel long distances (Mulder and Cochonat, 1996), features consistent with the units seen here that extend for several kilometers. The amplitude of the reflections that

671 distinguishes between these facies is likely a product of the
672 lithologic heterogeneity of the source material. On the eastern
673 side of Juan de Nova, this facies contains large stratified and
674 convolute-bedded blocks on a scale of several hundred meters
675 (Fig. 10C), interpreted as large blocks of coherent or deformed
676 sediment entrained within the mass movement.
677 The basinward or platform-dipping reflections in some
678 units containing Facies D suggest that a different process is
679 responsible for their deposition. A unit on the northwestern side
680 of Glorieuses thins basinward and displays both progradational
681 and retrogradational internal geometries (Figs. 11A, 11B). This
682 unit is interpreted as a turbidite lobe, as deposits with these
683 types of geometries have been interpreted elsewhere as
684 turbidites (e.g., Gervais et al., 2006). It is likely the subsurface
685 expression of the type of lobate deposits seen on the current
686 seafloor elsewhere (e.g., on Bassas da India; Fig. 8A). On the
687 northwestern side of Glorieuses, the unit seen in Figure 12
688 contains a series of organized structures with platform-dipping
689 reflections that are expressed on the seafloor surface. These
690 deposits are interpreted as a large MTD with depositional
691 thrusts and pressure ridges (Fig 12) gliding along a subsurface
692 decollement. Such features are known to form due to the
693 compressional regime encountered during some downslope
694 mass movements (Posamentier and Martinsen, 2011; Alsop et
695 al., 2017), however, this is one of the first times they have been

clearly documented in a predominantly carbonate system. Sedimentary compression ridges similar to these have been noted in analogous settings in the clastic realm—nearly identical features are described in recent, submarine sediments from multiple locations (e.g., Alfaro and Holz, 2014; Moscardelli et al., 2006; Frey-Martínez et al., 2005; Hampton and Lee., 1996; Joanne et al., 2013). Compressional features cannot explain all seafloor ridges near Glorieuses, however; smaller sediment waves are also present in the same area, and some of the seafloor topography seen in Figure 2A may be related to turbidity currents.

Transparent, continuous deposits in Facies E are form a channel levee, and interpreted to be the result of the overbank depositional processes associated with channelized sediment gravity flows. The generally low-amplitude nature of these deposits suggests that they are of uniform composition and fine-grained, an interpretation confirmed by the predominance of muds in core MOZ4-CS23 (Fig. 8D).

*5.1.3 Seafloor surface*

Backscatter (reflectivity) data has been reliably shown to predict sedimentological facies (Dartnell and Gardner, 2004), grain size (Clarke et al., 1996; McGonigle and Collier, 2014), and degree of induration of the seafloor (Mulder et al., 2017), though has not been used previously to differentiate between carbonate sands and muds. Here, high reflectivity values are

721 interpreted to denote areas of submarine volcanism, erosional
722 outcrops, and active sediment transfer where coarser-grained
723 (larger than silt-sized) facies are more abundant on the seafloor.
724 This assumption fits with observed geomorphology and is
725 preliminarily confirmed by core data. Backscatter data shows
726 that active deposition of coarse-grained material is currently
727 taking place through feeder channels that funnel sediment to
728 the basin floor (Figs. 2 and 3). High reflectivity values are
729 interpreted to be the result of carbonate sands (grainstones) on
730 the floors of incised channels, which respond differently to
731 acoustic soundings than surrounding muds. Although lithified
732 volcanic outcrops are also highly reflective, these are easily
733 distinguished from linear sediment pathways. High-reflectivity
734 sediments within channels may terminate on the basin floor in a
735 lobe, and channel forms may be bounded by elevated levees
736 (Fig. 9D-E). Undulatory surface morphologies within some
737 channels are interpreted as cyclic steps (c.f. Covault et al.,
738 2017). These types of bedforms, lobes and levees are associated
739 with deposition from turbidity currents (Shanmugam, 2000),
740 and this is interpreted to be the primary process of sediment
741 transfer from the platform top. Channel forms without
742 increased reflectivity are interpreted as inactive, as is the case
743 in the leveed channel noted in Fig. 9C. This channel and others
744 like it may have been cut off from active deposition in the past,
745 a hypothesis supported by the lack of recent sandy deposits in

746 the adjacent core (MOZ4-CS23). Individual channels may
747 therefore have a finite lifespan, and active channels and lobes
748 may switch with changes in sediment availability.

749 *5.2 Controls on deposition and geomorphology*

750 The nature of the volcanic edifice underlying each
751 platform ultimately influences the size, height, and overall
752 gradient of the slope profile, all of which influence the slope
753 depositional architecture. Volcanic cone morphologies lead to
754 an overall smaller platform top size, limiting the volume of
755 bioclastic carbonate sediment that can be produced and thus
756 reducing the available sediment supply to slopes. High
757 gradients in the upper slope lead to little carbonate deposition;
758 the majority of slope sedimentation takes place where gradients
759 are less than 10°. This upper slope bypass inhibits progradation
760 and lateral expansion of the platform top. Slope steepness is
761 also likely responsible for straight channel morphologies (Clark
762 et al., 1992) and the development of basin-floor fan systems, a
763 type of deposit rarely seen in modern carbonate settings
764 (Payros and Pujalte, 2008). The abundance of MTDs on the
765 lower slope and proximal seafloor may also be influenced by
766 slope steepness, although past studies (e.g., Hühnerbach and
767 Masson, 2004) note that the number of slope failures are is
768 relatively independent of inclination, even in volcanic islands.
769 Active regional tectonics may also directly influence platform
770 morphology (and thus deposition), as in the fault-generated

771 subaqueous terrace on Bassas da India. Processes occurring on
772 the terrace may likely affect the sedimentary character of
773 platform sediments; large sand dunes (Fig. 4B, inset; lithology
774 confirmed by sediment samples) suggest that sediments may be
775 winnowed and transported by bottom currents atop the terrace
776 before subsequently moving further downslope.
777 The direction and intensity of dominant trade winds have
778 long been known to have an effect on the facies distribution on
779 carbonate platforms (Dravis and Wanless, 2017) including on
780 Glorieuses (Jorry et al., 2016; Prat et al., 2016). In the Iles
781 Eparses, most platform tops show some degree of wind-related
782 asymmetry, especially on Glorieuses and Juan de Nova.
783 Platform tops also differ in terms of their geomorphology,
784 which likely has some influence over the nature and
785 distribution of slope sediments. Open platform tops without a
786 fringing reef (Glorieuses and Juan de Nova) have a submarine
787 bank with no barriers between the top and slope break, a
788 morphology that promotes continuous deposition and sediment
789 transfer (Fig. 2). Enclosed platform tops (Bassas da India) have
790 an interior lagoon with a mostly continuous fringing reef,
791 preventing continual transferal of large amounts of sediment
792 from the inner platform to the slope, and possibly affecting the
793 sedimentological character of platform top exports by confining
794 platform-top muds (Fig. 3). On the top of Europa, sediment
795 transfer is localized, showing a strong directionality to

sediment export in the form of a wide tidal channel. This channel is clearly the origin point for the largest single channel on the slope (labeled 'TC' on Fig. 4C). However, backscatter data (Fig. 3D) do not suggest that active sedimentation is appreciably increased within this specific channel axis when compared to the many other channels visible surrounding the island. Future studies of platform top sedimentology are needed to fully understand the way that sediment export is affected by platform top elements.

Wind-related asymmetry extends to the slope as well—the leeward sides of carbonate platforms elsewhere have been established to have their morphology affected by off-platform sediment transport (e.g., Hine et al., 1981). Here, leeward sides are generally smoother, with fewer high-relief outcrops. This is interpreted to be a product of increased sedimentation, which would promote faster erosion of any volcanic highs or remnant sedimentary outcrops, and would infill depressions and low areas with sediment. Windward sides of platforms are sometimes more rugose than leeward sides. This can also be attributed to increased abundance of outcrops of underlying basement, as well as from steep-sided arcuate slope failures. Decreased windward sedimentation may lead to oversteepened, sediment-starved windward slopes, which are more prone to failure.

*5.3 Summary and facies model*

Although facies models allow for real-world deviation from an idealized scenario, the character and distribution of sedimentary facies seen here is significantly different from previously established models of carbonate slopes elsewhere. Past models have generally not focused on steep, volcanic-cored platforms, however, these settings are clearly responsible for the generation of substantial amounts of carbonate sediment, and have a unique set of depositional features when compared to those elsewhere. The geomorphology, depositional elements, and sedimentary processes seen in the Iles Eparses are synthesized in a facies model shown in Figure 13.

In summary, sediment transfer to the deep sea in the Iles Eparses is a combination of processes at a variety of scales. Carbonate sediments on the platform top are transported onto the broad, steep upper slope through the action of wind- or tide-generated water movement, shallow currents, or density cascading (Fig. 13A). The slope becomes increasingly channelized basinward, with sediments moving down straight channel axes in gravity flows. Carbonate grainstones-packstones are ultimately deposited in the lower slope or proximal basin in the form of gravity flow deposits (turbidites and debrites), including levee and overbank deposits, where they are interbedded with hemipelagic foraminiferal muds. These interbedded gravity flow deposits and background muds (and possibly basement volcanics) may move further

846 downslope together in the form of large-scale mass transport
847 deposits that originate on the slope itself (Fig. 13B). MTDs
848 may in turn be subsequently reworked as new channels incise
849 into lower slope sedimentary deposits (Fig. 13C). Any given
850 slope deposit may therefore be the result of multiple
851 sedimentation processes, and a range of depositional elements
852 resulting from several different processes may be present on the
853 seafloor at any given time. Figure 13 shows a composite sketch
854 combining many of the observed geomorphologic and
855 depositional features seen across platforms, and general
856 characteristics are summarized in the chart in Table 3.

857 *5.4 Implications*

858 The synthesis of observed features and processes shown
859 in Figure 13 is one of the first detailed facies models for
860 sedimentary deposition on the slopes of carbonate atolls and
861 atoll-like carbonate platforms. It can be compared with similar
862 block diagrams on other carbonate slopes (e.g. Betzler et al.,
863 2014, Grammer and Ginsberg, 1992, Mulder et al., 2017,
864 Mullins and Cook, 1986, Mullins et al., 1984, and Payros and
865 Pujalte, 2008, among others). Although these are very different
866 types of carbonate platforms from those discussed here, such a
867 comparison is essential in determining which aspects of
868 carbonate deposition are more universal, and highlights the
869 differences between the settings discussed here and more
870 'traditional' carbonate platforms. In addition, facies on the

871 slopes of these platforms differ from those on other volcanic
872 islands. The island of La Réunion (Indian Ocean), for example,
873 is characterized by a steep-sided central volcanic cone rather
874 than a flat, carbonate-dominated platform top. Facies models
875 developed on the submarine slopes of La Réunion therefore
876 lack the extensive carbonate deposits seen here, and are instead
877 dominated by large-scale flank collapses, lava flow platforms
878 and deltas, and volcaniclastic fan systems (Babonneau et al.,
879 2011; Saint-Ange et al., 2013; Sisavath et al., 2011).
880 Elsewhere, the flanks of Madeira Archipelago (a series of
881 volcanic islands in the Atlantic Ocean) are also dominated by
882 numerous large, arcuate slope failures, as well as numerous
883 radial gully-channel systems more similar to those seen here
884 (Quartau et al., 2018). These channels, however, often show a
885 well-developed dendritic pattern in map view, and coalesce into
886 longer, larger channels that extend much further from the
887 islands than those in the Iles Eparses.
888 Of note in the Iles Eparses are the presence of clear,
889 unambiguous channel systems with lobate basin-floor fans.
890 This type of lobate fan system has rarely been described in
891 other modern carbonate settings: Payros and Pujalte (2008)
892 state that “Calciclastic submarine fans are rare in the
893 stratigraphic record and no bona fide present-day analogue has
894 been described to date.” Mullins and Cook (1986) also note the
895 paucity of unambiguous examples in the geologic record, and

James and Jones (2016) note that submarine fans do not typically form on carbonate slopes because of the linear, rather than point-sourced, nature of slope profiles. Terminal fans seen in the Iles Eparses are likely present because sediments are concentrated into relatively few active channels that reach the basin floor. Platform-derived sediment is distributed over a relatively small area, resulting in more focused distributary systems and promoting point-sourcing of deposition.

Although the deposits seen here are relatively recent in origin, the distribution and character of these sediments may be used as an analog for deposits elsewhere. Core taken on lower slopes almost always include some component of carbonate grainstones-packstones, a facies with more potential as a conventional hydrocarbon reservoir than the periplatform muds that make up the majority of core in inter-channel areas, MTDs, and levees. Goldstein et al. (2012) note the difference in reservoir potential between dispersed- and focused-flow carbonate slope systems in the Miocene of Spain; the Iles Eparses deposits are more similar to the latter. These types of small isolated platforms therefore have a different reservoir potential and sediment distribution than other, larger platforms with more dispersed depositional systems. The higher reservoir potential of more concentrated focused-flow grainstones should be tempered by the overall smaller volume, smaller distribution radius, and lower preservation potential of these types of

settings; the geologic record of atolls and carbonate platforms atop deep sea volcanoes is relatively sparse.

## 6. Conclusions

The Iles Eparses atolls, islands, and platforms are situated on isolated deepwater volcanic pedestals in and around the Mozambique Channel, making them genetically different from other, more well-known carbonate settings. This study provides a first look into the nature of carbonate slope sedimentation in this unique, little-known depositional environment, and presents the first detailed facies model for the types of atoll and atoll-like platforms discussed here. Slope sediments are a product of a range of gravity-dominated depositional processes, including hemipelagic rain, slope failure and downslope mass transport, and gravity flows (turbidites and debrites). Inherited topography of the underlying volcanic pinnacles results in steep upper slope gradients where little sedimentation takes place and arcuate slope failure scars are locally common. Platform-derived carbonates may be channelized in the lower slope, forming, in places, relatively straight channel systems that extend for tens of kilometers and may terminate in basin-floor lobes, a relatively rare occurrence in modern-day carbonate settings. Elsewhere on the lower slope, turbidites and mass transport deposits are present, with the subsurface seismic facies often taking the form of chaotic units interpreted as debris flows. Depositional thrusting and associated pressure

ridges are also present in some lower slope deposits. Slopes are usually asymmetric with respect to predominant wind direction, with leeward slopes usually having a lower rugosity than windward slopes and more spatially extensive toe-of-slope deposition. The lack of data in settings analogous to the Iles Eparses underscores the need for further research, and shows the importance of the observations reported here in expanding the known spectrum of depositional carbonate depositional environments.

## 7. Acknowledgements

The oceanographic expeditions PTOLEMEE, PAMELA-MOZ1 and PAMELA-MOZ4 and Elda Miramontes' fellowship were co-funded by TOTAL and IFREMER as part of the PAMELA (Passive Margin Exploration Laboratory) scientific project. This work was supported by the "Laboratoire d'Excellence" LabexMER (ANR-10-LABX-19) and co-funded by a grant from the French government under the program "Investissements d'Avenir". Thanks to Joseph Ronzier for writing and executing the Python script used in calculating slope rugosity. Thanks to Simon Courgeon for additional data contributions and helpful discussions related to this project, Sandrine Cheron and Audrey Boissier for XRD analysis, and Nicolas Gayet for SEM assistance. We also thank the captains and crews of the RVs *Atalante* and *Pourquoi Pas?* during the cruises where this data was collected.

971 **Figure Captions**

972 *Table 1*: General dimensions and associated volumes of
973 selected slope failure scars on Juan de Nova. Wedge diagram
974 shows conceptual method of volumetric calculation.

975 *Table 2*: Interpreted seismic facies found in lower slopes and
976 proximal basins. Interpretations are based on the amplitude,
977 orientation, and bounding relationships of seismic reflectors
978 within seismic units.

979 *Table 3*: Chart summarizing scale and character of selected
980 depositional elements observed in this study.

981 *Figure 1*: A) Location map of platforms and other geographic
982 and geologic features mentioned in this paper. Oceanic
983 circulation from Brietzke et al. (2017). COM-Comoros Islands;
984 MAY-Mayotte Island; GLO- Glorieuses Islands; JDN-Juan de
985 Nova; DR-Davie Ridge; ZV-Zambezi Valley ; BDI-Bassas da
986 India; EUR-Europa. B) Present-day dominant wind directions
987 from Metéo France, sourced from over 5000 individual
988 measurements from weather stations on the islands. Bassas da
989 India has no weather station, but is situated close enough to Ile
990 Europa that wind directions are not appreciably different (see
991 location in Figure 1A).

992 *Figure 2*: Detailed bathymetric and backscatter maps of slopes
993 of Iles Eparses platforms Glorieuses (A, B) and Juan de Nova
994 (C, D). Bathymetric maps are an overlaid combination of
995 absolute seafloor depth (color) and slope gradient (greyscale),

allowing both the slope relief and seafloor topography to be seen. Reflectivity maps use an arbitrary, sliding-scale color bar to best differentiate sedimentological and geomorphologic features. GG-Grande Glorieuse Island.

*Figure 3*: Detailed bathymetric and backscatter/reflectivity maps of slopes of Iles Eparses platforms Bassas da India and Europa. Same parameters as Figure 2. A, B) Bassas da India; C, D) Europa, TC-tidal channel.

*Figure 4*: Three-dimensional views of submarine platform slopes, focusing on slope morphology. Color gradient adjusted for each platform. A) Southeast-looking view of Glorieuses, showing the platform top, Glorieuses terrace and the linear escarpment most prominent on the northwestern side (magnified view in inset). B) Northward-looking view of Bassas da India, showing large submarine terrace and its profile and associated features, notably sand dunes and gullies found on the terrace surface in 350-600 meters water depth (insets). C) Southeastern-looking view of Europa, showing strike and dip profiles and location of seismic line in Figure 4D. Channel floor visible in both bathymetric and seismic data marked with an asterisk. Also of note is the steep, smooth upper slope surface, visible here on the leeward side of the platform. D) Europa seismic line 076 (PTO-mig076_v1500_g0). This line shows the relatively thin nature of sedimentary deposits in the

1020 mid-slope, the seismic character of the volcanic basement, and
1021 the higher-amplitude reflections in channel floors.
1022 *Figure 5*: A-B): Evidence of slope failure on Juan de Nova; A)
1023 Leeward slope, showing generally smooth upper slope surface
1024 and two large arcuate scarps, denoted 1 and 2 in Figure 5D. B)
1025 Windward slope, with several discrete scarps highlighted
1026 (numbers 3-6). Approximate volumetric calculations for each
1027 numbered scarp shown in Table 1. C) Quantitative rugosity
1028 analysis of Juan de Nova upper slope. 1st part shows conceptual
1029 method of quantification, second part applies the same method
1030 to the 600-m contour on Juan de Nova platform. On Juan de
1031 Nova, the windward side of the platform is significantly more
1032 rugose than the windward side.
1033 *Figure 6*: Examples of slope failure and/or erosion on Bassas
1034 da India and Europa, with along-strike profiles and dimensions.
1035 *Figure 7*: A) Seismic line 079 (PTO-mig079_v1500_g0), taken
1036 along the leeward side of Europa, showing sedimentary nature
1037 of the lower slope. The line is an oblique dip line, crossing
1038 channels and levees seen in Figures 8D and 8E, and clearly
1039 showing their contact with the underlying basement. B-D)
1040 Bathymetric profiles for the windward and leeward slopes of
1041 platforms. Bassas da India not included due to lack of data
1042 coverage on the windward side. Note extended lower slope on
1043 each leeward side; windward slopes often have a steeper
1044 descent to the basin floor.

*Figure 8*: Core data from the lower slopes and proximal basins of Iles Eparses. Exact locations of core shown in Figure 2. A-D) Lithologies and core photos from four seafloor piston cores. Core MOZ4-CS23 (D) contains an additional 23 meters above the selected section that is almost entirely composed of background foraminiferal ooze. (A) taken at 3089 m; (B) 3167 m; (C) 1909 m; (D) 2852 m. E) Grain-size profiles of the carbonate grainstone-packstone beds marked in red in above logs. F) Compositional data for selected intervals within carbonate grainstone-packstone beds. Locations denoted in A-D. Data shown only includes identifiable grains; unidentified grains constitute 30-40% of total grains observed. G) SEM images of carbonate grainstones in core MOZ1-KS04, interval 649-650 m, at the base of a relatively thick carbonate sand unit. Abbreviations: BF-benthic foraminifer; CA-calcareous algae; Ec-echinoid; Fo-Foraminifer; Ga-gastropod; PF-planktonic foraminifer. H) Analysis of muds/foraminiferal oozes; left side: SEM images; AN-aragonite needles; CM-clay minerals; Co-Coccolith. Right side: EDS spectra and XRD mineralogy of selected intervals.

*Figure 9*: Examples of channels and channel-related features on Iles Eparses slopes. A) Reflectivity map of northeastern side of Glorieuses, showing numerous sub-parallel active channels that do not terminate in lobe structures. B) and C) are overlays of reflectivity and slope data; B) Northwestern side of Bassas da

India, showing bifurcating channels, some of which terminate in a lobe. Image is an overlay of reflectivity and slope data. C) Northern side of Europa. Inactive channel crossed by seismic lines in D and E is outlined with dashed line. Other, active channels have higher backscatter values and fan outward at the slope base. D) Seismic strike line on the north side of Europa showing channel-levee complex. Note levee transparency, higher-amplitude asymmetric overbank deposits, and central channel. E) Interpretation of (D)

*Figure 10*: Lower slope seismic lines and interpretations. Description of seismic facies in text and in Table 2. Exact locations of lines shown in Figures 2 and 3. A) Bassas da India line 017 (PTO-mig017_v1500). B) Interpretation of seismic line above in (A). C) Juan de Nova line 234 (PTO-mig234_v1500_g0). D) Interpretation of seismic line above in (C). Colors delineate individual stratigraphic units, similar colors denote related units.

*Figure 11*: Lower slope seismic lines and interpretations, continued. A) Glorieuses Line 315 (mig315_v1500_g0). B) Interpretation of seismic line above in (A).

*Figure 12*: Glorieuses Line 319 (mig319_v1500_g0) and notes on interpretation.

*Figure 13*: A-C) Simplified diagram of sedimentation processes observed in core, seafloor bathymetry, and seismic data. A) Turbidite deposition resulting in interbedded carbonate

grainstone-packstones and seafloor muds B) Upper-middle slope failure, remobilizing previously deposited sediments (potentially including parts of the lithified platform) and redistributing them to the lower parts of the slope in the form of MTDs. C) Further deposition of carbonate grainstones-packstones in turbidites. Channelized deposits may erode into past MTDs and rework previously deposited material. D) Facies model that summarizes depositional elements and sedimentation processes in the Iles Eparses. Figure represents a synthesis of data from bathymetric, reflectivity, and seismic surveys of multiple platforms. Schematic only; not to scale.

1110 **References**


1111 Alfaro, E., Holz, M., 2014. Seismic geomorphological analysis
1112 of deepwater gravity-driven deposits on a slope system of the
1113 southern Colombian Caribbean margin. Marine and Petroleum
1114 Geology 57, 294-311.

1115 Alsop, G.I., Marco, S., Levi, T., Weinberger, R., 2017. Fold
1116 and thrust systems in Mass Transport Deposits. Journal of
1117 Structural Geology, 94, 98-115.

1118 Amblas, D., Ceramicola, S., Gerber, T.P., Canals, M., Chiocci,
1119 F.L., Dowdeswell, J.A., Harris, P.T., Huvenne, V.A., Lai, S.Y.,
1120 Lastras, G. and Iacono, C.L., Micalle, A., Mountjoy, J.J., Paull,
1121 C.K., Puig, P., and Sanchez-Vidal, A. 2018. Submarine
1122 canyons and gullies. In: Micallef, A., Krastel S., and Savini A.
1123 (eds) Submarine Geomorphology. 251-272, Springer Geology.
1124 Springer, Cham.

1125 Babonneau, N., Delacourt, C., Cancouët, R., Sisavath, E.,
1126 Bachèlery, P., Mazuel, A., Jorry, S.J., Deschamps, A.,
1127 Ammann, J. and Villeneuve, N., 2013. Direct sediment transfer
1128 from land to deep-sea: Insights into shallow multibeam
1129 bathymetry at La Réunion Island. Marine Geology, 346, 47-57.

1130 Bassias, Y., Roberts, G., Christoffersen, T., 2016. The nature of
1131 the crust offshore East Coast Africa When geology and seismic

meet potential fields in the search for hydrocarbons. East Africa: From Research to Reserves, Extended Abstract, The Geological Society of London 13-15 April 2016, 1-12.

Battistini, R., Cremers, G., 1972. Geomorphology and vegetation of Iles Glorieuses. Smithsonian Institution. Atoll Research Bulletin 159, 27 p.

Battistini, R., Gayet, J., Jouannic, C., Labracherie, M., Peypouquet, J.P., Pujol, C., Pujos-Lamy, A., Turon, J.L., 1976. Etude des sédiments et la microfaune des îles Glorieuses (Canal de Mozambique). Cahiers ORSTOM, Série Géologie 8, 147-171.

Benn, D., Evans, D.J., 2014. Glaciers and glaciation. Routledge, 816 p.

Berthois L., Battistini, R., 1969, Etude Sedimentologique de L'Ile Europa, Madagascar Revue de Geographie 15, 1-52.

Betzler, C., Lindhorst, S., Eberli, G. P., Lüdmann, T., Möbius, J., Ludwig, J., Schutter, I., Wunsch, M., Reijmer, J., Hübscher, C., 2014. Periplatform drift: the combined result of contour current and off-bank transport along carbonate platforms. Geology 42, 871-874.

1152 Betzler, C., Hübscher, C., Lindhorst, S., Lüdmann, T., Reijmer,
1153 J.J. and Braga, J.C., 2016. Lowstand wedges in carbonate
1154 platform slopes (Quaternary, Maldives, Indian Ocean). The
1155 Depositional Record, 2, pp.196-207.

1156 Blomeier, D.P.G., Reijmer, J. J., 2002. Facies architecture of an
1157 Early Jurassic carbonate platform slope (Jbel Bou Dahar, High
1158 Atlas, Morocco). Journal of Sedimentary Research 72, 462-
1159 475.

1160 Breitzke, M., Wiles, E., Krocker, R., Watkeys, M.K., Jokat, W.,
1161 2017. Seafloor morphology in the Mozambique Channel:
1162 evidence for long-term persistent bottom-current flow and
1163 deep-reaching eddy activity. Marine Geophysical Research 38,
1164 241-269.

1165 Carter, L., 2001. A large submarine debris flow in the path of
1166 the Pacific deep western boundary current off New Zealand.
1167 Geo-Marine Letters, 21, 42-50

1168 Clark, J.D., Kenyon, N.H., Pickering, K.T., 1992. Quantitative
1169 analysis of the geometry of submarine channels: implications
1170 for the classification of submarine fans. Geology, 20, 633-636.

1171 Clarke, J.E.H., Mayer, L.A. and Wells, D.E., 1996. Shallow-
1172 water imaging multibeam sonars: a new tool for investigating

1173 seafloor processes in the coastal zone and on the continental
1174 shelf. Marine Geophysical Researches, 18, 607-629.

1175 Courgeon, S., Jorry, S.J., Camoin, G.F., BouDagher-Fadel,
1176 M.K., Jouet, G., Révillon, S., Bachèlery, P., Pelleter, E.,
1177 Borgomano, J., Poli, E., Droxler, A.W., 2016. Growth and
1178 demise of Cenozoic isolated carbonate platforms: New insights
1179 from the Mozambique Channel seamounts (SW Indian Ocean).
1180 Marine Geology 380, 90-105.

1181 Courgeon, S., Jorry, S.J., Jouet, G., Camoin, G., BouDagher-
1182 Fadel, M.K., Bachèlery, P., Caline, B., Boichard, R., Révillon,
1183 S., Thomas, Y. Thereau, E., 2017. Impact of tectonic and
1184 volcanism on the Neogene evolution of isolated carbonate
1185 platforms (SW Indian Ocean). Sedimentary Geology 355, 114-
1186 131.

1187 Covault, J.A., Kostic, S., Paull, C.K., Sylvester, Z., Fildani, A.,
1188 2017. Cyclic steps and related supercritical bedforms: building
1189 blocks of deep-water depositional systems, western North
1190 America. Marine Geology, 393, 4-20.

1191 Dartnell, P., Gardner, J.V., 2004. Predicting seafloor facies
1192 from multibeam bathymetry and backscatter data.
1193 Photogrammetric Engineering & Remote Sensing 70, 1081-
1194 1091.

1195 Deutscher Wetterdienst, 2018, Klimatafel von Juan de Nova
1196 (Insel), Iles Desirades / Indischer Ozean / Frankreich
1197 https://www.dwd.de/DWD/klima/beratung/ak/ak_619700_kt.pd
1198 f. Retrieved June 20, 2018.

1199 Dravis, J.J., Wanless, H.R., 2017. Impact of strong easterly
1200 trade winds on carbonate petroleum exploration-Relationships
1201 developed from Caicos Platform, southeastern Bahamas.
1202 Marine and Petroleum Geology 85, 272-300.

1203 Dunbar, G.B. and Dickens, G.R., 2003. Late Quaternary
1204 shedding of shallow-marine carbonate along a tropical mixed
1205 siliciclastic–carbonate shelf: Great Barrier Reef, Australia.
1206 Sedimentology, 50, 1061-1077.

1207 Förster, R., 1975. The geological history of the sedimentary
1208 basin of southern Mozambique, and some aspects of the origin
1209 of the Mozambique Channel. Palaeogeography,
1210 Palaeoclimatology, Palaeoecology 17, 267-287.

1211 Frey Martinez, J., Cartwright, J., Hall, B., 2005. 3D seismic
1212 interpretation of slump complexes: examples from the
1213 continental margin of Israel. Basin Research, 17, 83-108.

1214 Gervais, A., Savoye, B., Mulder, T., Gonthier, E., 2006. Sandy
1215 modern turbidite lobes: a new insight from high resolution
1216 seismic data. Marine and Petroleum Geology, 23, 485-502.

1217 Gischler, E., 2011. Sedimentary facies of Bora Bora, Darwin's
1218 type barrier reef (Society Islands, South Pacific): the
1219 unexpected occurrence of non-skeletal grains. Journal of
1220 Sedimentary Research, 81,1-17.

1221 Goldstein, R.H., Franseen, E.K., Dvoretsky, R.A., Sweeney,
1222 R.J., 2012. Controls on focused-flow and dispersed-flow
1223 deepwater carbonates: Miocene Agua Amarga Basin, Spain.
1224 Journal of Sedimentary Research 82, 499-520.

1225 Grammer, G.M., Ginsburg, R.N., 1992. Highstand versus
1226 lowstand deposition on carbonate platform margins: insight
1227 from Quaternary foreslopes in the Bahamas. Marine Geology
1228 103, 125-136.

1229 Guillaume, M.M., Reyss, J.L., Pirazzoli, P.A., Bruggemann,
1230 J.H., 2013. Tectonic stability since the last interglacial offsets
1231 the Glorieuses Islands from the nearby Comoros archipelago.
1232 Coral Reefs 32, 719-726.

1233 Hampton, M., and Lee, H., 1996. Submarine Landslides,
1234 Reviews of Geophysics 34, 33-59.

1235 Harris, D.L., Webster, J.M., De Carli, E.V., Vila-Concejo, A.,
1236 2011. Geomorphology and morphodynamics of a sand apron,
1237 One Tree reef, southern Great Barrier Reef. Journal of Coastal
1238 Research, 64, 760.

1239 Hay W.W., 2014. Submarine Canyons. In: Harff J., Meschede
1240 M., Petersen S., Thiede J. (eds) Encyclopedia of Marine
1241 Geosciences. Springer, Dordrecht.

1242 Hine, A.C., Locker, S.D., Tedesco, L.P., Mullins, H.T.,
1243 Hallock, P., Belknap, D.F., Gonzales, J.L., Neumann, A.C.,
1244 Snyder, S.W., 1992. Megabreccia shedding from modern, low-
1245 relief carbonate platforms, Nicaraguan Rise. GSA Bulletin,
1246 104, 928-943.

1247 Hühnerbach, V. and Masson, D.G., 2004. Landslides in the
1248 North Atlantic and its adjacent seas: an analysis of their
1249 morphology, setting and behaviour. Marine Geology, 213, 343-
1250 362.

1251 James, N. P., Jones, B., 2016. Origin of Carbonate Sedimentary
1252 Rocks. John Wiley & Sons. 320 p.

1253 Janson, X., Kerans, C., Loucks, R., Marhx, M.A., Reyes, C.
1254 and Murguia, F., 2011. Seismic architecture of a Lower
1255 Cretaceous platform-to-slope system, Santa Agueda and Poza
1256 Rica fields, Mexico. AAPG bulletin, 95, 105-146.

1257 Joanne, C., Lamarche, G., Collot, J.Y., 2013. Dynamics of
1258 giant mass transport in deep submarine environments: the
1259 Matakaoa Debris Flow, New Zealand. Basin Research, 25, 471-
1260 488.

1261 Johnston, S.T., Thorkelson, D.J., 2000. Continental flood
1262 basalts: episodic magmatism above long-lived hotspots. Earth
1263 and Planetary Science Letters, 175, 247-256.

1264 Jorry, S., 2014. PTOLEMEE cruise, RV L'Atalante.
1265 http://dx.doi.org/10.17600/14000900

1266 Jorry, S.J., Camoin, G.F., Jouet, G., Le Roy, P., Vella, C.,
1267 Courgeon, S., Prat S., Fontanier C., Paumard V., Boulle J.,
1268 Caline B., Borgomano, J., 2016. Modern sediments and
1269 Pleistocene reefs from isolated carbonate platforms (Iles
1270 Eparses, SW Indian Ocean): A preliminary study. Acta
1271 Oecologica, 72, 129-143.

1272 Jouet, G., Deville, E., 2015. PAMELA-MOZ04 cruise, RV
1273 Pourquoi Pas ?. http://dx.doi.org/10.17600/15000700

1274 Kolla, V., Henderson, L. and Biscaye, P.E., 1976. Clay
1275 mineralogy and sedimentation in the western Indian Ocean.
1276 Deep Sea Research and Oceanographic Abstracts 23, 949-961.

1277 Lort, J.M., Limond, W.Q., Segoufin, J., Patriat, P., Delteil, J.R.,
1278 Damotte, B., 1979. New seismic data in the Mozambique
1279 Channel. Marine Geophysical Research, 4, 71-89.

1280 Lowe, D.R., 1982. Sediment gravity flows: II Depositional
1281 models with special reference to the deposits of high-density

1282 turbidity currents. Journal of Sedimentary Research, 52, 279-
1283 297.

1284 McGonigle, C. and Collier, J.S., 2014. Interlinking backscatter,
1285 grain size and benthic community structure. Estuarine, Coastal
1286 and Shelf Science, 147, 123-136.

1287 McIlreath, I.A., James, N.P., 1978. Facies models 13.
1288 Carbonate slopes. Geoscience Canada, 5, 189-199.

1289 Météo France, 2017.
1290 https://publitheque.meteo.fr/Donnees/DESC170531171564028
1291 9.KEYu07f7D3UO9xudD2U2fU9.html 1/2

1292 Milliman, J.D., Freile, D., Steinen, R.P. and Wilber, R.J., 1993.
1293 Great Bahama Bank aragonitic muds: mostly inorganically
1294 precipitated, mostly exported. Journal of Sedimentary
1295 Research, 63, 589-595.

1296 Moscardelli, L., Wood, L., Mann, P., 2006. Mass-transport
1297 complexes and associated processes in the offshore area of
1298 Trinidad and Venezuela. AAPG Bulletin, 90, 1059-1088.

1299 Mulder, T., Alexander, J., 2001. The physical character of
1300 subaqueous sedimentary density flows and their deposits.
1301 Sedimentology, 48, 269-299.

1302 Mulder, T. and Cochonat, P., 1996. Classification of offshore
1303 mass movements. Journal of Sedimentary Research, 66, 43-57.

1304 Mulder, T., Joumes, M., Hanquiez, V., Gillet, H., Reijmer,
1305 J.J.G., Tournadour, E., Chabaud, L., Principaud, M., Schnyder,
1306 J.S.D., Borgomano, J. Fauquembergue, K., 2017. Carbonate
1307 slope morphology revealing sediment transfer from bank-to-
1308 slope (Little Bahama Bank, Bahamas). Marine and Petroleum
1309 Geology, 83, 26-34.

1310 Mullins, H.T., Cook, H.E., 1986. Carbonate apron models:
1311 alternatives to the submarine fan model for paleoenvironmental
1312 analysis and hydrocarbon exploration. Sedimentary Geology,
1313 48, 37-79.

1314 Mullins, H.T., Heath, K.C., Buren, H., Newton, C.R., 1984.
1315 Anatomy of a modern open-ocean carbonate slope: northern
1316 Little Bahama Bank. Sedimentology, 31, 141-168.

1317 Olu, K., 2014. Rapport de fin de mission campagne Pamela-
1318 MOZ01. http://dx.doi.org/10.17600/14001000

1319 Payros, A., Pujalte, V., 2008. Calciclastic submarine fans: An
1320 integrated overview. Earth-Science Reviews, 86, 203-246.

1321 Pickering, K., Stow, D., Watson, M. and Hiscott, R., 1986.
1322 Deep-water facies, processes and models: a review and

1323 classification scheme for modern and ancient sediments. Earth-
1324 Science Reviews, 23, 75-174.

1325 Posamentier, H.W. and Kolla, V., 2003. Seismic
1326 geomorphology and stratigraphy of depositional elements in
1327 deep-water settings. Journal of Sedimentary Research, 73, 367-
1328 388.

1329 Posamentier, H.W., Martinsen, O.J. and Shipp, R.C., 2011. The
1330 character and genesis of submarine mass-transport deposits:
1331 insights from outcrop and 3D seismic data. In: Shipp, R.C.,
1332 Weimer, P., and Posamentier, H.W. (eds.), Mass-transport
1333 deposits in deepwater settings: Society for Sedimentary
1334 Geology (SEPM) Special Publication 96, 7-38.

1335 Prat, S., Jorry, S.J., Jouet, G., Camoin, G., Vella, C., Le Roy,
1336 P., Caline, B., Boichard, R., Pastol, Y., 2016. Geomorphology
1337 and sedimentology of a modern isolated carbonate platform:
1338 The Glorieuses archipelago, SW Indian Ocean. Marine
1339 Geology, 380, 272-283.

1340 Principaud, M., Mulder, T., Gillet, H. and Borgomano, J., 2015.
1341 Large-scale carbonate submarine mass-wasting along the
1342 northwestern slope of the Great Bahama Bank (Bahamas):
1343 Morphology, architecture, and mechanisms. Sedimentary
1344 Geology, 317, 27-42.

Quartau, R., Ramalho, R.S., Madeira, J., Santos, R., Rodrigues, A., Roque, C., Carrara, G. and da Silveira, A.B., 2018. Gravitational, erosional and depositional processes on volcanic ocean islands: Insights from the submarine morphology of Madeira Archipelago. Earth and Planetary Science Letters, 482, 288-299.

Raharimahefa, T. and Kusky, T.M., 2010. Environmental monitoring of Bombetoka Bay and the Betsiboka Estuary, Madagascar, using multi-temporal satellite data. Journal of Earth Science, 21, 210-226.

Reijmer, J.J., Swart, P.K., Bauch, T., Otto, R., Reuning, L., Roth, S. and Zechel, S., 2009. A Re-Evaluation of Facies on Great Bahama Bank I: New Facies Maps of Western Great Bahama Bank (pp. 29-46). International Association of Sedimentologists Special Publication 41, 29-46.

Saint-Ange, F., Bachèlery, P., Babonneau, N., Michon, L. and Jorry, S.J., 2013. Volcaniclastic sedimentation on the submarine slopes of a basaltic hotspot volcano: Piton de la Fournaise volcano (La Réunion Island, Indian Ocean). Marine Geology, 337, 35-52.

1365 Schott, F.A., Xie, S.P., McCreary, J.P., 2009. Indian Ocean
1366 circulation and climate variability. Reviews of Geophysics, 47,
1367 1-46.

1368 Shanmugam, G., 2000. 50 years of the turbidite paradigm
1369 (1950s—1990s): deep-water processes and facies models—a
1370 critical perspective. Marine and Petroleum Geology, 17, 285-
1371 342.

1372 Simpson, E.S.W., Schlich, R., Gieskes, J.M., Arch Girdley, W.,
1373 Leclaire, L., Marshall, B.V., Moore, C., Müller, C., Sigal, J.,
1374 Vallier, T.L., White, S.M., Zobel, B., 1974. Initial Reports of
1375 the Deep Sea Drilling Project, Sites 240-242, Volume 25,
1376 Washington (U.S. Government Printing Office) p. 65-176.

1377 Sisavath, E., Babonneau, N., Saint-Ange, F., Bachèlery, P.,
1378 Jorry, S.J., Deplus, C., De Voogd, B. and Savoye, B., 2011.
1379 Morphology and sedimentary architecture of a modern
1380 volcaniclastic turbidite system: The Cilaos fan, offshore La
1381 Réunion Island. Marine Geology, 288, 1-17.

1382 Talling, P.J., Masson, D.G., Sumner, E.J., Malgesini, G., 2012.
1383 Subaqueous sediment density flows: depositional processes and
1384 deposit types. Sedimentology, 59, 1937-2003.

1385 Tcherepanov, E.N., Droxler, A.W., Lapointe, P. and Mohn, K.,
1386 2008. Carbonate seismic stratigraphy of the Gulf of Papua

1387 mixed depositional system: Neogene stratigraphic signature and
1388 eustatic control. Basin Research, 20, 185-209.

1389 Testut, L., Duvat, V., Ballu, V., Fernandes, R.M., Pouget, F.,
1390 Salmon, C., Dyment, J., 2016. Shoreline changes in a rising sea
1391 level context: The example of Grande Glorieuse, Scattered
1392 Islands, Western Indian Ocean. Acta Oecologica, 72, 110-119.

1393 Van Sebille, E., Scussolini, P., Durgadoo, J.V., Peeters, F.J.,
1394 Biastoch, A., Weijer, W., Turney, C., Paris, C.B. and Zahn, R.,
1395 2015. Ocean currents generate large footprints in marine
1396 palaeoclimate proxies. Nature Communications, 6, 6521.

1397 Wiles, E., Green, A.N., Watkeys, M.K. and Jokat, W., 2017.
1398 Zambezi continental margin: compartmentalized sediment
1399 transfer routes to the abyssal Mozambique Channel. Marine
1400 Geophysical Research, 38, 227-240.

1401 Wilson, P.A. and Roberts, H.H., 1995. Density cascading: off-
1402 shelf sediment transport, evidence and implications, Bahama
1403 Banks. Journal of Sedimentary Research, 65, 45-56.

1404 Yamano, H., Cabioch, G., Pelletier, B., Chevillon, C.,
1405 Tachikawa, H., Lefêvre, J. and Marchesiello, P., 2015. Modern
1406 carbonate sedimentary facies on the outer shelf and slope
1407 around New Caledonia. Island Arc, 24, 4-15.

A: Geography

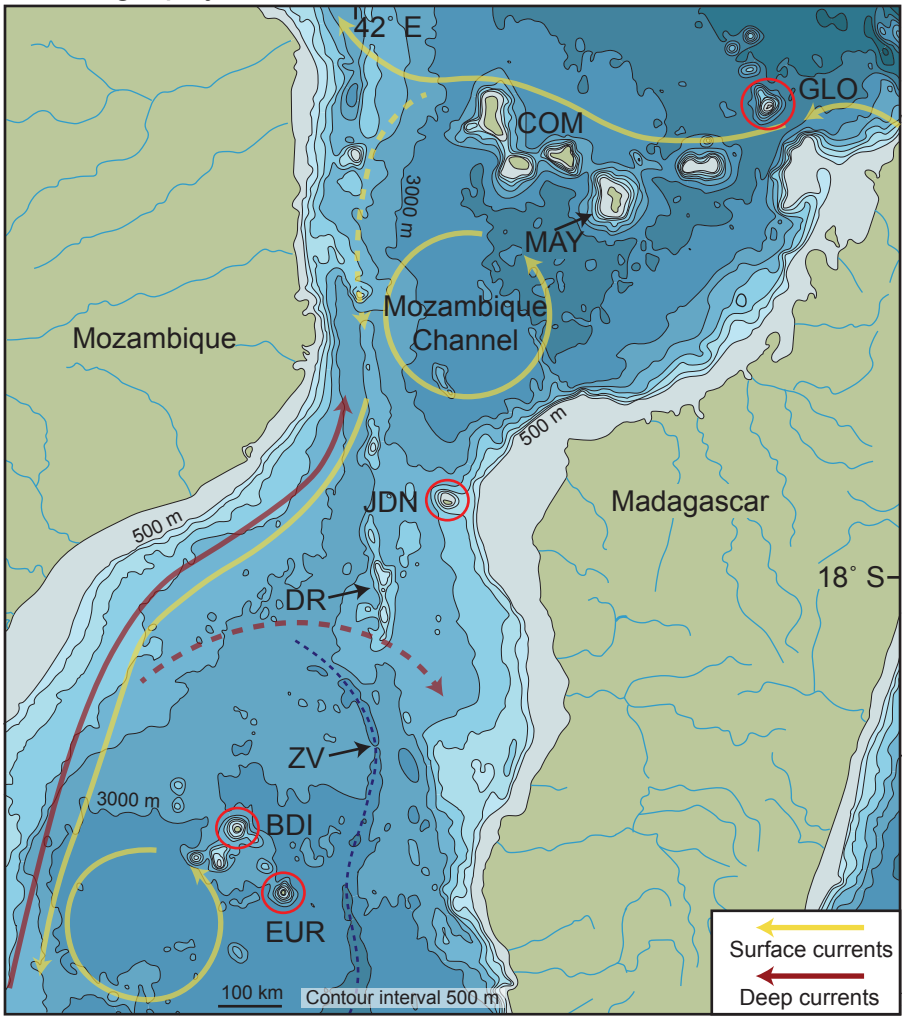


B: Wind direction

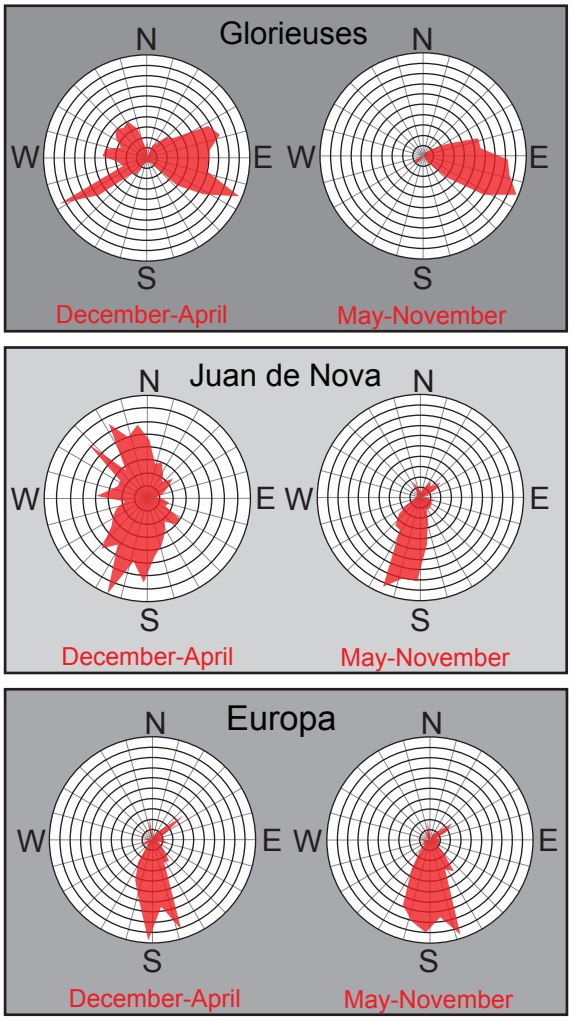

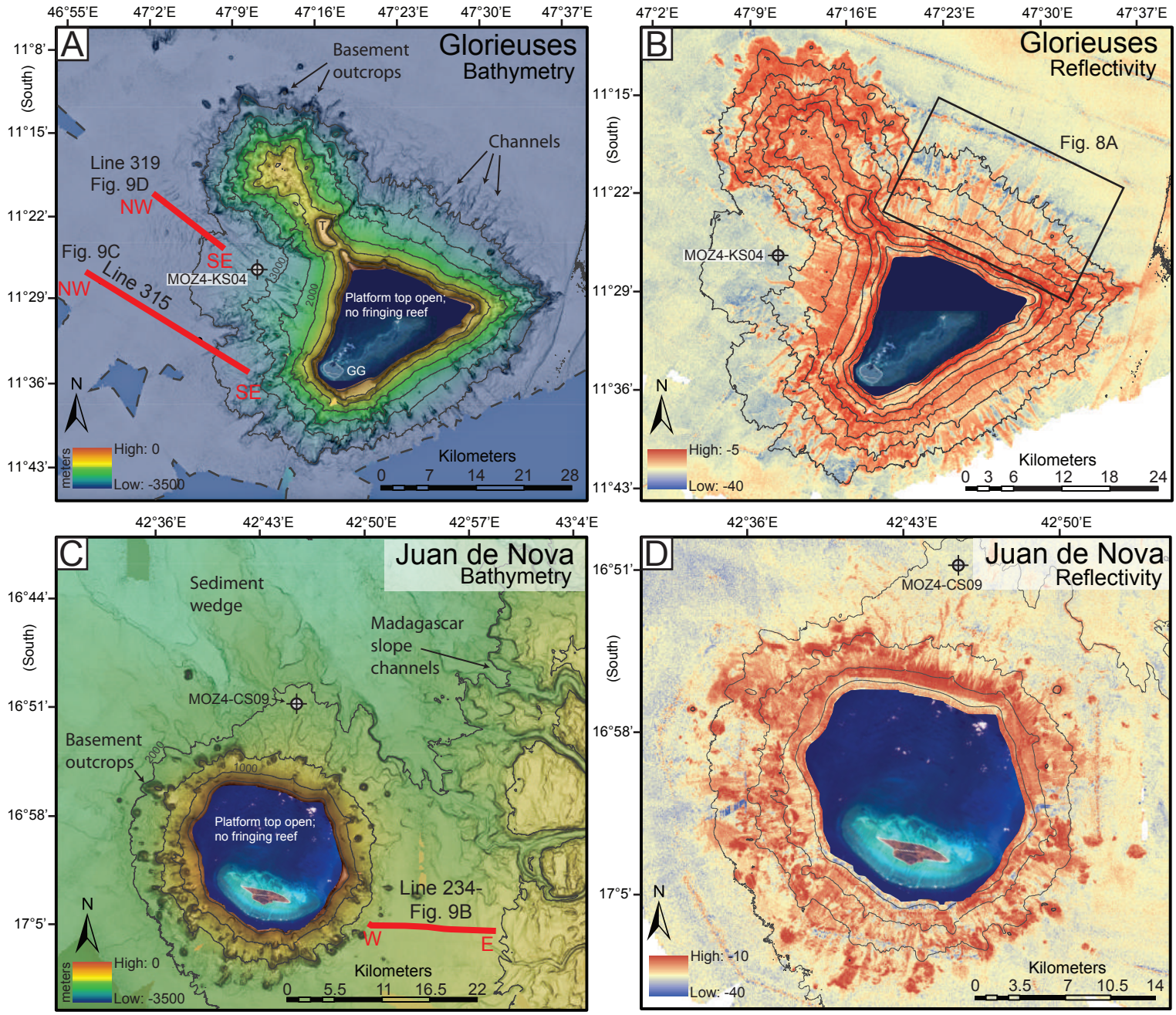
A
Glorieuses
Bathymetry
Basement outcrops
Channels
Line 319
Fig. 9D
NW
SE
Fig. 9C
Line 315
NW
SE
MOZ4-KS04
T
GG
Platform top open; no fringing reef
3000
2000
N
High: 0
Low: -3500
meters
Kilometers
0 7 14 21 28
B
Glorieuses
Reflectivity
Fig. 8A
MOZ4-KS04
N
High: -5
Low: -40
Kilometers
0 3 6 12 18 24
C
Juan de Nova
Bathymetry
Sediment wedge
Madagascar slope channels
MOZ4-CS09
Basement outcrops
2000
1000
Platform top open; no fringing reef
Line 234-
Fig. 9B
W
E
N
High: 0
Low: -3500
meters
Kilometers
0 5.5 11 16.5 22
D
Juan de Nova
Reflectivity
MOZ4-CS09
N
High: -10
Low: -40
Kilometers
0 3.5 7 10.5 14

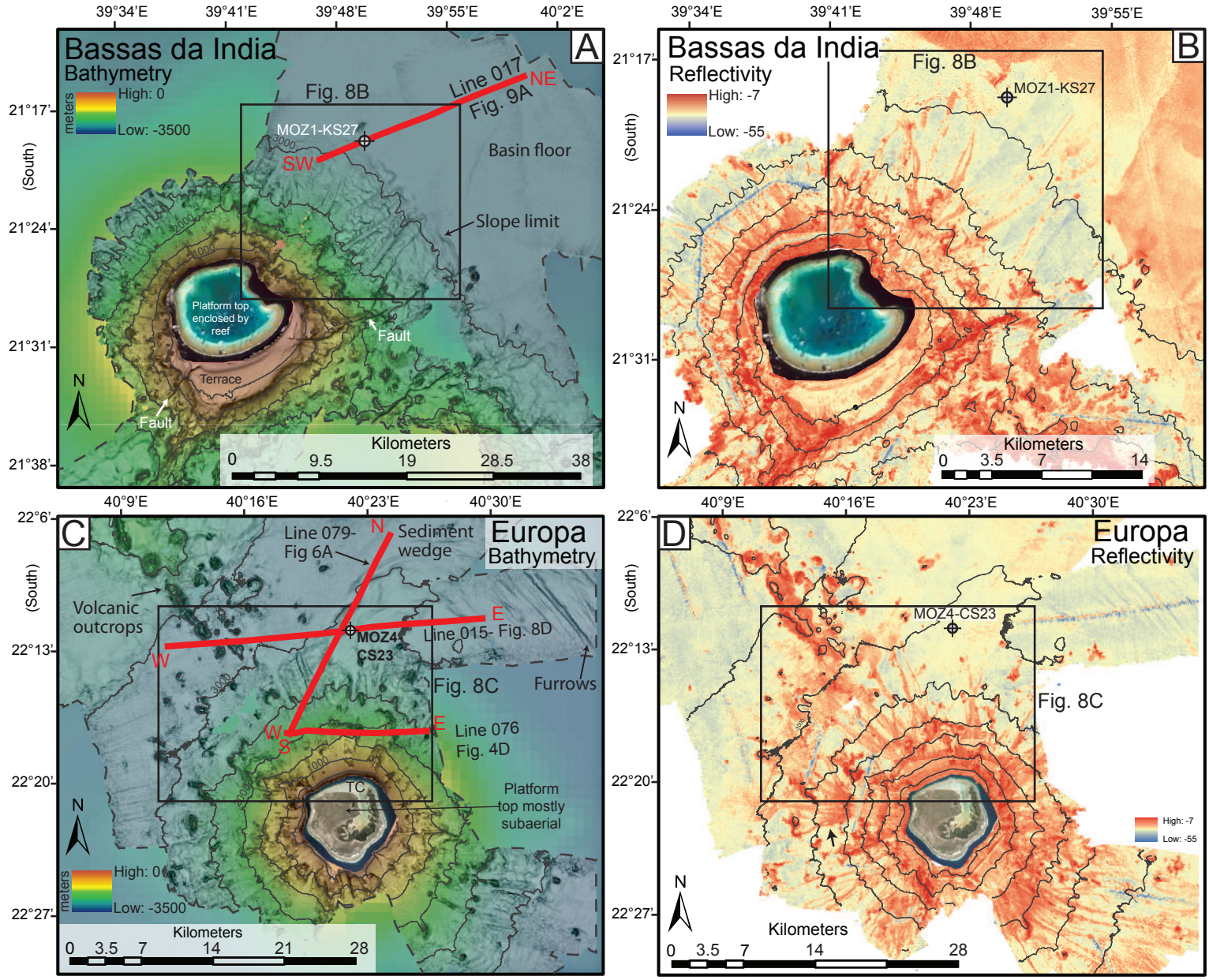
A
Bassas da India
Bathymetry
High: 0
Low: -3500
meters
Fig. 8B
Line 017
Fig. 9A
NE
SW
MOZ1-KS27
Basin floor
Slope limit
Platform top enclosed by reef
Fault
Terrace
Fault
N
Kilometers
0 9.5 19 28.5 38
B
Bassas da India
Reflectivity
High: -7
Low: -55
Fig. 8B
MOZ1-KS27
N
Kilometers
0 3.5 7 14
C
Europa
Bathymetry
Line 079-
Fig 6A
N
Sediment wedge
Volcanic outcrops
E
W
MOZ4-CS23
Line 015- Fig. 8D
Fig. 8C
Furrows
W
S
E
Line 076
Fig. 4D
TC
Platform top mostly subaerial
N
High: 0
Low: -3500
meters
Kilometers
0 3.5 7 14 21 28
D
Europa
Reflectivity
MOZ4-CS23
Fig. 8C
High: -7
Low: -55
N
Kilometers
0 3.5 7 14 28
39°34'E
39°41'E
39°48'E
39°55'E
40°2'E
21°17'
21°24'
21°31'
21°38'
(South)
40°9'E
40°16'E
40°23'E
40°30'E
22°6'
22°13'
22°20'
22°27'

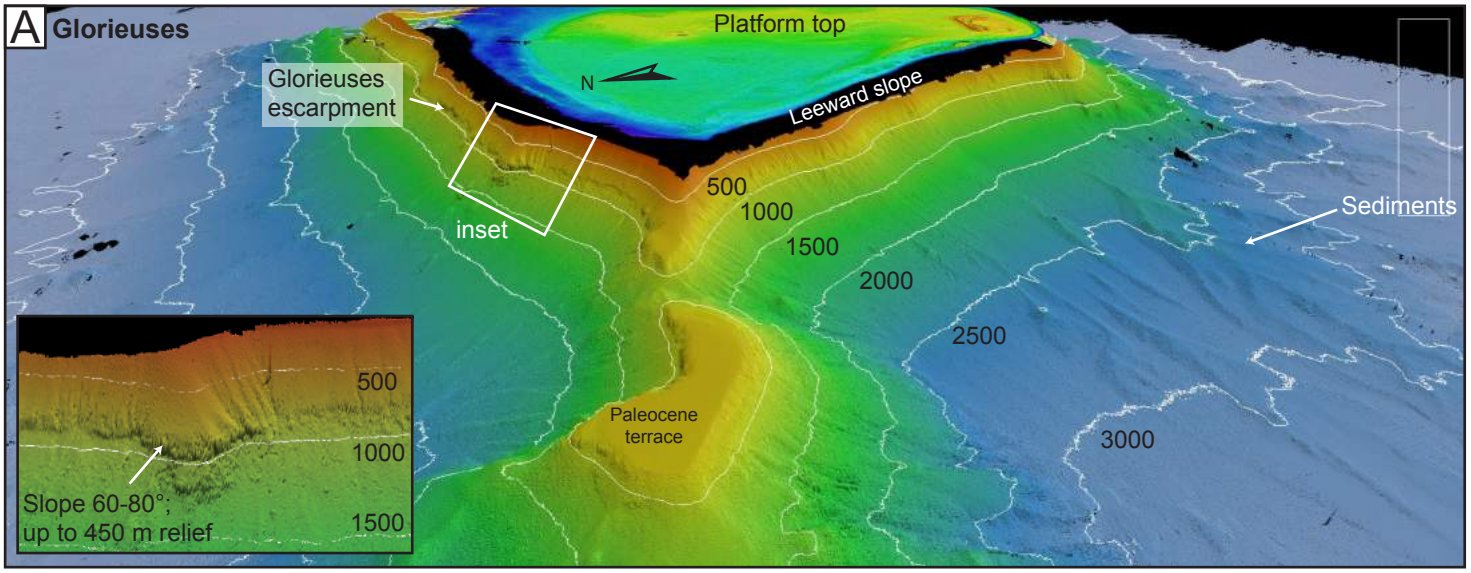
A Glorieuses
Platform top
N
Glorieuses escarpment
Leeward slope
inset
500
1000
1500
2000
2500
3000
Sediments
Paleocene terrace
Slope 60-80°; up to 450 m relief

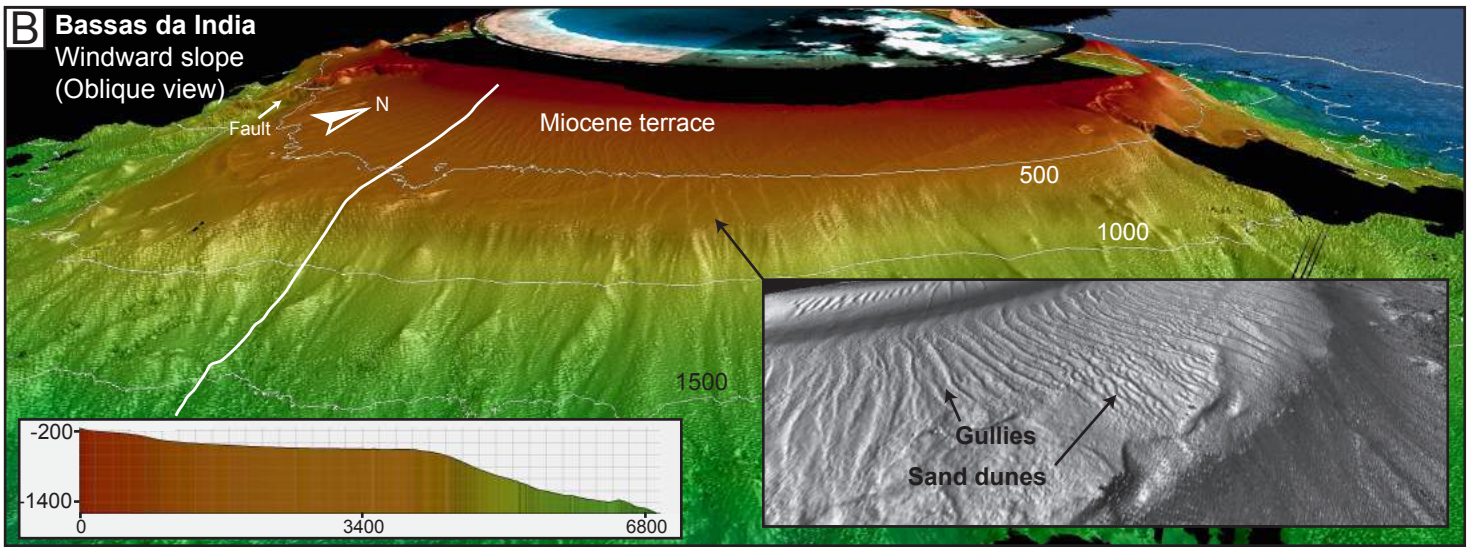
B Bassas da India
Windward slope
(Oblique view)
Fault
N
Miocene terrace
500
1000
1500
-200
-1400
0
3400
6800
Gullies
Sand dunes

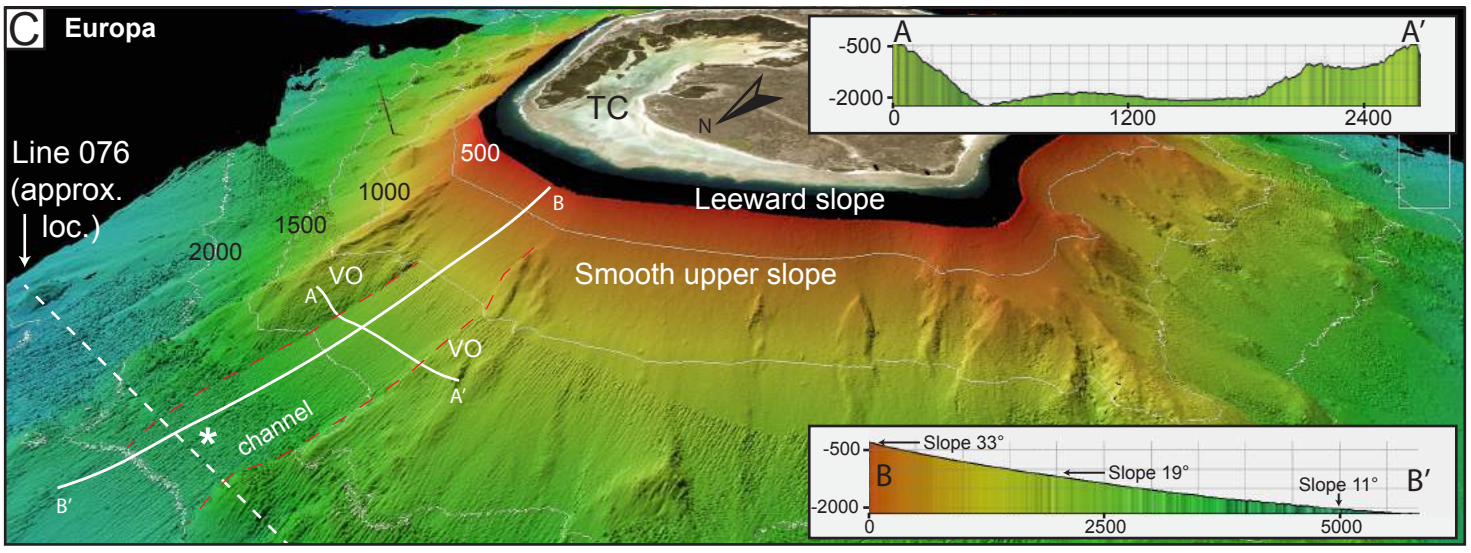
C Europa
TC
N
A
A′
-500
-2000
0
1200
2400
Line 076 (approx. loc.)
500
1000
1500
2000
B
Leeward slope
Smooth upper slope
VO
A
VO
A′
channel
B′
Slope 33°
Slope 19°
Slope 11°
B
B′
-500
-2000
0
2500
5000

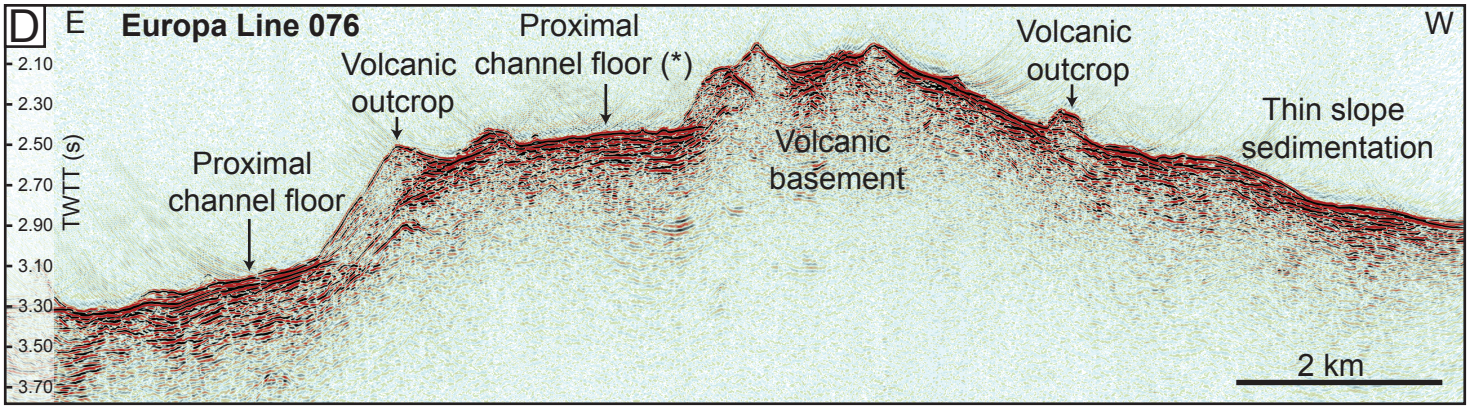
D E
Europa Line 076
W
Volcanic outcrop
Proximal channel floor (*)
Volcanic outcrop
Thin slope sedimentation
Proximal channel floor
Volcanic basement
TWTT (s)
2.10
2.30
2.50
2.70
2.90
3.10
3.30
3.50
3.70
2 km

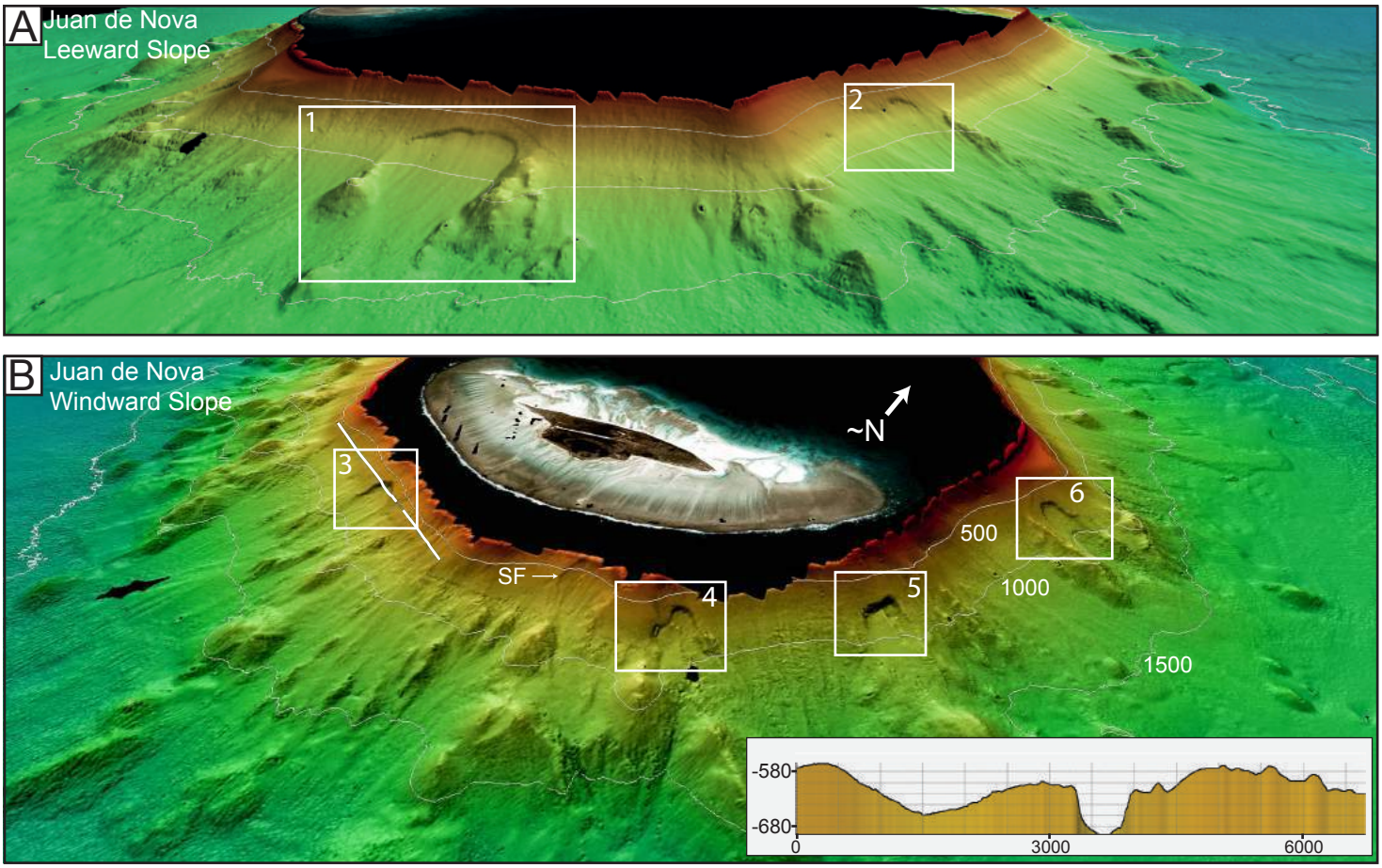
A
Juan de Nova
Leeward Slope
1
2
B
Juan de Nova
Windward Slope
~N
3
SF
4
5
6
500
1000
1500
-580
-680
0
3000
6000
C
Concept
Example
traced
contour
Platform
shape
correction
Leeward
Windward
Radii from leeward side
Std dev = X
Radii from windward side
Std dev = Y
Higher StD = less smooth slope
Results
600 m contour
South side (windward)
Std dev = 27.95
Radii length frequency
Adjusted radii length
North side (leeward)
Std dev = 18.85
Radii length frequency
Adjusted radii length

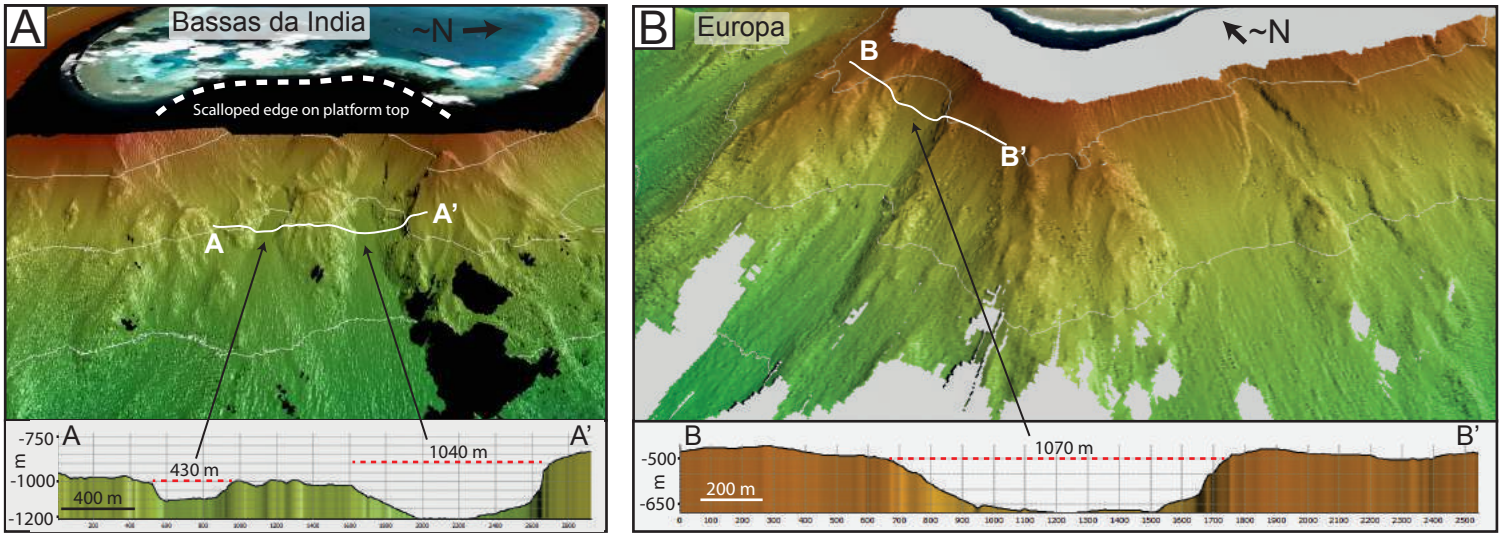
A
Bassas da India
~N
Scalloped edge on platform top
A
A'
-750
-1000
-1200
A
A'
430 m
1040 m
400 m
B
Europa
~N
B
B'
B
B'
1070 m
-500
-650
200 m

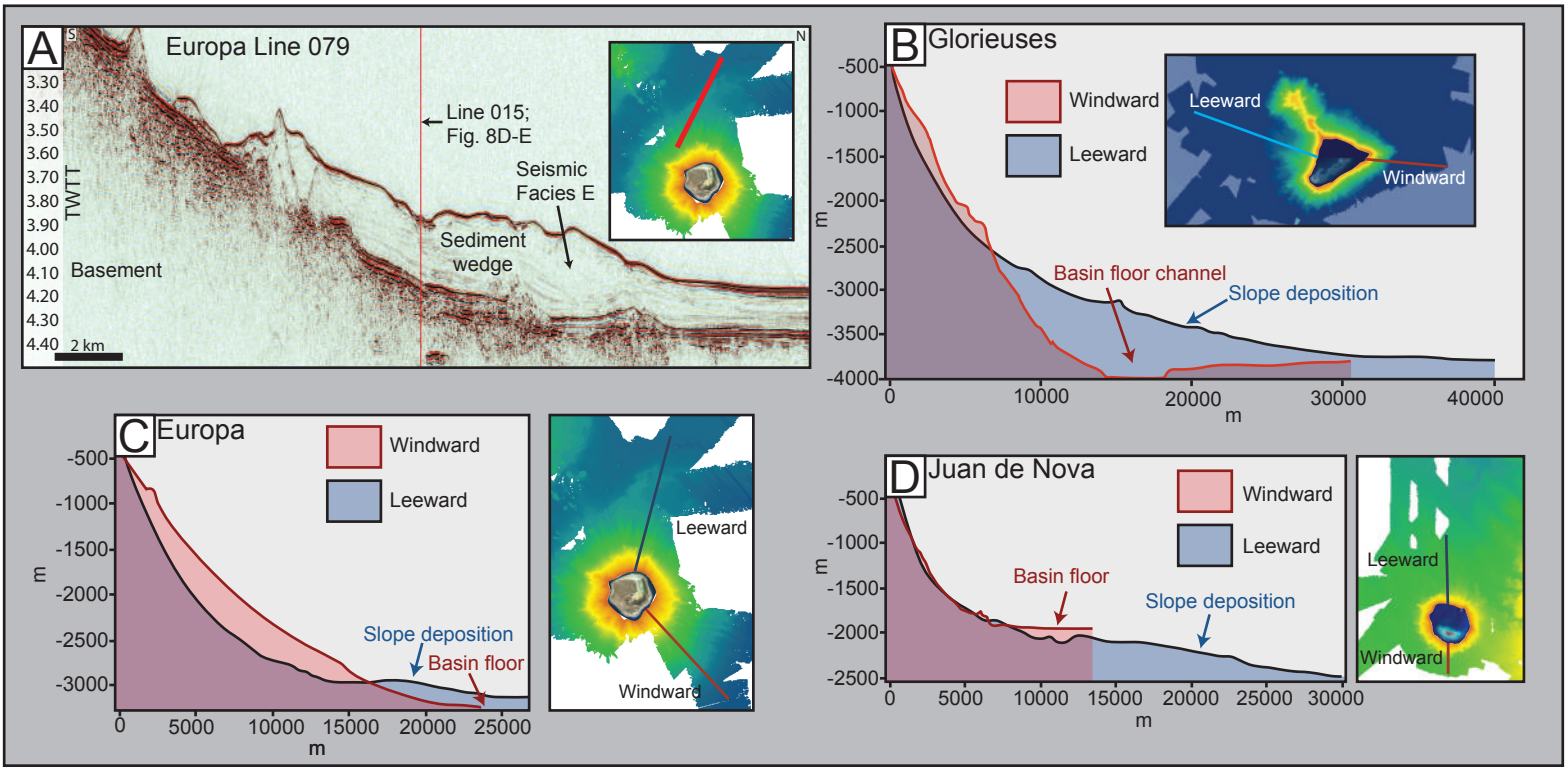
A
Europa Line 079
S
N
3.30
3.40
3.50
3.60
3.70
3.80
3.90
4.00
4.10
4.20
4.30
4.40
TWTT
Basement
2 km
Line 015;
Fig. 8D-E
Seismic
Facies E
Sediment
wedge
B Glorieuses
Windward
Leeward
Leeward
Windward
-500
-1000
-1500
-2000
-2500
-3000
-3500
-4000
m
Basin floor channel
Slope deposition
0
10000
20000
30000
40000
m
C Europa
Windward
Leeward
-500
-1000
-1500
-2000
-2500
-3000
m
Slope deposition
Basin floor
0
5000
10000
15000
20000
25000
m
Leeward
Windward
D Juan de Nova
Windward
Leeward
-500
-1000
-1500
-2000
-2500
m
Basin floor
Slope deposition
0
5000
10000
15000
20000
25000
30000
m
Leeward
Windward

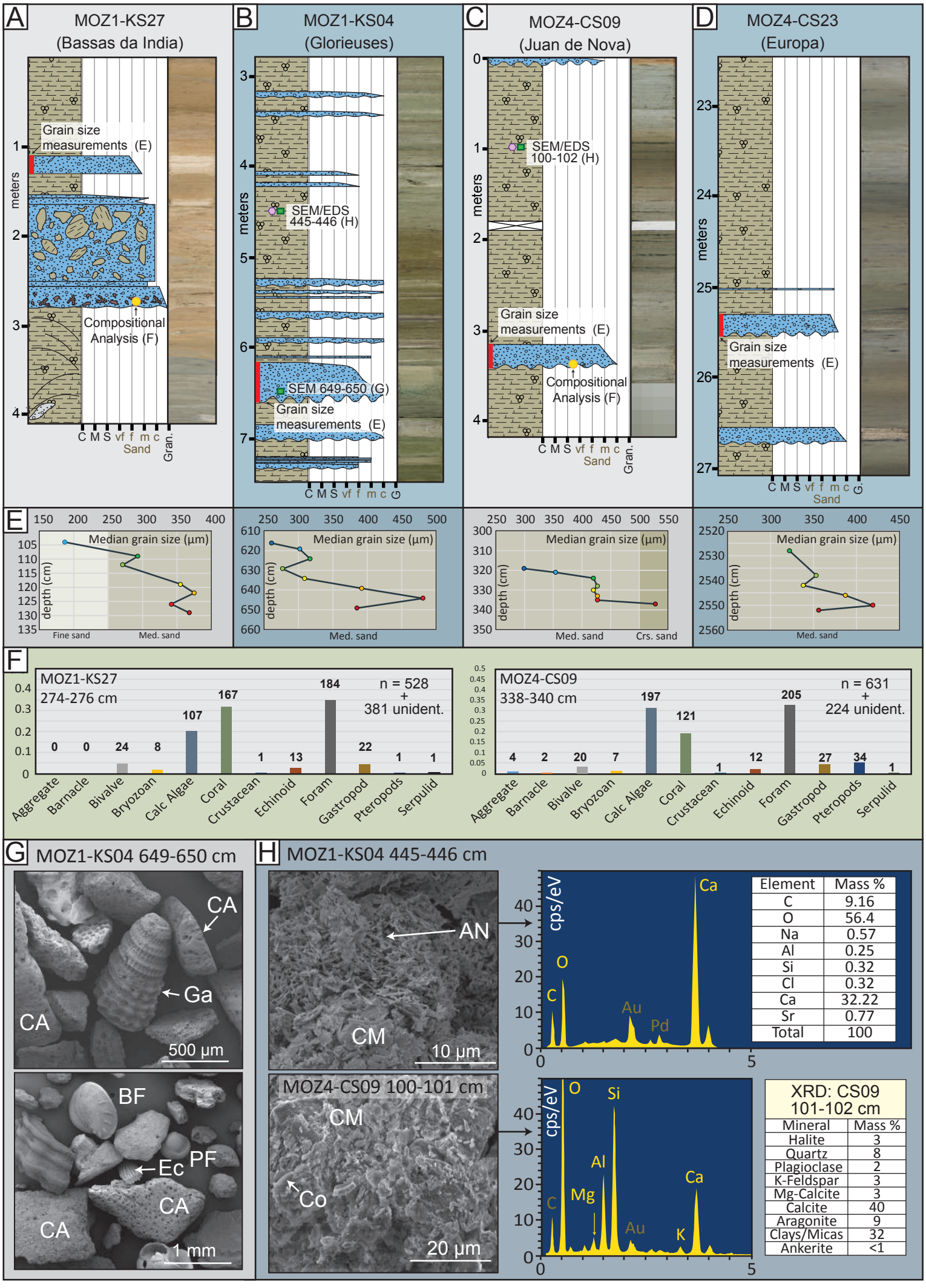
A
MOZ1-KS27
(Bassas da India)
Grain size
measurements (E)
Compositional
Analysis (F)
meters
C M S vf f m c
Sand
Gran.
B
MOZ1-KS04
(Glorieuses)
SEM/EDS
445-446 (H)
SEM 649-650 (G)
Grain size
measurements (E)
C
MOZ4-CS09
(Juan de Nova)
SEM/EDS
100-102 (H)
Grain size
measurements (E)
Compositional
Analysis (F)
D
MOZ4-CS23
(Europa)
Grain size
measurements (E)
E
Median grain size (µm)
depth (cm)
Fine sand
Med. sand
Crs. sand
F
MOZ1-KS27
274-276 cm
n = 528
+
381 unident.
0 0 24 8 107 167 1 13 184 22 1 1
MOZ4-CS09
338-340 cm
n = 631
+
224 unident.
4 2 20 7 197 121 1 12 205 27 34 1
Aggregate
Barnacle
Bivalve
Bryozoan
Calc Algae
Coral
Crustacean
Echinoid
Foram
Gastropod
Pteropods
Serpulid
G
MOZ1-KS04 649-650 cm
CA
Ga
500 µm
BF
Ec
PF
1 mm
H
MOZ1-KS04 445-446 cm
AN
CM
10 µm
cps/eV
Element | Mass %
C 9.16
O 56.4
Na 0.57
Al 0.25
Si 0.32
Cl 0.32
Ca 32.22
Sr 0.77
Total 100
MOZ4-CS09 100-101 cm
Co
20 µm
XRD: CS09
101-102 cm
Mineral | Mass %
Halite 3
Quartz 8
Plagioclase 2
K-Feldspar 3
Mg-Calcite 3
Calcite 40
Aragonite 9
Clays/Micas 32
Ankerite <1

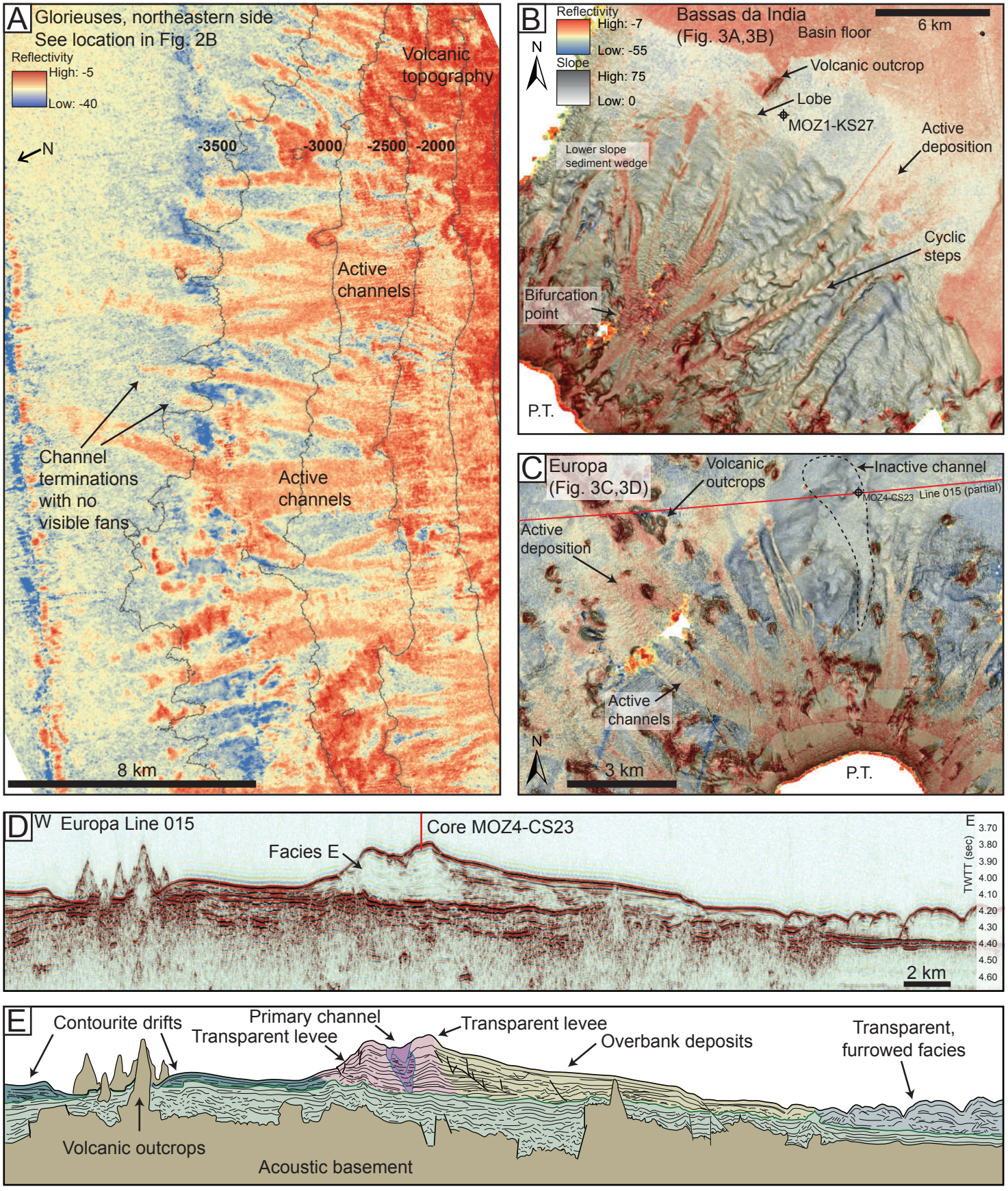
A
Glorieuses, northeastern side
See location in Fig. 2B
Reflectivity
High: -5
Low: -40
N
-3500
-3000
-2500
-2000
Volcanic topography
Active channels
Channel terminations with no visible fans
Active channels
8 km
B
Reflectivity
High: -7
Low: -55
Slope
High: 75
Low: 0
N
Bassas da India
(Fig. 3A,3B)
Basin floor
6 km
Volcanic outcrop
Lobe
MOZ1-KS27
Active deposition
Lower slope sediment wedge
Cyclic steps
Bifurcation point
P.T.
C
Europa
(Fig. 3C,3D)
Volcanic outcrops
Inactive channel
MOZ4-CS23
Line 015 (partial)
Active deposition
Active channels
N
3 km
P.T.
D
W
Europa Line 015
Core MOZ4-CS23
Facies E
E
TWTT (sec)
3.70
3.80
3.90
4.00
4.10
4.20
4.30
4.40
4.50
4.60
2 km
E
Contourite drifts
Primary channel
Transparent levee
Transparent levee
Overbank deposits
Transparent, furrowed facies
Volcanic outcrops
Acoustic basement

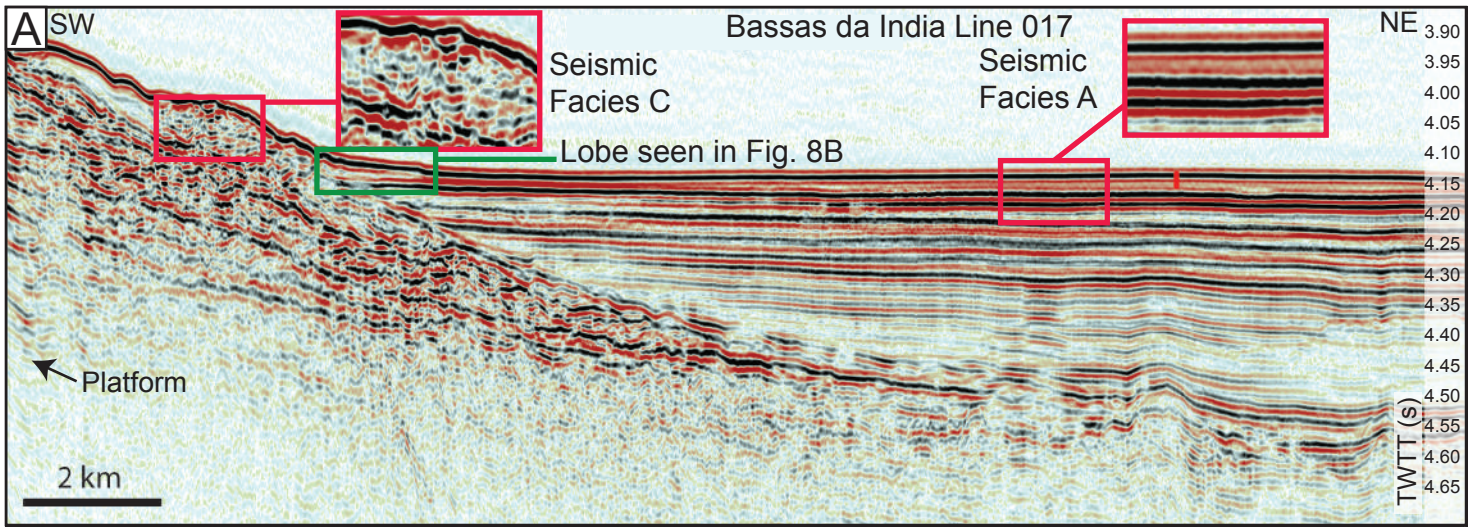
A
SW
NE
Bassas da India Line 017
Seismic
Facies C
Seismic
Facies A
Lobe seen in Fig. 8B
Platform
2 km
TWTT (s)
3.90
3.95
4.00
4.05
4.10
4.15
4.20
4.25
4.30
4.35
4.40
4.45
4.50
4.55
4.60
4.65

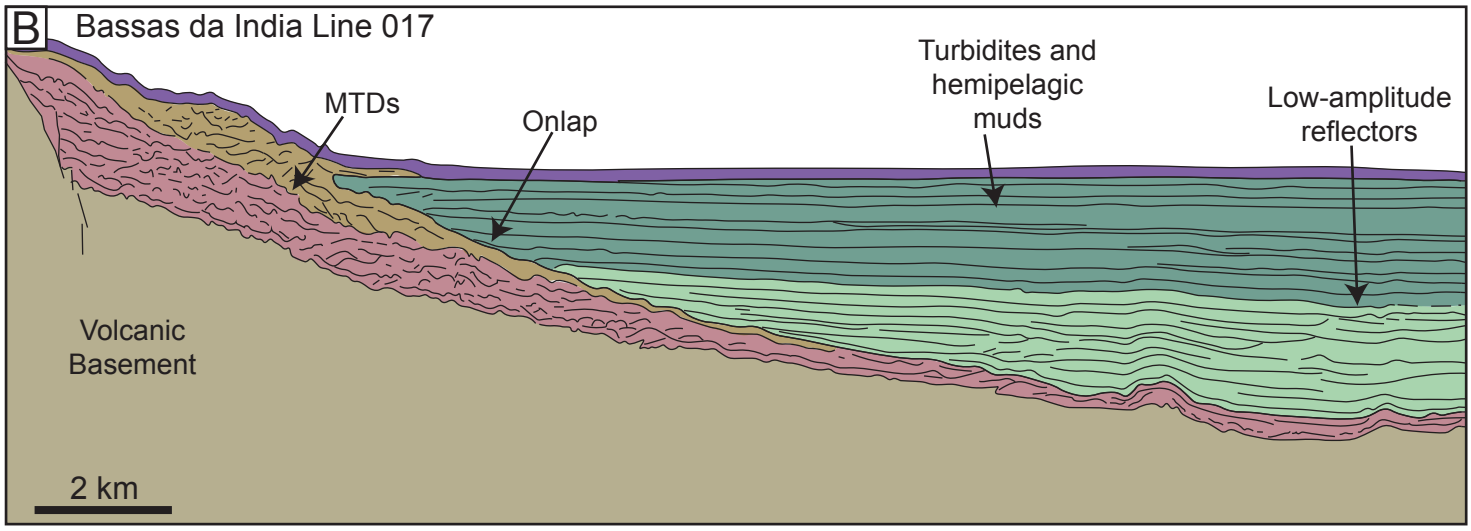
B
Bassas da India Line 017
MTDs
Onlap
Turbidites and
hemipelagic
muds
Low-amplitude
reflectors
Volcanic
Basement
2 km

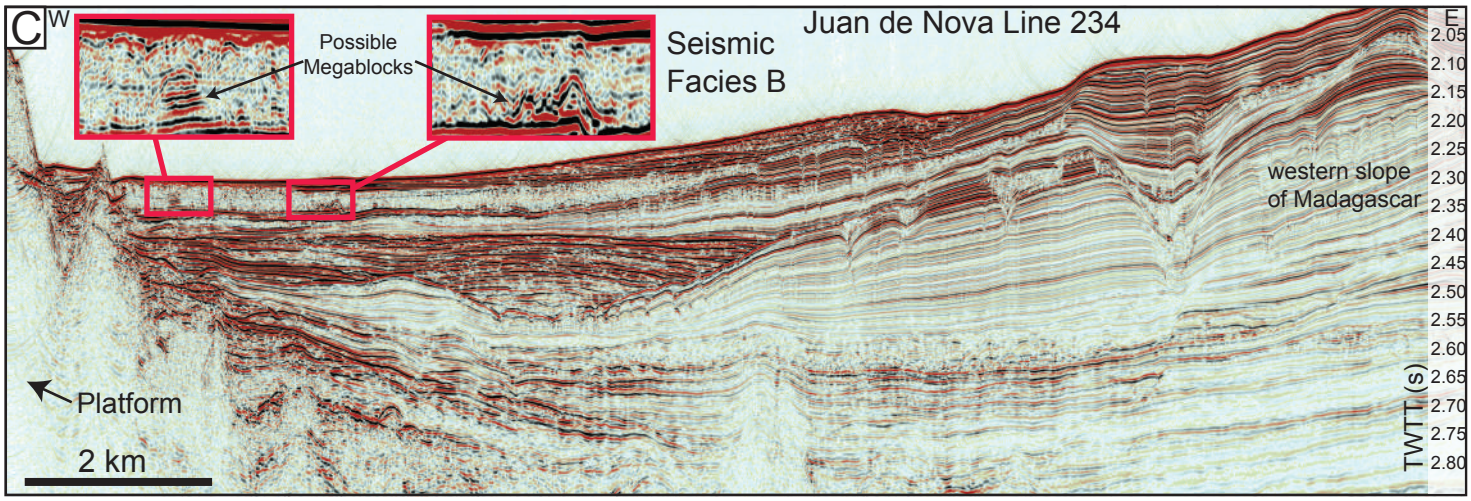
C
W
E
Possible
Megablocks
Seismic
Facies B
Juan de Nova Line 234
western slope
of Madagascar
Platform
2 km
TWTT (s)
2.05
2.10
2.15
2.20
2.25
2.30
2.35
2.40
2.45
2.50
2.55
2.60
2.65
2.70
2.75
2.80

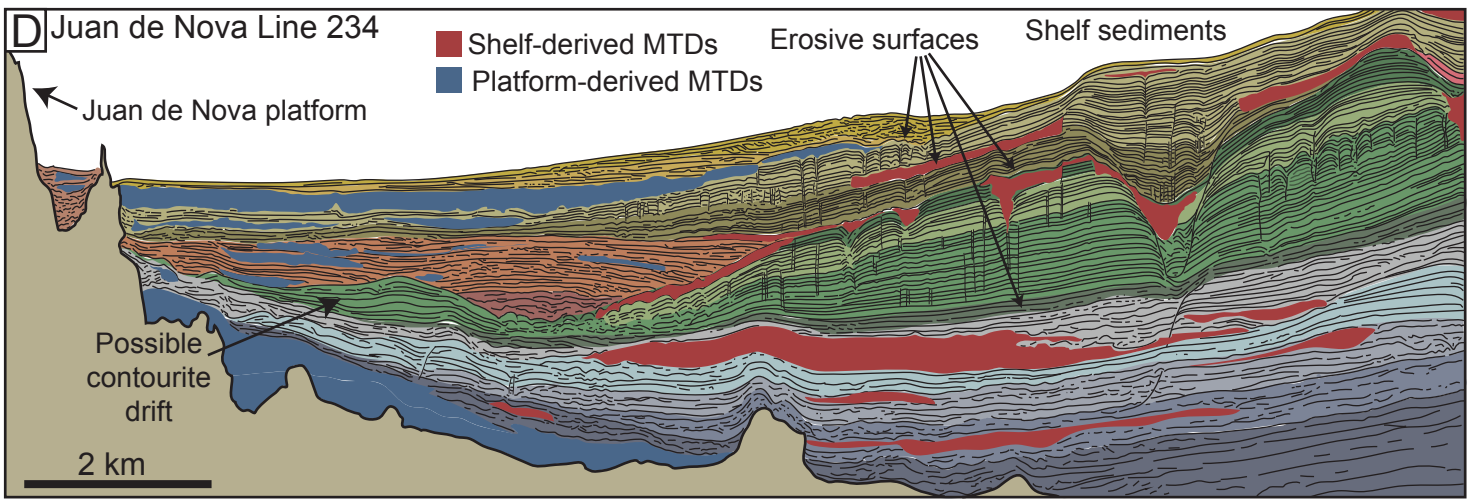
D
Juan de Nova Line 234
Shelf-derived MTDs
Platform-derived MTDs
Erosive surfaces
Shelf sediments
Juan de Nova platform
Possible
contourite
drift
2 km

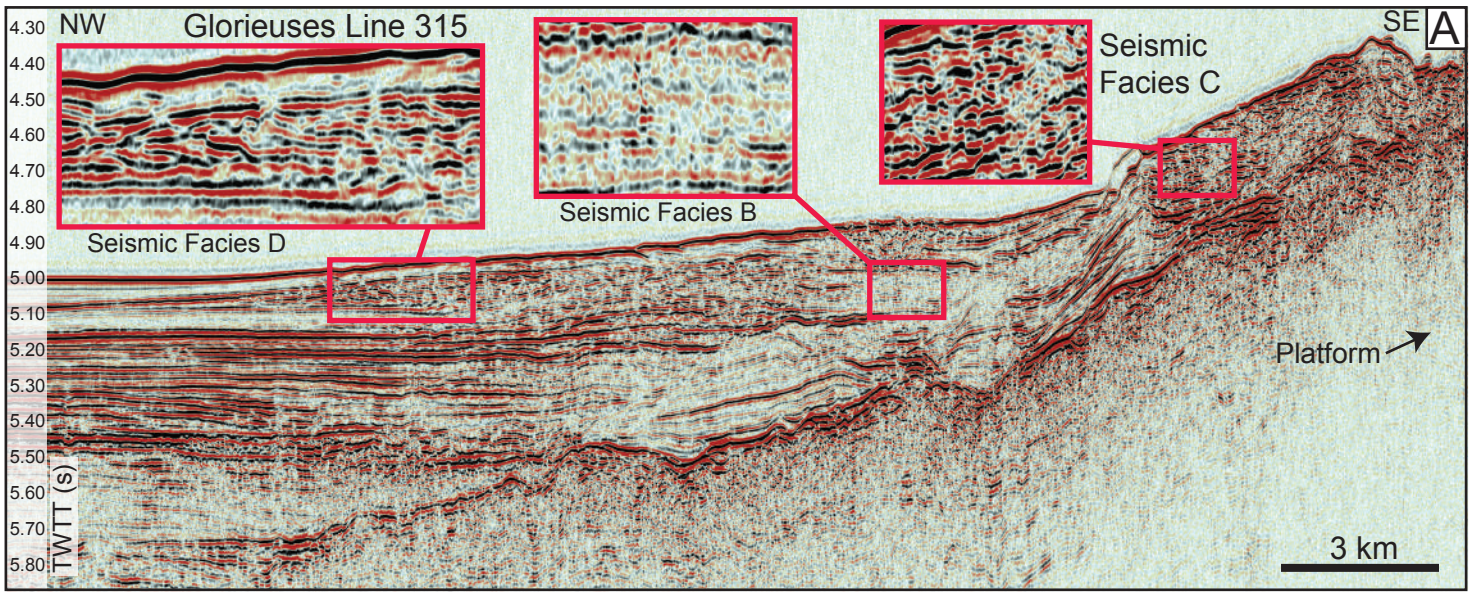


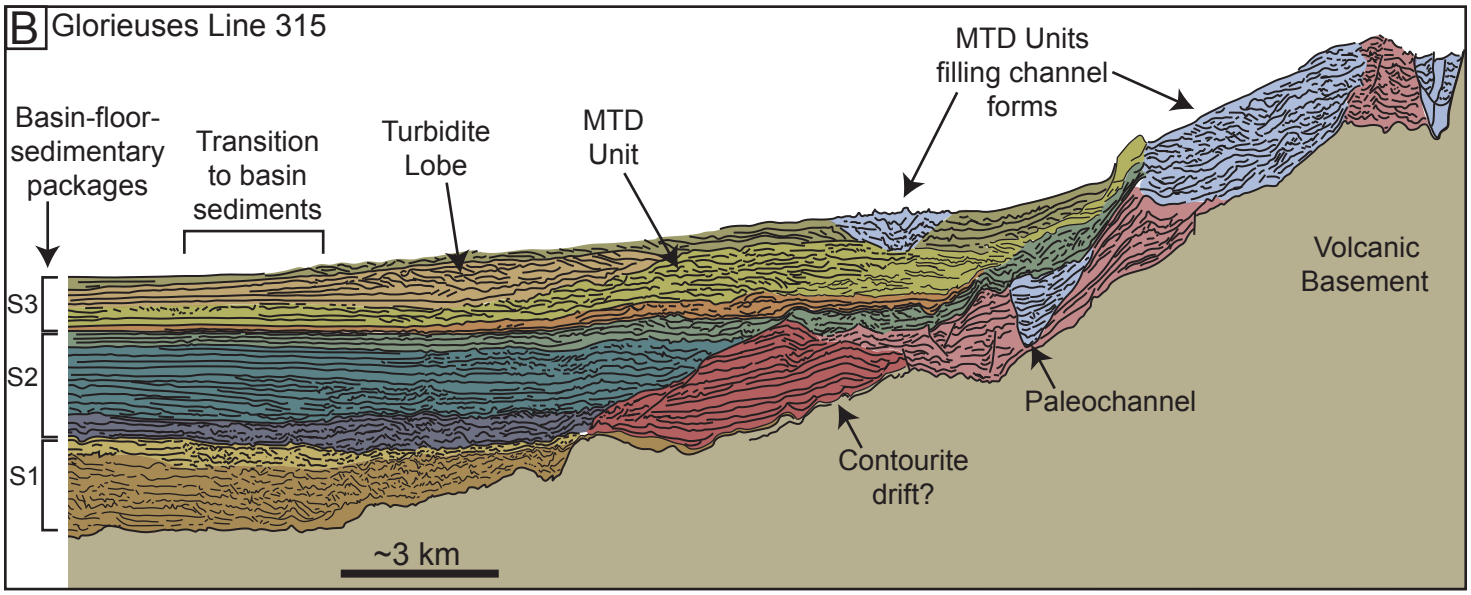


Colors= related units

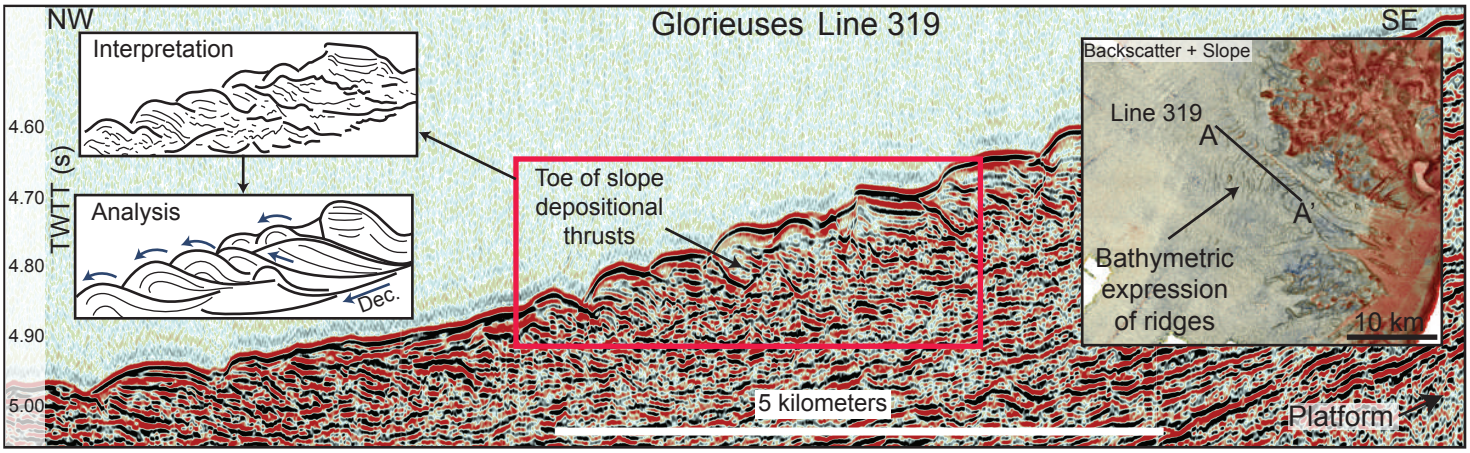
NW
Glorieuses Line 319
SE
Interpretation
Analysis
Dec.
4.60
4.70
4.80
4.90
5.00
TWTT (s)
Toe of slope
depositional
thrusts
Backscatter + Slope
Line 319
A
A'
Bathymetric
expression
of ridges
10 km
5 kilometers
Platform

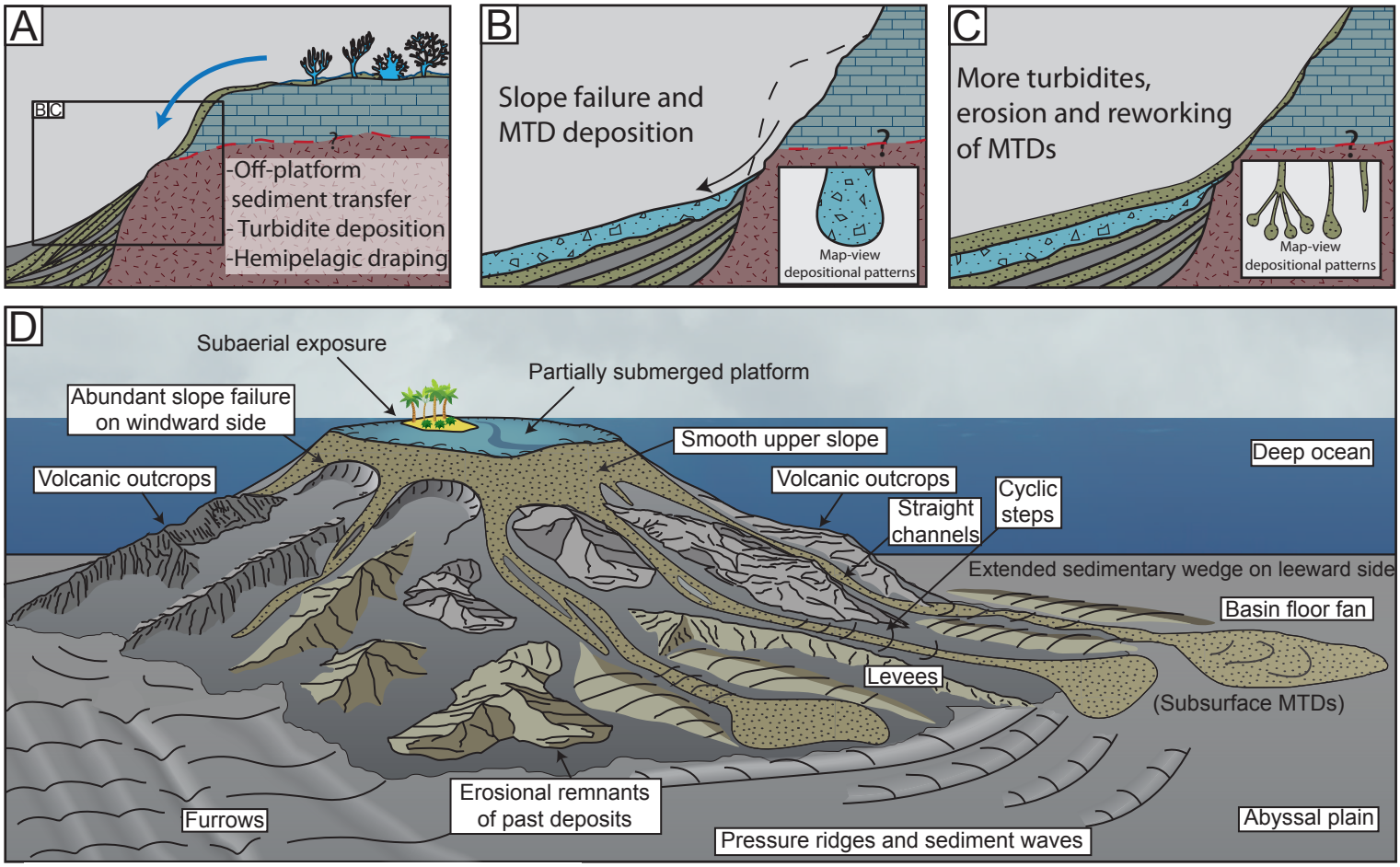
A
B|C
-Off-platform
sediment transfer
- Turbidite deposition
-Hemipelagic draping
B
Slope failure and
MTD deposition
Map-view
depositional patterns
C
More turbidites,
erosion and reworking
of MTDs
Map-view
depositional patterns
D
Subaerial exposure
Partially submerged platform
Abundant slope failure
on windward side
Smooth upper slope
Deep ocean
Volcanic outcrops
Volcanic outcrops
Straight
channels
Cyclic
steps
Extended sedimentary wedge on leeward side
Basin floor fan
Levees
(Subsurface MTDs)
Erosional remnants
of past deposits
Furrows
Pressure ridges and sediment waves
Abyssal plain

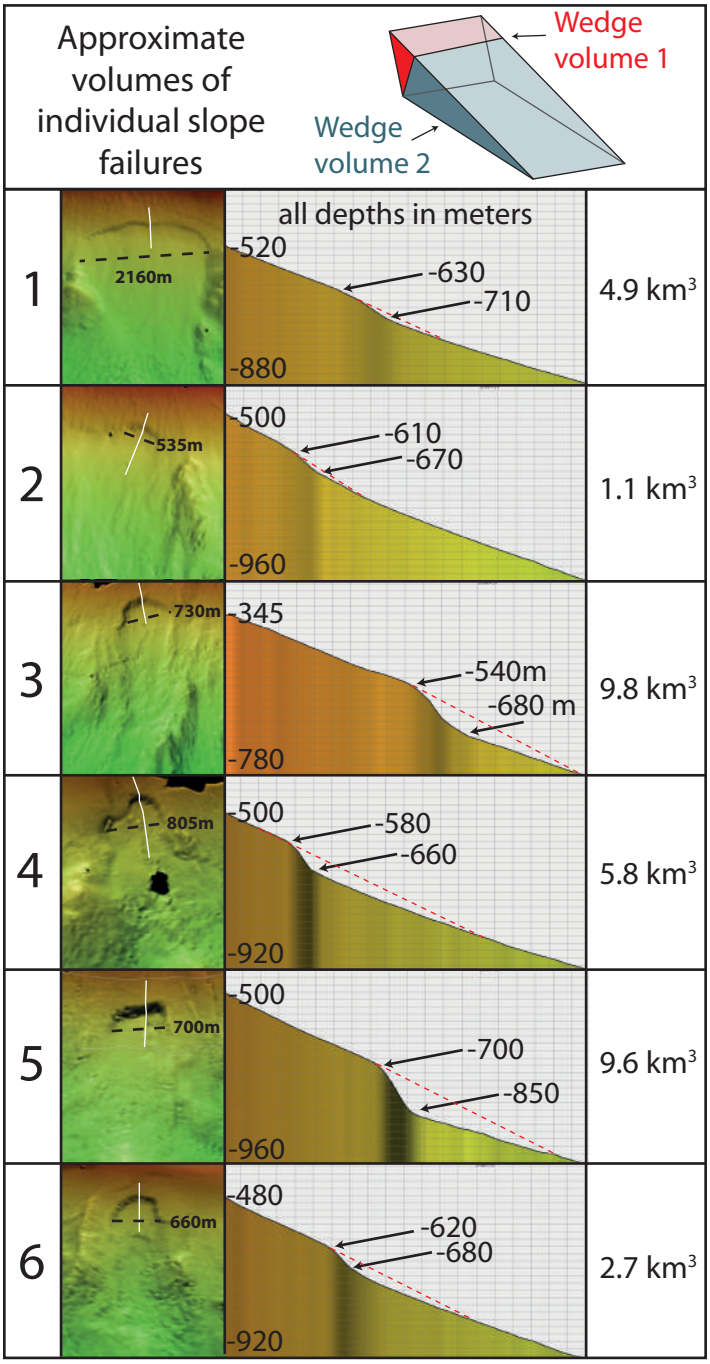
Approximate volumes of individual slope failures
Wedge volume 1
Wedge volume 2
all depths in meters
1
2160m
-520
-630
-710
-880
4.9 km³
2
535m
-500
-610
-670
-960
1.1 km³
3
730m
-345
-540m
-680 m
-780
9.8 km³
4
805m
-500
-580
-660
-920
5.8 km³
5
700m
-500
-700
-850
-960
9.6 km³
6
660m
-480
-620
-680
-920
2.7 km³

| Seismic Facies | Reflection Orientation | Reflection Continuity | Amplitude | Observed Distribution | Relationships with other Facies | Interpretation | Image |
|---|---|---|---|---|---|---|---|
| A (Continuous parallel) | Horizontal to subhorizontal; Parallel | Continuous | High | Basin floor surrounding all platforms | Onlaps other facies and units; transitions into | Basin-floor deposits; pelagic/hemipelagic sedimentation | 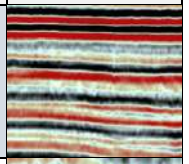 |
| B (Chaotic transparent) | Chaotic | Discontinuous | Low to mixed | Juan de Nova, Glorieuses | Interbedded; Pinches out distally | Mass transport deposits; debris flow; homogeneous composition | 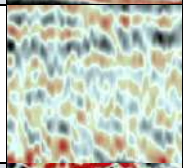 |
| C (Chaotic mixed) | Chaotic | Discontinuous | High to mixed | Bassas da India, Glorieuses | Interbedded; possibly erosional base | Mass transport deposits; debris flow; heterogeneous composition | 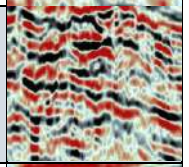 |
| D (Organized) | Inclined; Organized | Moderately continuous | Mixed | Glorieuses | Interbedded; Internal toplap and downlap | Turbidite lobe | 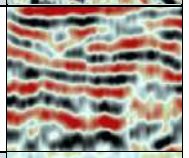 |
| E (Parallel transparent) | Parallel | Continuous | Low | Europa | Within a straigraphically distinct unit | Levee and overbank deposits related to submarine channels | 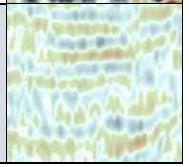 |

| Geomorphologic or Depositional Element | Gradient | Approximate scale | Map-view shape | Position relative to platform | Extent |
|---|---|---|---|---|---|
| Platform top | 0-3 degrees | 50-200 $km^2$ | Round/equant/ triangular | Top | N/A |
| Channels | 2-35 degrees; more similar to erosive shallow canyons ar slopes >10 degrees | Generally 6-9 km length, 200-400 meters width, with levees or erosional walls 10s of meters high | Linear, straight | Radial on all sides | Generally terminate 12-18 kilometers from platform top |
| Fans | 1-3 degrees | On the order of 1.5 x 3 km, individually variable | Cone/fan-shaped | Leeward sides of BDI and EUR | At terminal end of some channels, 12-15 km from platform top |
| Slope failure scars | generally >22 degrees | On Juan de Nova, ~2-50 km in volume, 500-2000 meters across. Elsewhere, larger but less frequent | Arcuate wedge on JDN | Upper slope, more frequent on windward side | Scars confined to upper slope; deposits may extend into lower slope or basin |
| MTDs | Variable but generally found on lower slopes of gradient <10 and usually <5 degrees. | ~7 km | Wedge in cross-section; unknown in map view | Occur on all sides; more abundant on leeward sides | Visible in seismic up to 35 meters from platform top |